Università degli Studi della Calabria

Dottorato di Ricerca in Ingegneria Chimica e dei Materiali

SCUOLA DI DOTTORATO " PITAGORA " IN SCIENZE INGEGNERISTICHE

Tesi

Membrane Distillation in Integrated Seawater Desalination Systems

Settore Scientifico Disciplinare CHIM07 – Fondamenti chimici delle tecnologie

Supervisori

Ch.mo Prof. Enrico DRIOLI

Dott.Efrem CURCIO

Candidato

Xiaosheng Ji

Ciclo XXIII

Il Coordinatore del Corso di Dottorato

Ch.mo Prof. Raffaele MOLINARI

A.A. 2009-2010

INDEX

Summary 5

Sommario 8

CHAPTER ONE 11

Membrane Desalination 11

1.1 Desalination 11
1.2 Desalination market 12
1.3 Desalination technology 14
1.4 Membrane technology market 15
1.5 Reverse Osmosis 16
1.6 Limited of reverse osmosis 18
1.7 Potential of Membrane Distillation in Desalination 20
1.8 Principles of Membrane Distillation 22
1.9 Membrane Distillation Materials 23
References: 25

CHAPTER TWO 28

Membrane Distillation 28

2.1 Theoretical 28
2.2 Driving Force and Vapour-Liquid Equilibrium 28
2.3 Heat transfer 29
2.3.1 Heat transfer in boundary layers 31
2.3.2 Heat transfer across membrane 32
2.4 Mass transfer 34
2.4.1 Mass transfer in the boundary layers 34
2.4.2 Mass transfer across the membrane 35
References: 40

CHAPTER THREE 42

Membrane Fouling 42

3.1 Introduction 42
3.1.1 Particulate and colloidal fouling (Suspended Solids) 43
3.1.2 Scaling 44
3.1.3 Organic fouling 48
3.1.4 Microbial fouling / Biofouling 50
3.2 Fouling in Membrane Distillation 51
3.2.1 Scaling in MD 51
3.2.2 Natural organic matter (NOM) fouling 53
3.2.3 Biological fouling in MD 54

3.2.4 Wetting and cleaning 55
References: 57

CHAPTER FOUR 59

Experimental Activity on CaCO3 Scaling in Presence of Humic Acid 59

4.1 Introduction 59
4.2 Theory of CaCO3 scaling 60
4.3 Materials and methods 61
4.4 Results and discussion 64
4.5 Conclusions 73
References: 75
Appendix A 78

CHAPTER FIVE 81

The effect of sulfate in Nanofiltration-Membrane Crystallization system 81

5.1 Introduction 81
5.2 Materials and Methods 82
5.3 Results and discussion 84
5.4 Economical aspects 91
5.5 Conclusions 91
References: 92

CHAPTER SIX 94

Membrane Bioreactor For Water Treatment 94

6.1 Introduction 94
6.2 Compare MBR with CAS 94
6.3 MBR configuration 97
6.4 Membrane materials and modules 99
6.5 MBR Market Overview 99
6.6 Challenges for developing MBR technology 100
6.7 Objective 101
References: 102

CHAPTER SEVEN 103

Removal of the Organic matter by Submerged Ultrafiltration 103

7.1 Introduction 103
7.2 Materials and methods 104
7.3 Results and Discussions 107
7.4 Conclusions 118
References: 120

CHAPTER EIGHT 123

Membrane Distillation /Crystallization of Reverse Osmosis brines 123

8.1 Introduction 123

8.2 Theory 124
8.3 Materials and methods 126
8.4 Results and discussion 129
8.5 Conclusions 138
References: 139
CONCLUSIONS 142

Summary

The scarcity of fresh water is considered of vital importance by civil, industrial, and agricultural sectors nowadays. Pollution and exploitation of groundwater aquifers and surface water have led to a decrease in quantity and quality of available natural water resources in many regions. In addition, higher living standards, especially in industrial countries, result in higher per capita water consumption and intensified water scarcity. To solve these problems, some strategies could be used, such as sustainable water resources management, wastewater treatment and desalination technologies.

Membrane distillation (MD) is a thermal membrane separation process that involves transport of vapor through microporous hydrophobic membranes and operated on the principle of vapor-liquid equilibrium. The driving force of the process is supplied by the vapor pressure difference caused by temperature gradient imposed among the liquid-vapor interfaces. In particular, the MD process has many advantages over conventional desalination processes such as multi-stage flash (MSF), reverse osmosis (RO), and multiple effect distillation (MED). The advantages of MD compared with these processes are as follows:

(1) Lower operating temperature and vapor space required than MSF and MED.

(2) Lower operating pressure than RO.

(3) 100% (theoretical) rejection of non-volatile solute.

(4) Performance not limited by high osmotic pressure or concentration polarization.

Membrane fouling is a major obstacle for efficient use of membrane technology for natural waters treatment, and increases the use of cleaning chemicals (consequently introducing a waste problem), ultimately shortens membrane life. Membrane fouling is mostly due to specific adsorption, gel layer formation and membrane pore plugging. Gel or cake layer formation may be caused by a variety of particulate substances including inorganic precipitates such as $CaCO_3$, $CaSO_4$, and several metal hydroxides, organic materials such as proteins, natural organic matter (NOM), colloids, humic acids and other macromolecular materials, and biological components such as micro-organisms and products of their metabolism. All of these components are

present, in various extents, into seawater.

The results of experimental research emphasise the significant role played by microporous membranes in the heterogeneous nucleation mechanisms that control scaling in Membrane Distillation. For better understanding the complex phenomena of inorganic fouling, supersaturation, morphological and physicochemical properties of the membrane should be considered carefully. Supersaturation is mainly decided by the chemistry of the solutions and partially affected by concentration polarization phenomena. Induction times, determined by DLS measurements, will be significantly reduced if precipitation occurs in presence of membranes, thus $CaCO_3$ nucleation process will be accelerated.

DCMD tests, carried out on a semi-pilot plant for 35 h, demonstrated that scaling significantly reduced the transmembrane permeate flux by 33 %. With the help of humic acid at low concentration, the nucleation and growing rate of vaterite crystals were retarded, and supersaturation was also reduced. Besides, $CaCO_3$ deposition on the membrane surface (exacerbated at high ionic strength) also contributed – with minor extent with respect to scaling - to the decrease in the system performance.

Membrane Bioreactor (MBR), a compact-built purification system, combines the biological degradation step and the membrane separation step. Firstly, the influent is feed to the bio-reactor where the organic components are oxidized by the activated sludge at the same time. Then, the aqueous activated sludge solution passes through a membrane filtration unit and consequently the water is separated from the sludge. Finally, the sludge returns to the bio-reactor, while the permeate is discharged or re-used as particle-free effluent.

At the sole filtration stage, on the purpose of reducing flux value, TOC could be removed up to 63 % by using 70 kDa MWCO membrane, although polarization phenomena was in favor of the decrease in TOC rejection for higher trans-membrane fluxes. For this reason, removing TOC increased the overall efficiency of the proposed system by stimulating biodegradation before membrane filtration.

The study confirmed the ability of MDC to extremely concentrate RO brines which achieved a total water recovery factor above 90 % and an analogous volumetric

reduction of the waste to be discharged. Transmembrane fluxes in the order of 10^{-4} kg $m^{-2}s^{-1}$ reduced concentration polarization on membrane surface where heterogeneous nucleation took place. The possibility of preventing encrustations or irremovable deposits of solids due to uncontrolled supersaturation was recognized as a crucial task in order to achieve long-term stability of MDC.

All these results outline the potential impact of MDC on the economical and environmental aspects of membrane desalination industry, and more research efforts in this field should be encouraged.

Sommario

La scarsità di acqua dolce è considerata, al giorno d'oggi, di vitale importanza per i settori civile, industriale, agricolo.L'inquinamento e lo sfruttamento delle falde acquifere sotterranee e di superficie hanno portato a una diminuzione della quantità e qualità delle risorse idriche naturali disponibili in molte regioni. Inoltre, gli standard di vita più elevati, soprattutto nei paesi industriali, provocano un aumento dei consumi pro capite di acqua e intensificato la scarsità d'acqua. Per risolvere questi problemi, alcune strategie potrebbero essere utilizzate, come la gestione sostenibile delle risorse idriche, trattamento delle acque reflue e le tecnologie di dissalazione.

La distillazione a membrana (MD) è un processo di separazione termica a membrana che comporta il trasporto di vapore attraverso membrane microporose idrofobiche ed è gestito secondo il principio di equilibrio liquido-vapore. La forza motrice del processo è fornita dalla differenza di pressione di vapore causata dal gradiente di temperatura imposto tra le interfacce liquido-vapore. In particolare, il processo di MD ha molti vantaggi rispetto aitradizionali processi di dissalazione, come flash multi-stadio (MSF), osmosi inversa (RO), e distillazione effetto multiplo (MED). I vantaggi di MD rispetto a questi processi sono i seguenti:

(1) bassa temperatura di esercizio e ridotto spazio necessario a vapore MSF e MED.

(2) pressione di esercizio inferiore rispetto RO.

(3) 100% (teorico) la reiezione del soluto non volatile.

(4) Le prestazioni non limitate dalla alta pressione osmotica o dagli effetti di polarizzazione per concentrazione.

L'intasamento delle membrane è uno dei principali ostacoli per un uso efficiente delle tecnologie a membrana per il trattamento naturale delle acque, e aumenta l'uso di prodotti chimici di pulizia (di conseguenza l'introduzione di un problema dei rifiuti), riducendo, in ultima analisi, la vita della membrana. Il fouling delle membrane è dovuto principalmente all' adsorbimento specifico, alla formazione di strato di gel e tamponamento dei pori della membrana. La formazione di strati di gel o di torta può essere causato da una varietà di sostanze tra cui il particolato di precipitati inorganici

come $CaCO_3$, $CaSO_4$, e idrossidi di metalli diversi, materiali organici come proteine, la materia organica naturale (NOM), colloidi, acidi umici e altri materiali macromolecolari, e dei componenti biologici come microrganismi e prodotti del loro metabolismo. Tutte queste componenti sono presenti, in varia misura, nell' acqua di mare.

I risultati della ricerca sperimentale hanno teso a sottolineare il ruolo significativo svolto da membrane microporose nei meccanismi di nucleazione eterogenea che controllano the scaling nella distillazione a membrana. Per una migliore comprensione dei complessi fenomeni di sporcamento inorganico, sovrasaturazione, proprietà morfologiche e fisico-chimiche della membrana devono essere considerate con attenzione. La sovrasaturazione è principalmente controllata dalla chimica delle soluzioni e in parte influenzata da fenomeni di polarizzazione per concentrazione. I tempi di induzione, determinati mediante misurazioni DLS, saranno notevolmente ridotti se la precipitazione si verifica in presenza di membrane, quindi il processo di nucleazione $CaCO_3$ sarà accelerato.

Le prove DCMD, effettuate su un impianto semi-pilota per 35 h, hanno dimostrato che lo scaling ha ridotto significativamente al 33% il flusso transmembrana permeato Con l'aiuto di acidi umici a bassa concentrazione, la nucleazione e la velocità di crescita dei cristalli di vaterite sono stati ritardati, e la sovrasaturazione è stato anche ridotta. Inoltre, la deposizione di $CaCO_3$ sulla superficie della membrana (aggravato ad alta forza ionica) ha contribuito anche - con misura minore rispetto alla rappresentazione in scala - alla diminuzione delle prestazioni del sistema.

Un bioreattore a membrana (MBR), che è un sistema di depurazione compatto , combina la fase di degradazione biologica e la fase di separazione a membrana. In primo luogo, è l'affluente è alimentato al bio-reattore in cui vengono ossidati i componenti organici del fango attivo. Quindi, la soluzione acquosa a fanghi attivi passa attraverso un gruppo di filtrazione a membrana e di conseguenza l'acqua viene separata dal fango. Infine, i fanghi vengono riciclati al bio-reattore, mentre il permeato viene scaricato o riutilizzato come effluente priva di particelle.

Nella fase di filtrazione, al fine di ridurre il valore del flusso, TOC potrebbe essere

rimosso fino al 63% con una membrana 70 kDa MWCO, anche se i fenomeni di polarizzazione favore sono favoriti da maggiori flussi transmembrana Per questo motivo, la rimozione di TOC aumentata l'efficienza complessiva del sistema proposto, stimolando la biodegradazione prima della filtrazione a membrana.

Lo studio ha confermato la capacità di MDC di concentrare brine per un fattore di recupero di acqua superiore al 90% e una riduzione analoga volumetrica dei rifiuti da scaricare. I flussi transmembrana nell' ordine di 10^{-4} kg $m^{-2}s^{-1}$ riducono la polarizzazioneper concentrazione sulla superficie della membrana in cui la nucleazione eterogenea ha avuto luogo. La possibilità di prevenire incrostazioni o depositi inamovibili dei solidi a causa di supersaturazione incontrollata è stato riconosciuta come un compito cruciale per il raggiungimento di una stabilità a lungo termine di MDC.

Tutti questi risultati delineano l'impatto potenziale di MDC sugli aspetti economici e ambientali del settore dissalazione a membrana, maggiori sforzi di dovrebbero essere concentrati su questo filone di ricerca..

CHAPTER ONE

Membrane Desalination

1.1 Desalination

In recent years, the scarcity of fresh water has been considered as a primary issue by civil, industrial, and agricultural sectors. Water scarcity, which occurs not only in arid regions, may be caused by mismatch between water supply and water demand: Pollution and exploitation of groundwater aquifers and surface water have led to the decrease in quantity and quality of available natural water resources in many regions. The ongoing growth of population, industry and agriculture further increases water demand. In addition, higher living standards, especially in industrial countries, result in higher per capita water consumption and intensified water scarcity. To overcome these obstacles, researchers are seeking some strategies such as sustainable water resources management, wastewater treatment and desalination technologies, etc [1].

Take China as an example, the total volume of water resource is 21,812.4 billion m^3 (occupying the 6th place in the world), nevertheless the per-capita water resource volume is only 1/4 of that of the world average and serious summer drought conditions tend to occur in the northwest so much so that it is classified as one of the most poorest water shortage countries in the world. In more than 300 cities, water shortage has already become a serious problem, especially in the northern coastal area and several islands (like Tianjin, Beijing, Hebei, Shandong, Henan, Shanxi, Liaoning, Ningxia, etc).The coastal area occupies about 15 % of the whole country, has a coastline longer than 18,000 km, over 6,500 islands and population accounting for more than 40 % of the whole country, and is also the most developed economical area in China. Water shortage has already become the bottleneck on development of social progress and economy [2].

On the other hand, a low contamination use such as cooling water taken from rivers, which contributes highly to water abstraction figures in some countries such as China and India, may create much less water stress than agricultural or urban use.

Frequently, part of the water is less accessible or of lower quality. As soon as the convenient water resources are utilized, a hard competition for water arises between agriculture, industry and the public water users. This competition may lead to higher water prices, constricted economic development and social problems in regions with limited water access. As a result, the general welfare of a country under water stress conditions is threatened. Exploitation of natural fresh water resources combined with higher water demand has led to an increased demand for alternative fresh water resources. Since about 97.5 % of the water is present as oceans on the earth, desalination will unavoidably become a feasible method in the next decades. Desalination provides such an alternative source, offering water otherwise not accessible for irrigational, industrial and municipal use [1].

1.2 Desalination market

There are desalination facilities in more than 100 countries, especially in those oil-rich, water-poor countries in the Middle East, like Saudi Arabia, the United Arab Emirates and Kuwait. The continued proliferation of desalination facilities has built up a global market with more than $8 billion, with continued rapid growth rate. Two-thirds of the world's desalination plants are located in Gulf Cooperation Council (GCC) countries [3].

Desalination markets have expanded in the last decades. The global market for desalinating seawater and brackish water to generate new supplies of potable water will grow at a compound annual growth rate of 9.5 % over the next 10 years, effectively tripling the market in size to reach a capacity of 54 billion cu meters per year.

The market with the greatest installed capacity is the Gulf Region (Middle East), where low cost of fossil fuel led to preferred application of thermal desalination processes. The Mediterranean market follows, ahead of the American and Asian markets. The Gulf region will continue to be the greatest market for new desalination equipment because of a rapid growth in population and necessary replacement of

over-aged plants. A doubling in capacity until 2015 is expected. The countries around the Mediterranean Sea will experience the largest growth rate with a smaller expansion expected in Asia until 2015.

Asia will become a fast growing market in the long run, due to its enormous population and economic growth that will most likely lead to a water demand that cannot be satisfied with conventional water sources. According to the industrial tracking and survey results by Desalination Association of China in 2008, 56 seawater desalination plants were established in China till December in 2008 the total capacity is 276,100 m^3/d. The gross desalination productivity in China has reached 295,000 m^3/d, increased by 46 % compared with that in 2007. Moreover, the productivity of programs under construction has reached to 268,000 m^3/d, in which 82,500 m^3/d is in bidding progress or conceptual design. Productivity of desalination programs on plan in China has reached 200,000 m^3/d.

A survey has been carried out of 46 desalination plants in Australia that have capacities greater than 10 kL/day. Operating plants, all except one utilising reverse osmosis (RO) as the desalination process, have a total output of 294 ML/day, while the outputs for plants under construction amount to 976 ML/day, and for proposed plants 925 ML/day. The total current desalted water usage is 153 ML/day for potable supplies and 141 ML/day for industrial purposes. By the year 2013 this will amount to 1,734 ML/day for potable and 461 ML/day for industrial supplies. The most dramatic increase is occurring in the major cities where the installed production capacity of seawater desalination will increase tenfold from 45 GL/year in 2006 to over 450 GL/year by 2013 [4].

The largest growth market will be the Mediterranean Rim, where Algeria, Libya, and Israel are anticipating capacity increases in excess of 300 %. With desalination back on the political agenda in Spain, the total increase in capacity in the Mediterranean region will be 179 %. For example, in Mallorca, desalination capacities expanded from 450,000 m^3/y to 17,210,000 m^3/y [5].

1.3 Desalination technology

Desalination processes were developed to obtain fresh water from the seawater. Desalination technologies can be classified into thermal and membrane based desalination by separation mechanism. Tradition desalination processes are mainly thermal based, including multi stage flash (MSF), multi effect evaporation (MEE) / multi effect distillation (MED), vapor compression (VC) and solar desalination. Membrane based separation processes include reverses osmosis (RO) and electro-dialysis (ED).

Thermal desalination separates salt from water by evaporation and condensation, whereas in membrane desalination water diffuses through a membrane, while salts are almost completely retained. An overview of available desalination techniques is given in Table 1.1.

Table 1.1 Applied desalination technologies

Thermal desalination technologies	Membrane desalination technologies
Multi-stage flash distillation (MSF)	Reverse osmosis (RO)
Multi-effect distillation (MED)	Nanofiltration (NF)
Vapour compression distillation (VCD)	Electrodialysis (ED)

Among these available technologies, MSF distillation and RO dominate the existing plants. Multi-stage flash distillation (MSF) is the most frequently applied and still preferred in the Middle East. Reverse osmosis is the most common membrane based desalination option in seawater and brackish water desalination, dominating in the area around Mediterranean Sea.

Thermal desalination is more energy intensive than membrane based desalination, but can better deal with more saline water and deliver even higher permeate quality. Table 1.2 demonstrates the differences in key operational data between thermal and membrane desalination technologies. Energy consumption of reverse osmosis is the lowest among all options for seawater desalination, making it most cost efficient in

regions with high energy cost. Especially in brackish water desalination, reverse osmosis offers great advantages over thermal desalination technologies due to its much lower energy consumption at low salt concentration. The variable cost of thermal desalination plants are almost independent of feed water salinity, while membrane process variable cost is nearly proportional to the feed water salinity and therefore lower in brackish water than in seawater desalination, making reverse osmosis and electrodialysis the most economic processes. For all desalination technologies, costs have steadily decreased in the last decades. Generally, thermal desalination is more cost intensive than reverse osmosis desalination. Comparing the thermal separation processes, the advantages of Membrane technology are operational simplicity, good compatibility and synergy between different membrane operations in integrated systems, low energetic requirements, good stability under a wide range of operative conditions, high eco-compatibility, easy control and scale-up, large flexibility. All these specialties make membrane technology as a powerful tool in the logic of the process intensification.

Table 1.2 Key operational data of thermal and membrane desalination technologies [5]

	MSF	RO	Electrodialysis
Thermal energy consumption [kWh/m^3]	12	0	0
Electrical energy [kWh/m^3]	35	0.4	–7 1
Typical salt content of raw water	30,000–100,000	1,000–45,000	100–3,000
Product water quality (ppm TDS)	<10	<500	<500

1.4 Membrane technology market

The application of membrane desalination in seawater desalination has substantially increased in the last 30 years. The reverse osmosis membrane market is expanding at an annual rate in excess of 8% fueled by the intensifying worldwide water shortage and the need to preserve water resources from environmental

perspective. Today, more than 2,000 reverse osmosis (RO) installations are being operated worldwide, with an overall production higher than 800 MGD. The total worldwide market for RO membrane system was worth of 670 billion won as of 2008 and is growing at 10.3 % annually [6].

1.5 Reverse Osmosis

Reverse Osmosis is by far the most widespread type of membrane desalination process. It is capable of rejecting nearly all colloidal or dissolved matter from an aqueous solution, producing the brine and the permeation which consists of almost pure water.

Reverse Osmosis is a (differential) pressure driven separation technique. The membrane of Reverse Osmosis is based on a property of certain polymers called semi-permeability. By applying a pressure difference, the permeating component(s), in most applications nearly exclusively water, are forced through the membrane. In order to overcome the feed side osmotic pressure, fairly high feed pressure is required. In seawater desalination it commonly ranges from 55 to 68 bars. Operating pressures for the purification of brackish water are lower due to the lower osmotic pressure caused by lower feed water salinity. Besides its application for production of drinking water, reverse osmosis is also applied in the treatment of effluent water and separation of organic and inorganic compounds from aqueous solution for industrial applications. Although Reverse Osmosis has also been used to concentrate organic substances, its most frequent use lies in seawater desalination applications.

The Reverse Osmosis desalination plant process includes seven stages [7], they are: water abstraction, pre-treatment, pumping system, membrane separation unit, energy recovery system, post-treatment and control-system (see Figure 1.3 and Figure1.4).

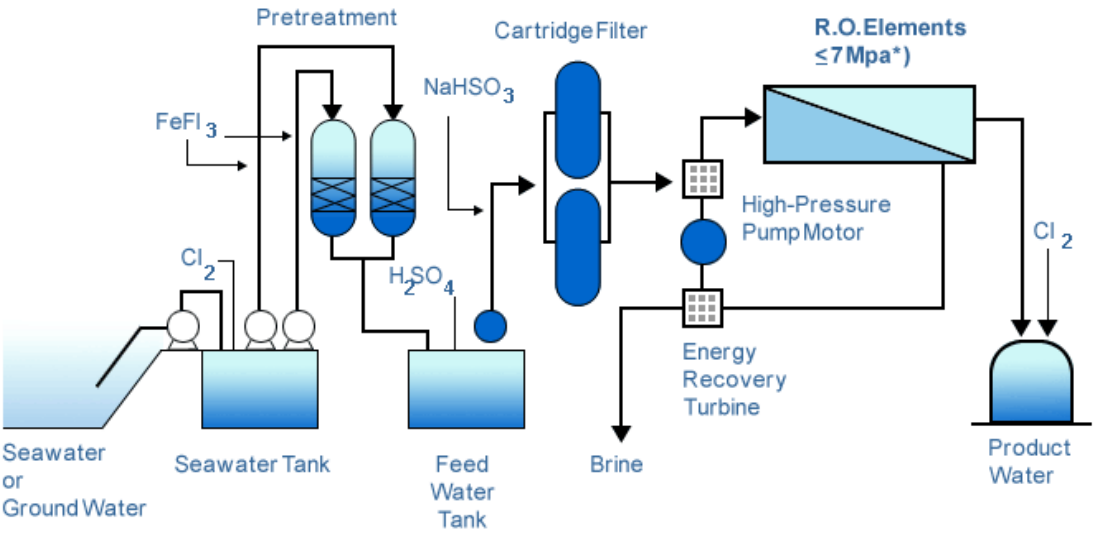

Figure 1.3 Reverse Osmosis treatment process

Figure 1.4 Existing RO Plant [8]

In fact, pressure-driven membranes such as microfiltration (MF) and ultrafiltration (UF) are the new trends in designing the pretreatment systems for desalination plants and they can be used as a substitute for the conventional pretreatment technologies. MF can remove suspended solids and lower the silt density index (SDI) while in UF, not only suspended solids and large bacteria are retained, but also (dissolved) macromolecules, colloids and small bacteria. MF and UF pretreatment leaded to a better control of membrane biofouling, increased the membrane lifetime, and limited

the cleaning frequency of the plant. Furthermore, permeate fluxes measured at the successive high-pressure membrane filtration unit increase up to 30 %, thus resulting in higher reliability and better overall economics of the desalination system. In RO desalination, the capital and operating costs are the major drivers for process selection and due to relatively low water recovery in RO plants, any cost saving incurred in the pretreatment system will strongly affect the cost of water produced. Actually, the MF/UF was predicted to contribute for about 10 % reduction in the total water cost [9]. It has been reported that a reduction of 39 % in the operating and maintenance costs can be achieved when replacing the conventional pretreatment with MF or UF. Besides, the elimination of flocculation, recarbonation and filtration steps will decrease the power and chemical costs and reduce the plant space which leads to a significant reduction in the plant capital costs [10].

Moreover, nanofiltration (NF) is today used in softening, disinfection, and removal of organic materials and metals. The installation of NF as a pretreatment will lead to a breakthrough in the application of RO due to its capability of effectively removing dissolved organic compounds, scale forming hardness ions, and bivalent ions. As consequence, the osmotic pressure of RO feed and retentate streams is decreased, thus allowing the system to be operated at high water recovery factors (70 %) with minor scaling problems [11]. At this stage, the integrated pressure-driven membrane (MF/UF-NF-RO) system is characterized by global water recovery factors up to 50 %, energy saving of 25-30 %, less consumption of chemicals and additives, smaller land space, and less amount of discharged wastes [12, 13].

1.6 Limited of reverse osmosis

Currently, reverse osmosis (RO) is one of the most prevalent technologies for seawater desalination. Although the utilization of RO, also in combination with other pressure driven membrane operations such as microfiltration (MF), ultra-filtration (UF) and nano-filtration (NF) as pre-treatment to the RO stage, has led fundamental contribution in terms of overall process economics, one of the main problems still

open is the management of the salts concentrates. Recovery rates in brackish water reverse osmosis (BWRO) applications are limited by the risk of scale precipitation and are typically in the range of 75 %–80 %. In seawater reverse osmosis systems (SWRO) recovery rates may at most reach 60 % due to limited feed pressure and increased energy consumption at elevated salt concentrations. Feed pressure typically reaches 55-65 bars in SWRO and BWRO desalination uses moderate feed pressures of 10–15 bars. This would result in a significant residue of high concentrated solutions to be disposed-off. At present, the most frequent disposal practice for brines is a direct discharge into lakes, lagoons, rivers, ocean and sanitary sewer. Because disposal options are limited, disposal is associated with high additional costs and environmental damage has to be expected.

However, the promulgation of more and more stringent environmental protection regulations will preclude this low-cost possibility in the near future. In the last years, several process engineering strategies have been implemented in order to accomplish the concept of ‘zero-liquid’ or ‘quasi-zero-liquid’ discharge in seawater reverse osmosis desalination. Delivery of fresh water from seawater desalination plants demands piping and pumping systems to transport product water from coastal regions to residential areas, which increase cost. High availability of brackish water in residential areas makes expensive deli piping and pumping unnecessary. In this context, membrane contactors (MCs) technology is expected to offer alternative design-pathways for brine management [14].

Another crucial drawback of RO membranes is their weakness against fouling due to the presence of colloidal, particulate, dissolved organics and inorganic matter in feed water, as well as biological growth in the RO system. Therefore, it is required to install a pretreatment step for the feed water before going to the RO unit. The conventional pre-treatment were based on mechanical treatment (media filters, cartridge filters) followed by extensive chemical treatment like flocculation, coagulation, acid treatment and disinfection. The main problems in using the conventional pretreatment is that it does not represent a complete barrier to colloids and suspended particles and produces unsteady feed water quality and quantity. In

addition, this pretreatment is known to be complex, labor intensive and space consuming. Furthermore, it consumes large amount of chemicals which are used for coagulant dosages to provide surface charge neutralization, chlorination to limit biological growth, and flocculation-sedimentation sequences.

1.7 Potential of Membrane Distillation in Desalination

Membrane distillation (MD) is a methodology having a great potential as concentration process carried out at low temperature. MD is not affected by concentration polarization phenomenon, whereas it represents the critical limit for pressure driving processes such as NF or RO. Production of high purity distillate, absence of limitation caused by fouling, lower energy consumption with respect to conventional evaporation or distillation operations are additional advantages of this technique, especially when coupled with solar energy or utilizing low-grade heat source [15-17]. MD systems powered by solar energy have been shown cost competitive with reverse osmosis in remote areas [18, 19].

In 2004, researchers at the University of Texas at El Paso (UTEP) in collaboration with the Swedish firm SCARAB DEVELOPMENT AB studied methods coupling solar pond technology with desalination to create a zero discharge system, and MD was one of the technologies that were investigated as part of the zero discharge concepts [20, 21]. Moreover, when combine MSF and MED modes into one air gap membrane distillation module. The process promised to decrease desalination costs to 0.26 $/m^3**,** using low-grade waste steam or heat as driving force. For comparison, the unit cost of water produced by conventional thermal desalination is around 1.00 $/m^3 for MED and 1.40 $/m^3 for MSF, while it is around 0.5 $/m^3 for RO [22-24].

The Configurations of MD integrated pressure-driven membranes system is illustrated in Figure 1.5:

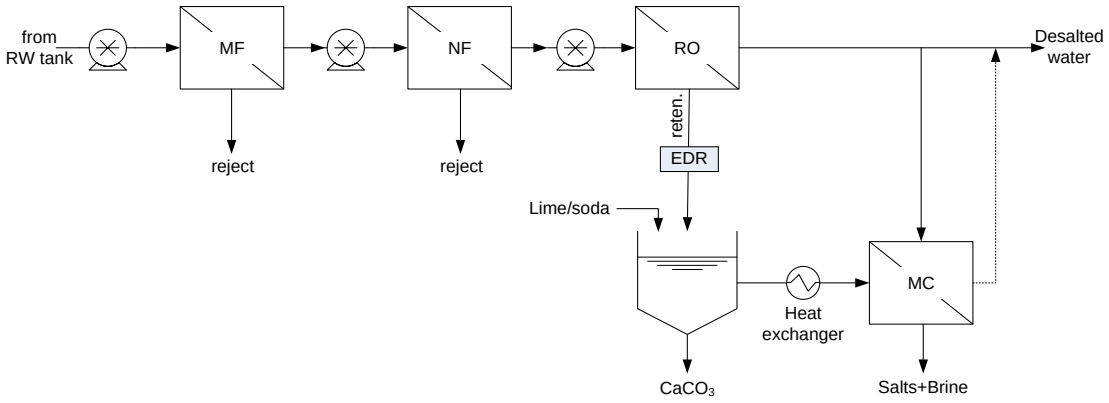

Figure 1.5 MD integrated pressure-driven membranes system

Configurations of MD integrated pressure-driven membranes system are summarized in Table.1.6. It demonstrated that integrated membrane system will offer essential improvements in efficiency, water cost and environmental impact. The total water cost decreased as the water recovery was increased due to the fact that smaller intake/discharge facilities and lower membrane surface area were required since higher flux values were obtained at higher recoveries.

Table 1.6 Several integrated membranes systems

	RO	MF— NF— RO MC	MF— NF— RO MC	MF— NF— RO MC MD	MF— NF— RO MC MC
Water recovery	45%	71.9%	70.6%	88.4%	92.4%
Brine reduction	0	48.5%	45.6%	79.2%	86.4%
Improvement of Permeate quality	0	47.7%	46.4%	57.7%	59.5%
Water cost ($/m^3)	0.50-0.70	0.64	0.56	0.71	0.69

Membrane distillation (MD) is a thermal membrane separation process that involves transport of vapor through microporous hydrophobic membranes and operated on the principle of vapor-liquid equilibrium as a basis for molecular separation. The driving force of the process is supplied by the vapor pressure difference caused by temperature gradient imposed between the liquid-vapor

interfaces. In particular, the MD process can be used as a substitute for conventional desalination processes such as multi-stage flash (MSF), reverse osmosis (RO), and multiple effect distillation (MED). The advantages of MD compared with these processes are as follows:

(1) lower operating temperatures and vapor space required than MSF and MED；

(2) lower operating pressure than RO；

(3) 100 % (theoretical) rejection of non-volatile solute；

(4) performance not limited by high osmotic pressure or concentration polarization.

Since MD is a thermally driven process, operating pressures are generally on the order of zero to a few hundred kPa, relatively low compared to pressure driven processes RO. Lower operating pressures translate to lower equipment costs and increased process safety. Another benefit of MD stems from its efficiency in terms of solute rejection. Since MD operates on the principles of vapor-liquid equilibrium, 100 % (theoretical) of ions, macromolecules, colloids, cells, and other non-volatile constituents are rejected; RO is not to achieve such high levels of rejection. When applied to desalination, a well designed MD system typically achieves water fluxes as high as 75 kg/m^2/h, which is comparable to RO. Since MD operates at pressures significantly lower than those encountered in the pressure-driven processes, the mechanical demands on these micro-porous membranes is greatly reduced.

1.8Principles of Membrane Distillation

MD processes have several configurations depending on the way by which the vapor is recovered in the permeate side. In general, MD systems may be classified into four different categories as follows [25–31]:

(1) An aqueous solution colder than the feed solution is maintained in direct contact with the permeate side of the membrane giving rise to the configuration known as direct contact membrane distillation (DCMD). The transmembrane temperature difference induces a vapor pressure difference. Consequently, volatile molecules evaporate at the hot liquid/ vapor interface, cross the membrane in vapor phase and

condense in the cold liquid/vapor interface inside the membrane module.

(2) A stagnant air gap is interposed between the membrane and a condensation surface. In this case, the evaporated volatile molecules cross both the membrane pores and the air gap to finally condense over a cold surface inside the membrane module. This MD configuration is called air gap membrane distillation (AGMD).

(3) A cold inert gas sweeps the permeate side of the membrane carrying the vapor molecules and condensation takes place outside the membrane module. This type of configuration is termed sweeping gas membrane distillation (SGMD).

(4)Vacuum is applied in the permeate side of the membrane module by means of a vacuum pump. The applied vacuum pressure is lower than the saturation pressure of volatile molecules to be separated from the feed solution. In this case, condensation occurs outside of the membrane module. This MD configuration is termed vacuum membrane distillation (VMD).

Among the other MD configurations DCMD is simplest to operate - does not require vacuum pump as in vacuum membrane distillation (VMD), nor condenser as in sweep gas membrane distillation (SGMD) or cooling surface as in air gap membrane distillation (AGMD) - and the distillation process can be carried out in any desired membrane configuration (flat sheet, spiral wound, capillaries or hollow fibers). Thus, DCMD can be conveniently applied for investigations in which water is the major fluxing component, such as in desalination [32–35].

1.9 Membrane Distillation Materials

The main requirements for MD process are that the membrane must not be wetted and only vapor and noncondensable gases are present within its pores. The pores size of the membranes used in MD lies between 10 nm and 1um. To avoid pore wettability, the membrane material must be hydrophobic with high water contact angle and small maximum pore size. Hydrophobic microporous membranes such as those made from polypropylene (PP), polyethylene (PE), polytetrafluoroethylene (PTFE), and polyvinylidene fluoride (PVDF) meets these requirements. However pore wettability

may occur and permeate quality may be affected if solutions with surface active components are brought in direct contact with the membrane surface or if the transmembrane hydrostatic pressure exceeds the liquid entry pressure (LEP), which is characteristic of each membrane. MD is therefore, a process mainly suited for applications in which the major component is water [36].

References:

[1] E. El-Zanati, K.M. El-Khatib. Integrated membrane based desalination system. Desalination, 2007, 205: 15.

[2] Congjie Gao, Jia Xu. Development of seawater desalination technology in China. EU-CHINA WORKSHOP 2009.

[3] Water desalination report, 2008. IDA Desalination Year Book 2007-2008.

[4] Manh Hoang, Brian Bolto, Carolyn Haskard, Olga Barron, Stephen Gray, Greg Leslie. Desalination in Australia report 2009.

[5] C. Fritzmann, J. Löwenberg, T. Wintgens and T. Melin. Desalination, 2007, 216 (1-3, 5): 1-76.

[6] Membrane Separation Technologies 2009, Global Industry Analysts, Inc.

[7] www.biosystemsasia.com

[8] www.ci.wellington.fl.us/html/Departments/Util.

[9] M. Wilf and M.K. Schierach. Improved performance and cost reduction of RO sweater systems using UF pretreatment. Desalination, 2001, 135: 61.

[10] G.L. Leslie et al., Proc. AWWA. Water Reuse Conference, Florida, 1998.

[11] N. Hilal et al. A comprehensive review of nanofiltration membranes: treatment, pretreatment modeling, and atomic force microscopy. Desalination, 2004, 170: 281.

[12] M.M. Nederlof, J.C. Kruithof, J.S. Taylor, D. van der Kooij and J.C. Schippers. Comparison of NF/RO membrane performance in integrated membrane systems. Desalination, 2000, 131: 257.

[13] E. Drioli, A. Criscuoli, E. Curcio. Integrated membrane operations for seawater desalination. Desalination, 2002, 147: 77.

[14] E. Curcio, E. Drioli. Membrane distillation and related operations. Separation & Purification Reviews, 2005, 34: 35.

[15] F. Banat, R. Jumah and M. Garaibeh. Exploitation of solar energy collected by solar stills for desalination by membrane distillation. Renewable Energy, 2002, 25: 293.

[16] Z. Ding, L. Liu, M.S. El-Bourawi and R. Ma. Analysis of a solar-powered membrane distillation system. Desalination, 2005, 172: 27.

[17] J. Koschikowski, M. Wieghaus and M. Rommel. Solar thermal-driven desalination plants based on membrane distillation. Desalination, 2003, 156: 295.

[18] G.L. Morrison, Sudjito, A.G. Fane and P, Hogan. Solar heated membrane distillation, Proc. of the Biennial Congr.of the Int. Solar Energy Soc., Sydney, Australia, Pergamon, 1992: 2329-2334.

[19] P.A. Hogan, Sudjito, A.G. Fane and G.L. Morrison. Desalination by solar heated membrane distillation. Desalination, 1991, 81: 81-90.

[20] www.scarab.se

[21] J. Walton, H. Lu, C. Turner, S. Solis and H. Hein. Solar and waste heat desalination by membrane distillation. 98-FC-81-0048, DWPR n. 81, El Paso TX, 2004.

[22] J.H. Hanemaaijer, J. van Medevoort, A.E. Jansen, C. Dotremont and E. van Sonsbeek. Memstill membrane distillation - a future desalination. Desalination, 2006, 199: 175.

[23] B. Van der Bruggen. Desalination by distillation and by reverse osmosis – trends towards the future. Membrane Technology, February/2 (2003) 6.

[24] C. Fritzmann, J. Löwenberg, T. Wintgens and T. Melin. State-of-the-art of reverse osmosis desalination. Desalination, 2007, 216: 1.

[25] K.W. Lawson, D.R. Lloyd. Membrane distillation. J. Membrane Sci., 1997, 124: 1-25.

[26] J.I. Mengual, L. Pe˜na. Membrane distillation. Colloid Interf. Sci., 1997, 1: 17-29.

[27] R.W. Schofield, A.G. Fane, C.J.D. Fell. Heat and mass transfer in membrane distillation. J. Membrane Sci., 1987, 33: 299–313.

[28] M. Khayet, M.P. Godino, J.I. Mengual. Theory and experiments on sweeping gas membrane distillation. J. Membrane Sci., 2000, 165: 261-272.

[29] F.A. Banat, J. Simandl. Theoretical and experimental study in membrane distillation. Desalination, 1994, 95: 39-52.

[30] S. Bandini, C. Gostoli, G.C. Sarti. Separation efficiency in vacuum membrane distillation. J. Membrane Sci., 1992, 73: 217-229.

[31] S. Kimura, S.I. Nakao, S.I. Shimatani. Transport phenomena in membrane distillation. J. Membrane Sci., 1987, 33 (3): 285–298.

[32] K.W. Lawson and D.R. Lloyd. Membrane distillation. II. Direct contact membrane distillation. J. Membrane Sci., 1996, 120: 123.

[33] B. Li and K.K. Sirkar. Novel membrane and device for direct contact membrane distillation-based desalination processes. Ind. Eng. Chem. Res., 2004, 43: 5300.

[34] L. Martínez-Díez, M. I. Vázquez-González, F. J. Florido-Díaz. Study of membrane distillation using channel spacers. J. Membrane Sci. 1998, 144: 45.

[35] E. Drioli, E. Curcio, A. Criscuoli, G. Di Profio. Integrated system for recovery of $CaCO_3$, NaCl and $MgSO_4 \cdot 7H_2O$ from nanofiltration retentate. J. Membrane Sci., 2004, 239: 27.

[36] A. Gabelman and S.-T. Hwang. Hollow fiber membrane contactors. J. Membrane Sci., 1999, 159: 61.

CHAPTER TWO

Membrane Distillation

2.1 Theoretical

In MD, mass transfer of water vapor through a micro-porous hydrophobic membrane coupled with heat transfer through the membrane and heat transfer to and from the membrane surfaces. The separation process in MD is characterized by both simultaneous heat and mass transfer, since mass (vapor) transport through membrane pores occurs as a result of the difference in temperature and composition between the feed and the permeate.

2.2 Driving Force and Vapour-Liquid Equilibrium

For small changes of the number of moles in the two phases (caused by the mass transfer across the membrane), the variation of the Gibbs free energy (G) is:

$$dG = \sum_i (u_i' - u_i'')dn_i' \qquad (2.1)$$

Equation (2.1) expresses a general concept: the driving force for the mass transport of a component from one phase to the other is given by the difference in the chemical potential of the two phases caused by changes in temperature, pressure and activity. In equation (2.2), n_i is the mole of i-th component transferred and is related to transmembrane flux J_i by:

$$\frac{dn_i}{dt} = AJ_i \qquad (2.2)$$

where t indicates the time and A the membrane area. As previously stated, the hydrostatic pressure gradient across the membrane is negligible in MD, and the driving force of process is the partial pressure difference across the membrane, established by a temperature difference between the two contacting solution, or by vacuum, air gap, or sweep gas in the permeate side. In the frequent case of non-ideal mixtures, the vapour-liquid equilibrium is mathematically described in terms of partial pressure (p_i), vapour pressure of pure i (p_i 0), and activity coefficient ji,

according to the well-known thermodynamic relationship:

$$p_i = Py_i = p_i^0 a_i = p_i^0 \xi_i x_i \tag{2.3}$$

In equation (2.3), P is the total pressure, a_i the activity, and x_i and y_i are the liquid and vapour mole fraction, respectively. The vapour pressure p^0 of a pure substance varies with temperature according to the Clausius-Clapeyron equation:

$$\frac{dp^0}{dT} = \frac{\lambda}{RT^2} \tag{2.4}$$

where λ is the latent heat of vaporization (λ =9.7 cal/mol for water [1]), R the gas constant, and T the absolute temperature. At the pore entrance, the curvature of the vapour-liquid interface is generally assumed to have a negligible effect on the equilibrium; however, possible influences on the vapour pressure value can be estimated by the Kelvin equation:

$$p^0_{convex} = p^0 \exp\left(\frac{2\gamma_L}{rcRT}\right) \tag{2.5}$$

where r is the curvature radius, γ_L the liquid surface tension, and c the liquid molar density. The expression for activity coefficient in diluted aqueous ionic solutions can be derived from the Debye-Hückel theory:

$$\log \xi_{\pm} = -|Z_+ Z_-| \varphi \sqrt{I} \tag{2.6}$$

Here $\xi_{\pm}$ is the activity coefficient of the electrolyte, ψ is a constant that depends on the temperature and solution permittivity, z is the ion valence, and I the ionic strength of the solution given by:

$$I = \frac{1}{2}\sum_i Z_i^2 C_i \tag{2.7}$$

In an aqueous solution at 25℃ the constant ψ is 0.509 $(\text{mol kg}^{-1})^{1/2}$ [2].

2.3 Heat transfer

A schematic representation of Heat transfer process in MD is shown in Figure 2.1.

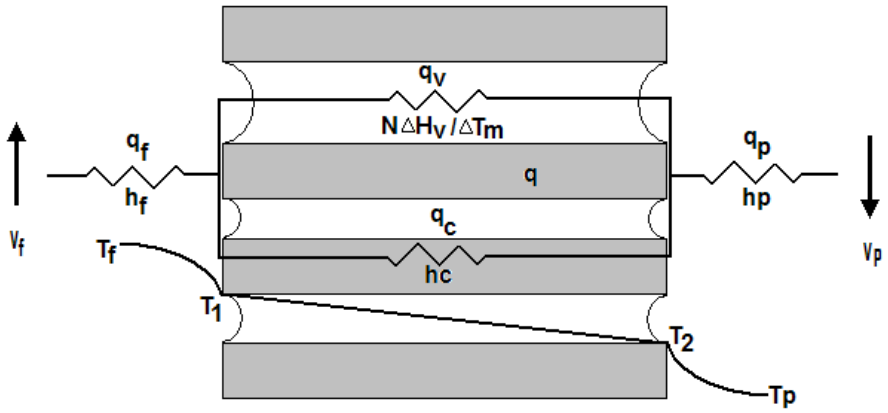

Figure 2.1 Heat transfer resistances in DCMD

Heat transfer in MD processes is always coupled with mass transfer. Heat transfer processes is divided into three parts [3]:

(1) first, heat is transferred from the heated feed solution across the thermal boundary layer to the membrane surface q_f;

(2) second, the heat passes through the membrane in the form of vapor latent heat q_v and heat conduction q_c through the membrane structure;

(3) finally, the heat is removed from the cold permeate side of membrane surface through the boundary layer q_p.

The boundary layers next to the membrane surface may contribute significantly to overall heat transfer resistance [4-7].

The heat transfer processes equations for three steps in heat flows in and around the membrane are [8]:

- along the module at feed and permeate sides:

$$Q_f = c_{pf}\left(\dot{m}_f - NA\right)T_f \qquad (2.8.a)$$

$$Q_p = c_{pp}\left(\dot{m}_p - NA\right)T_p \qquad (2.8.b)$$

- across the membrane:

$$Q_m = Q_V + Q_C \qquad (2.9)$$

- within the boundary layers at feed and permeate sides:

$$Q_f = h_f\left(T_f - T_1\right) \qquad (2.10.a)$$

$$Q_p = h_p\left(T_2 - T_p\right) \tag{2.10.b}$$

- overall heat balance at the steady state:

$$Q_f = Q_m = Q_p \tag{2.11}$$

Hence, the total heat transferred across the membrane is expressed as [4]:

$$Q = H\Delta T \tag{2.12}$$

The overall heat transfer coefficient of the MD process is given by:

$$H = \left[\frac{1}{h_f} + \frac{1}{h_c + N\Delta H_v / \Delta T_m} + \frac{1}{h_p}\right]^{-1} \tag{2.13}$$

where each *h* represents the corresponding heat transfer coefficient shown in Figure 2.1, *N* is the molar flux, ΔH_v is the heat of vaporization.

2.3.1 Heat transfer in boundary layers

The liquid heat transfer coefficients depend on the physical properties of the solution as well as on the hydrodynamic conditions acting on the MD system. It is important to minimize the boundary layer resistances by maximizing the boundary layer heat transfer coefficients h_f and h_p. This is to allow the MD system to supply large quantity of heat to the surface of the membrane to vaporize the liquid. In MD processes, the interfacial temperatures (T_1 and T_2) are often differ significantly from the measured temperatures of bulk solutions at the feed and permeate sides (T_f and T_p). This phenomenon is called the temperature polarization [8, 9]. It causes reduction in the driving force of the MD process due the decrease in the vapor pressure difference across the membrane. The interfacial temperatures (T_1 and T_2) cannot be measured directly, and they are significantly affected by applied membrane physical properties and interfacial film heat transfer coefficient (h_f and h_p). The temperature polarization coefficient (*TPC*) is used to evaluate the efficiency of MD systems by quantifying the magnitudes of the boundary layer resistances relative to the total heat transfer resistance of the MD system. The TPC is defined as [4, 7]:

$$TPC = \frac{T_1 - T_2}{T_f - T_p} \tag{2.14}$$

The recommended *TPC* range is from 0.4 to 0.7 for satisfactory designed system [4]. The boundary layer heat transfer coefficients may be measured experimentally or they often estimated from empirical correlations based on dimensionless numbers, like *Nusselt* (*Nu*), *Reynolds* (*Re*) and *Prandtl* (*Pr*) numbers. The most often relationships is:

$$Nu = C\,\mathrm{Re}^{a}\,\mathrm{Pr}^{b}\left(\frac{\mu_b}{\mu_m}\right)^{c} \qquad and \qquad h_i = \frac{Nu_i\, k_i^T}{d_{h_i}} \tag{2.15}$$

where C, a, b and c are the coefficients depending on the channel configuration of the heat exchanger and flowing character of the streams [8].

2.3.2 Heat transfer across membrane

The heat transfer across the membrane is two parts [9]:

(1) q_c transferred by both conduction through the membrane material.

(2)q_v the latent heat of vaporization associated with the vapor flowing through the membrane.

Heat transfer models for calculating membrane interfacial temperatures T_1 and T_2 were developed on the assumptions of linear temperature distribution across the membrane and an associated isenthalpic flow of vapor in early literature [6, 10]. In these models, the total heat flux through the membrane Q_m is the sum of the heat conduction q_c and the latent heat of vaporization q_v is:

$$Q_m = \left[N\,H_T + \frac{k_m}{s}\left(T_1 - T_2\right)\right] \tag{2.16}$$

Hence, combination of equation (2.3) with equation (2.13) to measure the interfacial temperatures:

$$T_1 = \frac{\left(K_m / s\right)\left(T_p + \alpha T_f\right) + h_f T_f - NH_T}{\left(K_m / s\right)\left(1+\alpha\right) + h_f} \tag{2.17.a}$$

$$T_2 = \frac{(K_m / s)(T_f + \alpha^{-1} T_p) + h_p T_p + N H_T}{(K_m / s)(1 + \alpha^{-1}) + h_p} \qquad (2.17.b)$$

With $\alpha = h_f / h_p$

From above equations, latent heat of vaporization is promoting the permeate flux, whereas heat conduction across the membrane is considered as heat loss since there is no corresponding mass transfer. It was shown that 20-50 % of the total heat transferred in MD process is lost by conduction in literature [11]. The conduction heat transfer coefficient k_m is usually estimated from vapor and solid phase thermal conductivities as:

$$k_m = \varepsilon k_v + (1 - \varepsilon) k_s \qquad (2.18)$$

where k_s and k_v are the heat transfer coefficients of the solid membrane material and the vapor within the membrane pores, respectively and k_s is generally one order of magnitude greater than k_v [10].Therefore, heat loss by conduction can be reduced by increasing the porosity.

MD heat transfer models are based on the assumptions of nonlinear temperature distribution across the membrane and non-isenthalpic flow of vapor [7]. Therefore, the total heat flux through the membrane is given by:

$$Q_m = N H_{TV} + k_m \frac{dT}{dx} \qquad (2.19)$$

where H_{TV} is the transporting vapor enthalpy at a temperature T, and x is the distance to the direction of vapor flux. Since the temperature inside the membrane in MD changes within a range of few degrees and assuming the condensation temperature of vapor T_2 as reference temperature, the enthalpy at temperature T can be written in the form:

$$H_{TV} = h_v\{T_2\} + C_p(T - T_2) \qquad (2.20)$$

where $h_v\{T_2\}$ is the heat of vaporization measured at T_2 and C_p is the specific heat of the vapor. Substituting equation (2.20) into equation (2.19) with separation of variables and integration yields:

$$q_m = \frac{N C_p (T_1 - T_2)}{1 - e^{-N C_p s / k_m}} + N h_v \qquad (2.21)$$

2.4 Mass transfer

Mass transfer in MD is achieved by convective and diffusive transport of water vapor across the microporous hydrophobic membrane for which the driving force is the difference in water vapor pressure on either side of membrane. The possible mass transfer resistances in MD by using an electrical analogy are illustrated in Figure 2.2 [12]:

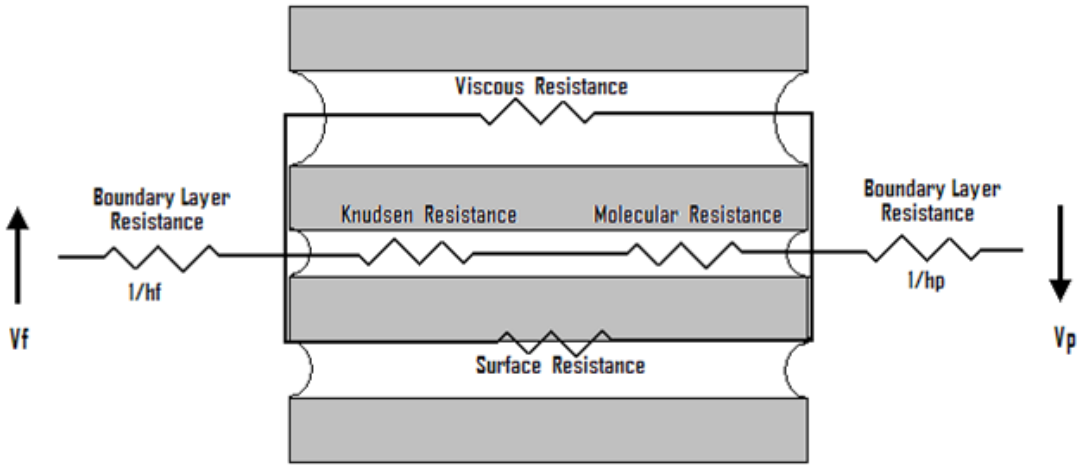

Figure 2.2 Mass transfer resistances in DCMD

The mass transport phenomena including two transportation steps [13]:

(1) mass transport through boundary layers on both sides of membrane.

(2) mass transport through the membrane structure.

2.4.1 Mass transfer in the boundary layers

It is often convenient to operate MD with pure water in order to minimize the boundary layers resistances to mass transfer. However, the presence of concentrated feed layer along the surface of the membrane can scientifically affect the global resistance to mass transfer. This phenomenon is called concentration polarization which results in reduction of the driving force across the membrane [18]. A mass balance across the feed side boundary layer gives the relationship between molar flux N, the mass transfer coefficient k_f, and the solute molar concentrations at the

membrane interface c_m and at the bulk location c_b:

$$N = k_f \ln\left(\frac{C_m}{C_b}\right) \tag{2.22}$$

The boundary layer mass transfer coefficient k_f can be obtained by experiments or be estimated using empirical correlation of dimensions less numbers like Sherwood (*Sh*), Reynolds (*Re*) and Schmidt (*Sc*) numbers. These empirical relationships and usually expressed in the form:

$$Sh = b1\,\mathrm{Re}^{b2}\, Sc^{b3}\left(\frac{\mu_b}{\mu_m}\right)^{b4} \quad with \quad Sh = \frac{k_f d_h}{D},\ \mathrm{Re} = \frac{\rho v d_h}{\mu},\ Sc = \frac{\mu}{\rho D} \tag{2.23}$$

where d_h is the hydraulic diameter, D the binary diffusion coefficient in the liquid, v the fluid velocity, ρ the fluid density, μ the dynamic viscosity of the fluid. These correlations are still applicable for the case of a non-circular flow channel, by using equivalent diameter of the flow channel d_e defined as in [4]:

$$d_e = 4S / L_p \tag{2.24}$$

where S is the cross-sectional area and L_p is the length of wetted perimeter of the flow channel.

2.4.2 Mass transfer across the membrane

Resistances to mass transfer within the membrane structure are three species [8]:

(1) viscous or momentum resistance, due to transfer of momentum through the indirect contact with capillary walls via molecule-molecule collision terminating at molecule-wall collision.

(2) molecular resistance, from collision of a diffusing molecule with other molecules.

(3) Knudsen resistance, collisions between molecules and membrane walls.

A major difference among MD models which Modeling of mass transfer within the membrane pores was described in many experimental and theoretical studies found in the literature [4.6.7.11] is in the arrangement of the transport resistances in the circuit. In most cases, one or more of the resistances may be omitted. The vapor transport in

MD processes is related to the kinetic theory of gases. Accordingly, the vapor transport mechanism depends upon the mean free path length ψ, which can be calculated based on the average process operating conditions (pressure and temperature), and the mean diameter of the membrane pores d_p. The value of ψ, defined as the average distance the molecule of diffusing species travels between two successive collisions, can be calculated from the kinetic theory of gases [15]:

$$\psi = \frac{k_B T}{P\sqrt{2}\pi\sigma_B^2} \tag{2.25}$$

where k_B is the *Boltzmann* constant (1.381×10^{-23} J/K) and σ_B is the collision diameter of the molecule. For the binary mixture of water vapor and air, the mean free path of water in air $\psi_{w\text{-}a}$ may be evaluated at the average membrane temperature T_m as in using:

$$\psi_{w-a} = \frac{k_B T_m}{\pi\left((\sigma_w + \sigma_a)/2\right)^2 P} \frac{1}{\sqrt{1+\left(M_w / M_a\right)}} \tag{2.26}$$

where σ_w and σ_a are the collision diameters for water vapor (2.641×10^{-10} m) and air (3.711×10^{-10} m) [16], and M_w & M_a the molecular weight water and air. The mean free path in the DCMD experiments at a typical operating temperature of 40^{o}C calculated using equation (30) is 0.11 μm. Compare the above equations, the mass transfer efficient will be reduced by the air trapped within the membrane pores.

Generally, the mass transport across the membrane occurs in three regions as shown in Figure 2.3 [7]:

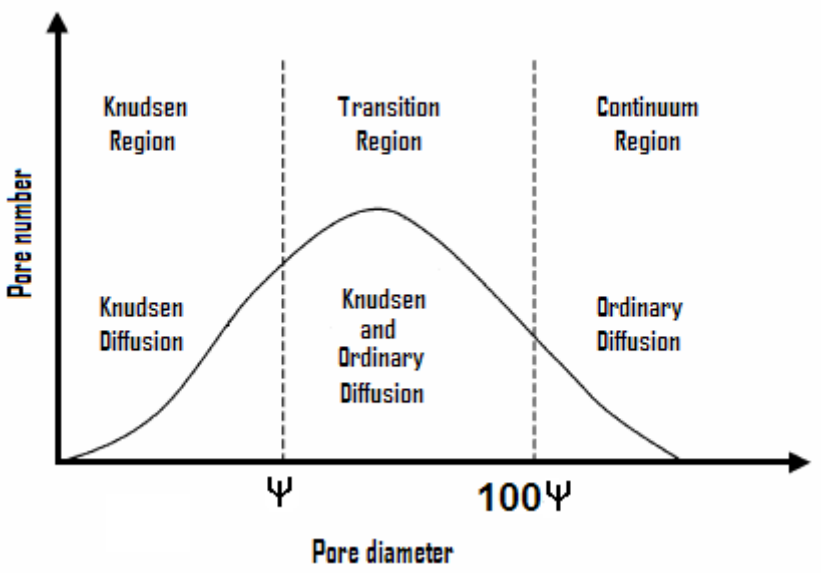

Figure 2.3 Mass transport regions and associated transport mechanisms with pore size distribution.

Mass transport regions including:

(1) Knudsen region/ Knudsen diffusion;

(2) Transition region/ Molecular diffusion;

(3) Continuum region/ Poiseuille flow.

The predominance, coexistence or transition between all of three regions can be estimated by comparing the mean free path ψ of the diffusing molecules to the mean pore diameter d_p of the membrane [7].

In Knudsen region ($d_p < \psi$), the molecule-wall collisions dominate over the molecule-molecule collisions and the mass transport mode is Knudsen diffusion.

In Transition region ($\psi < d_p < 100\psi$), mass transport takes place within the combination on Knudsen and ordinary molecular diffusion.

In Continuum region ($d_p > 100\psi$), the average membrane diameter is large compared to the free mean path of the vapor and the molecule-molecule collision are dominant. Thus, the transport mechanism is the classical viscous (*Poiseuile*) diffusion. In this region, the membrane pores may contain air. The presence of air in the pores hinders the diffusion of vapor and results in lower flux than the maximum achievable flux for the particular membrane and conditions.

Therefore, substantial increase in flux can be achieved by removing the air from the feed (de-aeration) or reducing the pressure of the liquids boundering the membrane (i.e. limiting the total vapor pressure in the pores) [15]. The basic models used to describe water transport in MD system relate the mass flux (N) to the driving force represented by the vapor pressure difference at both liquid-vapor interfaces, via proportionally coefficient (C) as in [4.11.17].

$$N = C\left[p\left(T_{fm}\right) - p\left(T_{pm}\right)\right] \tag{2.27}$$

where $p(T_{fm})$ and $p(T_{pm})$ are the vapor pressure of transporting fluid at the membrane feed and permeate sides, respectively, and C is the membrane distillation coefficient which is a function of membrane physical properties (pore size, porosity, thickness, and membrane pore tortuosity), transporting fluid physical properties (molecular weight and diffusivity), and operating temperature. There are mainly two different models that describe the vapor flux across the membrane; i.e. the Dusty-Gas Model (DGM) [4] and the model proposed by Schofield et al [11]. The DGM will be used in this study for its simplicity because it is based on the well-developed kinetic theory rather than the arguments required by the momentum transfer method. The complete form of the DGM takes into account surface, Knudsen and viscous diffusions. The DGM, without the surface diffusion, as the following expression [18-20]:

$$\frac{X_i^D}{D_e^k} + \sum_{j=1\neq i}^{n} \frac{p_j X_i^D - p_i X_j^D}{D_{ij}^0} = \frac{-1}{R_G T} \nabla p_i$$

$$X_i^V = \frac{-p_i B_o}{R_G T \mu} \nabla I \tag{2.28}$$

$$D_{ij}^0 = K_1 I D_{ij}, \quad D_e^k = K_o \left(\frac{8 R_G T}{\pi M_i}\right)^{1/2}, \quad K_0 = \frac{2\varepsilon r}{3\tau} \qquad B_o = \frac{\varepsilon r^2}{8\tau} \qquad K_1 = \frac{\varepsilon}{\tau}$$

where p the partial pressure, M_i the molecular weight, μ the vapor viscosity, r the pore radius, ε the membrane porosity, τ the membrane tortuosity and R_G is the gas constant. K_o and B_o are constants that can be calculated based on membrane properties or obtained from gas permeation experimental data of non-condensable pure gas such

as hydrogen, helium or air.

The average pore diameter of the membranes used in this study was 0.2 μm, and thus comparable to the mean free path of water vapor molecules (0.1 μm at 40 ℃ as calculated earlier). Therefore, the reduced Knudsen-molecular diffusion transition form of the Dusty-Gas Model (DGM) was applied for describing the vapor flux of pure water across the membrane [10]:

$$N = -\frac{1}{RT_{avg}}\left(\frac{D_w^k D_{w-a}^0}{D_{w-a}^0 + p_a D_w^k}\right)\frac{\Delta p}{\delta} M \qquad (2.29.a)$$

with:

$$D_w^k = \frac{2\varepsilon r}{3\tau}\sqrt{\frac{8RT_{avg}}{\pi M}} \qquad (2.29.b)$$

and

$$D_{w-a}^0 = 4.46 \cdot 10^{-6}\frac{\varepsilon}{\tau}T_{avg}^{2.334} \qquad (2.29.c)$$

where $D^o_{w\text{-}a}$ is the pressure independent binary diffusion coefficient of water-air [21], T_{avg} is the average membrane surface temperature on the feed and permeate sides, and Δp, the partial pressure gradient of water through both membrane surfaces generated by a temperature gradient and/or a concentration difference, is the driving force to mass transfer in DCMD.

References:

[1]. Reid, R.C., Prausnitz, J.M., and Sherwood, T.K. The properties of gases and liquids, 3rd ed.; McGraw-Hill: New York, 1997.

[2]. Atkins, P.W. (1990) Physical Chemistry, 4th ed.; Oxford University Press:Oxford.

[3] S. Bandini and G.C. Sarti. Heat and mass transport resistances in vacuum membrane distillation. AIChEJ, 1999, 45(7): 1422-1433.

[4] K.W. Lawson and D.R. Lloyd. Membrane distillation. II. Direct contact membrane distillation, J. Membrane Sci., 1996, 120: 123.

[5] B. Li and K.K. Sirkar. Novel membrane and device for direct contact membrane distillation-based desalination processes. Ind. Eng. Chem. Res., 2004, 43: 5300.

[6] Z. Ding, R. Ma, A.G. Fane. A new model for mass transfer in direct contact membrane distillation. Desalination, 2002, 151: 217.

[7] J. Phattaranawik, R. Jiraratananon, A.G. Fane. Heat transport and membrane distillation coefficients in direct contact membrane distillation. J. Membrane Sci., 2003, 212: 177.

[8] A.O. Imdakm, T. Matsuura. Simulation of heat and mass transfer in direct contact membrane distillation (MD): The effect of membrane physical properties. J. Membrane Sci., 2005, 262: 117.

[9] A. Gabelman, S.-T. Hwang. Hollow fiber membrane contactors. J. Membrane Sci., 1999, 159: 61.

[10] E. Curcio, E. Drioli. Membrane distillation and related operations - a review. Separation & Purification Rev., 2005, 34: 35.

[11] R.W. Schofield, A.G. Fane, C.J.D. Fell. Gas and vapour transport through microporous membrane. II. Membrane distillation. J. Membrane Sci., 1990, 53: 173.

[12] L. Martínez-Díez, M. I. Vázquez-González, F. J. Florido-Díaz. Study of membrane distillation using channel spacers. J. Membrane Sci., 1998, 144: 45.

[13] E. Drioli, E. Curcio, A. Criscuoli, G. Di Profio. Integrated system for recovery of $CaCO_3$, NaCl and $MgSO_4 \cdot 7H_2O$ from nanofiltration retentate. J. Membrane Sci., 2004, 239: 27.

[14] M. Courel, M. Dornier, G.M. Rios, M. Reynes. Modeling of water transport in osmotic

distillation using asymmetric membrane. J. Membrane Sci., 2000, 173: 107.

[15] R.D. Present. Kinetic Theory of Gases. McGraw-Hill, New York, 1958.

[16] R.A. Albert, R.J. Silbey. Physical Chemistry, 2nd ed. Wiley, New York, 1997.

[17] L. Martínez-Díez, F. J. Florido-Díaz. Theoretical and experimental studies on desalination using membrane distillation. Desalination,2001, 139: 373.

[18] C.M. Guijt, I.G. Racz, J.W.v. Heuven, T. Reith, A.B.d. Haan. Modeling of a transmembrane evaporation module for desalination of seawater. Desalination, 1999, 126: 119.

[19] K.W. Lawson, D.R. Lloyd. Membrane distillation. J. Membrane Sci., 1997, 124: 1-25.

[20] R.W. Schofield, A.G. Fane, C.J.D. Fell. Gas and vapour transport through microporous membrane. II. Membrane distillation. J. Membrane Sci., 1990, 53: 159-171.

[21] R.H. Perry, D. Green, Perry's Chemical Engineers' Handbook, 6th Edition, McGraw Hill, New York, 1984.

CHAPTER THREE

Membrane Fouling

3.1 Introduction

Membrane fouling refers to the phenomenon where "foulants" (suspended particles, colloids, natural organic matter, bacteria etc.) accumulate on and within membrane that, in turn, leads to performance deterioration such as lowered permeate flux and salt rejection [1]. Fouling is a major obstacle for efficient use of membrane technology for treatment of natural waters [2]; in particular, fouling increases the use of cleaning chemicals (consequently introducing a waste problem) and ultimately shortens membrane life.

Membrane fouling is in most part due to specific adsorption, gel layer formation and membrane pore plugging. Gel or cake layer formation may be caused by a variety of particulate substances including inorganic precipitates such as $CaCO_3$, $CaSO_4$, and several metal hydroxides, organic materials such as proteins, natural organic matter (NOM), colloids, humic acids and other macromolecular materials, and biological components such as micro-organisms and products of their metabolism [3]. All of these components are present, in various extents, into seawater.

The rate and extent of membrane fouling are influenced by operating conditions, such as the applied pressure and cross flow velocity [4]. Applied pressure governs the initial permeate flux and the resulting convective transport of foulants towards the membrane surface. Higher permeate flux results in severe fouling due to higher permeation drag and more compressed foulant layers [5]. Thus, although higher operating pressures allow higher initial permeate flux, the exacerbation of fouling phenomena may counteract this advantage.

In addition, solution chemistry (pH and ionic composition) plays a significant role in determining foulant–foulant and foulant–membrane electrostatic double layer interactions and hence membrane performance [6, 7, 8].

3.1.1 Particulate and colloidal fouling (Suspended Solids)

Natural resources for drinking water usually contain particles and colloids like Suspended Solids, including silicates, sand, sludge, clay, salt precipitates and microorganisms.

Generally, not a consideration with properly constructed and maintained ground water systems, suspended solids can be a major concern when treating surface water or reclaiming municipal and agricultural wastewater. Suspended solids in feed water for membrane processes can consist of inorganic materials, such as clays, insoluble metal oxides, and organic substances such as colloidal color.

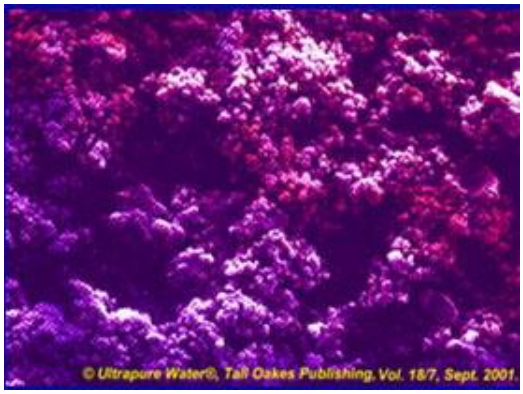

Figure 3.1 Colloidal fouling

In the RO system, when the active carbon let out from the pre-treatment process produces is sub particulate fouling.

Figure 3.2 Active carbon fouling

The oxides of several metals are extremely insoluble of principal concern in membrane plants are the oxides of ferric iron (Fe^{3+}) and Manganese (Mn^{3+}).

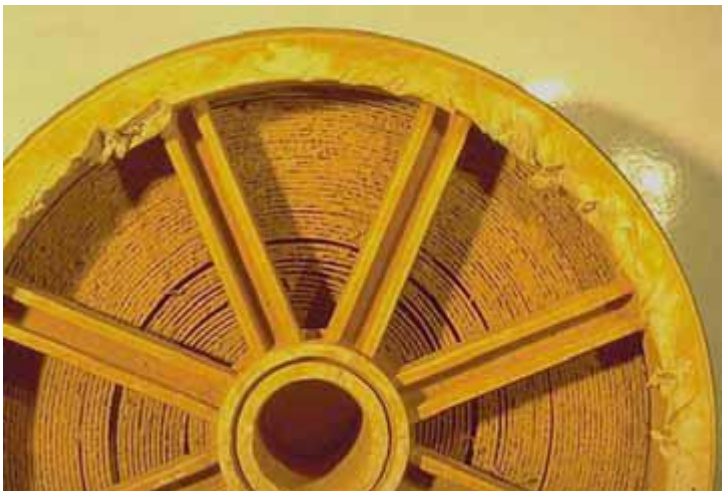

Figure 3.3 oxides of ferric iron

It is wise to limit iron and manganese in the feed water to not more than 3 mg/L of iron, and not more than 0.1 mg/L of manganese. Values above this may cause problems of coprecipitation with other constituents such as silica, and in drinking water systems may cause excess concentrations in the permeate. Relatively high levels of iron may also influence the effectiveness of scale inhibitors, possibly leading to premature precipitation of scale-forming compounds. The feed water system should be kept anaerobic, so that iron and manganese remain in the soluble divalent or "-ous" state, rather than be oxidized to the insoluble trivalent, or "-ic" state.

3.1.2 Scaling

Scaling of the membrane surface occurs due to the precipitation of sparingly soluble salts. As water passes through the membrane, dissolved minerals from the feed water become concentrated in the reject stream. If the concentrations of minerals in the reject stream exceed their solubility products, crystals will precipitate onto the membrane. Scaling occurs first in the last elements of an RO system because the feed water is more concentrated near the end of the process.

Figure 3.4 Scaling on membrane surface

The following is a list of some of the types of scale that may occur on the membrane systems:

• Calcium and Magnesium Carbonates

• Calcium and Magnesium Sulfates

• Metal Oxides

• Silica

• Strontium and Barium Sulfates

Calcium carbonate ($CaCO_3$) scaling is the most common form of mineral scale found in membrane process operations. $CaCO_3$ precipitation usually takes place toward the end of an RO system. The tendency for $CaCO_3$ scaling has been traditionally predicted by the Langelier Saturation Index (LSI) method.

$$LSI = pH - pHs \quad (3.1)$$

Where pHs = pH of solution if it were in equilibrium with $CaCO_3$

$$pHs = pCa + pAlk + C(T,TDS) \quad (3.2.a)$$

$$pCa = \log \text{ of Ca concentration} \quad (3.2.b)$$

$$pAlk = \log \text{ of MO Alkalinity} \quad (3.2.c)$$

C (T,TDS) = Constant to include temperatue (T) and TDS

At higher ionic strengths the Stiff and Davis Index is a more accurate predictor of scaling tendency：

$$SD = pH - pHSD \quad (3.3.a)$$

$$pHSD = pCa + pAlk + K(T,IS) \quad (3.3.b)$$

where K is constant to include temperature and ionic strength. If pH>pHs (or pHSD), then the water is saturated with calcium carbonate, if pH<pHs, then the water is unsaturated. A positive value indicates a tendency toward precipitation.

Sulfate of calcium, strontium and barium are also very important scaling in membrane system. Barium and strontium sulfates ($BaSO_4$ and $SrSO_4$) are extremely insoluble, but fortunately are able to be controlled at very high levels of supersaturation, due to the tendency to form very slowly. Commonly used values for $BaSO_4$ are 40 to 60 times saturation.

Figure 3.5 $CaSO_4$ on membrane surface

Silica

Silicon is the most abundant element on Earth's crust in the form of several silicon-containing minerals [9, 10]. It is widely and abundantly distributed throughout the earth, both in pure state and as silicates. Silica occurs naturally in amorphous and crystalline forms. Quartz, tridymite, or cristobalite are crystalline forms of silica and the solubility is very low, approximately 5-6 mg/L, while amorphous silica solubility is about l00-120 mg/L at neutral pH and temperature of 25℃ [11].In water sources

silica can occur in three different forms [12]:

• Monomer silica, or silicic acid, $Si(OH)_4$: soluble or reactive silica.

• Polymerized silicic acid: colloidal or unreactive silica.

• Particulate silica.

Presence of silica in water is due to the dissolution of silica based on the following reaction:

$$SiO_2 + 2H_2O = Si(OH)_4 \quad (3.4)$$

In natural waters, silica solubility is in the range of 1-30 ppm, in well waters 20-100 ppm and in brackish waters in excess of 1000 ppm [13].

High silica levels often lead to undesirable silica formation and deposition in water systems. Silica occurs in varying concentrations in all natural waters.

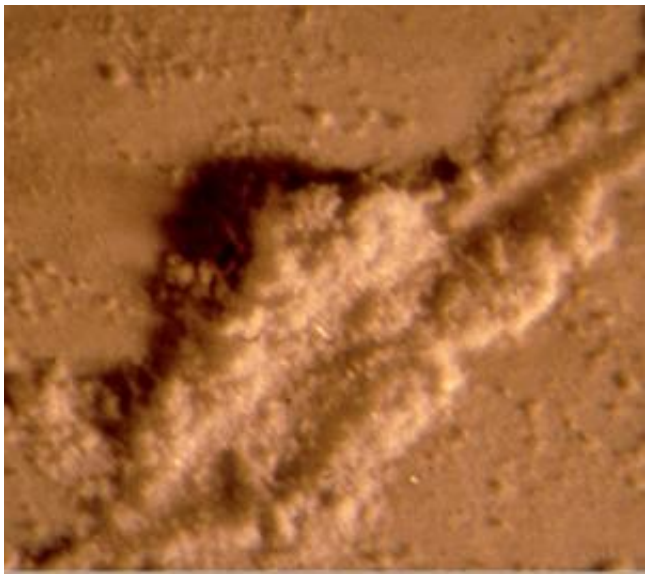

Figure 3.6 Silica fouling on membrane surface

The silica fouling potential is dependent on the concentration of dissolved silica exceeding the amorphous silica equilibrium solubility of the solution. The solubility of silica is greatly affected by parameters such as temperature, pH, and presence of other salts. For example, silica solubility of 1500 ppm at ambient temperature can be achieved with pH of 11 [14]. Silica supersaturation in water is thermodynamically controlled by the solubility of amorphous silica at these conditions. Soluble silica in

water is initially in monomeric state as monosilicic acid ($Si(OH)_4$) and is mostly un-ionized at natural pH levels. At alkaline pH, silica may co-precipitate with soluble metals to form magnesium silicate (Mg_2SiO_4) or calcium silicate (Ca_2SiO_4). Furthermore, silica may be adsorbed onto the surface of insoluble metal hydroxide compounds, such as $Mg(OH)_2$ or $MgCO_3$ [15].

Silica is very weakly ionised and is generally considered to exist as undissociated (ortho-) silicic acid (H_4SiO_4) in most naturally occurring waters with pH up to approximately 8.0. Various authors have studied and found that solubility of undissociated (unionised) silica in water is about 120 to 150 ppm at 25℃ and pH below 8. As pH increases, the degree of ionization increases; at a pH of 8.5 only 10 % of the monosilicic acid is ionized and the dissociation constant (pKa) for the first stage of dissociation is approximately 9.7, indicating that silica is approximately 50 % ionised at pH of 9.7, the other 50 % exist as undissociated (ortho) silicic acid [16].

The polymerization of monomer silica has been accepted as the key factor to the formation of amorphous silica deposits. Once deposited, silica scale is extremely difficult to remove without damaging the membrane. Traditional RO operations limited silica concentration in the concentrate to 150 mg/L. However, some facilities have successfully operated at higher concentrations, while other has been able to operate as high as 250 mg/L. A maximum value of 120 mg/L is recommended for hollow fiber membranes. Heavy metals in the feed water in small concentrations can cause premature polymerization of silica as a complex with the metal. Because reduction of silica in the feed water is typically very costly, the primary strategy for controlling silica fouling has been by water recovery.

3.1.3 Organic fouling

Organic fouling originates from the interaction between organic compound present in the feed water with the membrane surface. Organic matter present in natural waters is undesirable because it is responsible for color in the water, formation of carcinogenic by-product during water disinfection.

There are three types of bulk organic matter in drinking water treatment and wastewater reuse [17]:

(1) Allochthonous natural organic matter (NOM) dominated by humic substances derived from runoff and leaching of vegetative debris from terrestrial sources within a watershed.

(2) Autochthonous or algal organic matter consisting of extracellular and intracellular macromolecules and cellular debris.

(3) Wastewater effluent consisting of background (drinking water) NOM plus soluble microbial products derived from biological wastewater treatment.

Natural organic matter present in seawater at concentration of 2-3 ppm, but in more significant amount at higher concentrations [18].

Figure3.7. Membrane organics fouling

Figure 3.8 Membrane humic acid fouling

3.1.4 Microbial fouling / Biofouling

It is caused by microorganisms which are accumulated and attached at the membrane surface. Bio-fouling results in an increase of salt passage and pressure drop, and a decrease of the flux.

The general development of a biofouling can be divided into three phases [19]:

(1) The *induction phase*, with primary colonization. Adhesion is essentially proportional to the cell density in the water phase and occurs owing to weak physicochemical interactions.

(2) The logarithmical growth phase, when cell growth on the surface contributes more to biofilm accumulation than does the adhesion of planctonic cells.

(3) The *plateau phase*, when biofouling growth (adhesion and cell multiplication) and cell detachment are in balance. This phase is mainly controlled by nutrient concentration and the resultant growth rate, the mechanical stability of the biofouling, and the effective shear forces. It is independent of the concentration of cells in the raw water. Original surface properties of the membrane are masked by the biofilm.

Figure 3.9 Microbial fouling on membrane surface

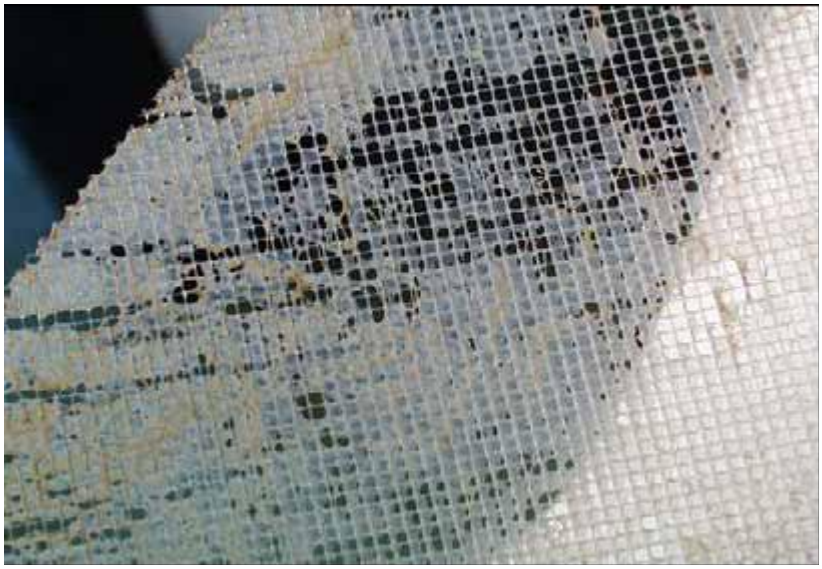

Figure 3.10 Microbial fouling on membrane grid

Even in clear brackish well waters, the potential for biofouling can exist. Earlier in the history of RO, cellulose acetate membranes were frequently attacked by a variety of bacteria. The results were often rapid increase in both flux and salt passage, as holes appeared in the membrane surface. More typical however was the loss of flux due to biofouling over days or weeks, resulting in significant increase in power requirements, and often a change in salt passage. However, since chlorine in limited doses could be tolerated by this membrane material, disinfection of the system was possible, and some level of control could be exercised. With the advent of polyamide and other non-celluclosic membrane materials, the use of chlorine, or other strong oxidants, within the membrane system became unacceptable, due to the potential for membrane degradation. However, these membrane materials typically are resistant to biological attack.

3.2 Fouling in Membrane Distillation

3.2.1 Scaling in MD

Since many feed waters contain sparingly soluble salts, the ability to use MD for treating these waters is contingent on MD not being susceptible to scaling when these salt solutions become supersaturated. However, as reported in the literature,

membrane pores/surfaces may be clogged or membrane pores may get wetted by deposits [20, 21]. This may be aggravated by the fact that certain salts, such as $CaSO_4$ (both in anhydrite and gypsum forms) and $CaCO_3$, have an inverse solubility with respect to temperature.

There have been reports in the literature of permeate flux decrease due to scaling of MD modules by calcium carbonate. Investigations carried out by Karakulski et al (2002) [22] showed that a direct purification of natuarl water by MD results in the deposition of significant amounts of $CaCO_3$, on the membrane surface. Preliminary softening of water in NF process resulted in the decrease of fouling. Addition of small amounts of HCL to the feed (pH = 5) permitted to carry out the MD process without a decline of the efficiency.

During the concentration of tap water (also softened by NF process), Karakulski et al. (2005) have found that the silicon compounds precipitated in the feed, and they were deposited at the inlets of the capillary membranes. In particular, EDS analysis revealed that this deposit was mainly composed of Si, with smaller amounts of the following elements: Fe, Ca, Zn and Cl. This resulted in a rapid decline of the MD module efficiency. Moreover, the wettability of a fraction of the membrane pores caused a decline of the module efficiency by 30 % after 1100 hours of the process duration. Drying of membranes allows restoring the initial module efficiency for a short period only [23].

The effect of iron oxides (iron and steel corrosion is the major reason of formation of iron oxides in an aqueous solution) deposit on the membrane permeability and wettability during the MD process was evaluated by Gryta (2007) [24]. Various forms of iron oxides (maghemite, lepidocrocite, akaganéte and hematite) were identified as a result of corrosion of the MD pilot plant. These oxides exhibit a high potential to accumulate not only on the membrane surface, but also within the pores. The precipitates formed on the membrane surface are characterised by a high porosity. Thus, despite of the complete coverage of the membrane surface by them, the permeate flux was reduced only by several percentages. Rinsing the module with a concentrated HCl solution can dissolve deposit of iron oxides. However, this is associated with the

penetration of the HCl solution into the pores occupied by the deposit, which initiated the process of membrane wettability. Consequently, for the studied case the permeate flux decreased from 800 to 650 L/m^{2}d during the 100 hours of MD. Moreover, the electrical conductivity of the obtained distillate was increased from 3 to 20 μS/cm.

The scaling potential of $CaSO_4$ in DCMD modules has been recently investigated at different saturation index (SI) by He et al. (2008) [25]. Below are summarized some of their results:

(1) the induction period for the $CaSO_4$ (showing inverse solubility) precipitation decreased with increasing feed brine temperature and increasing degree of supersaturation and showed dependencies of classical homogeneous nucleation theory only for higher supersaturation;

(2) even at higher supersaturation in the bulk solution and in presence of precipitation at the membrane surface, there was no significant drop in the permeate production rate;

(3) the precipitate formed was found to be gypsum and not anhydrite;

(4) for gypsum scaling at the membrane surface, concentration polarization effects are more important than temperature polarization effects;

(5) MD modules must be protected from recycling large amounts of suspended crystalline material which could damage the membrane surface, especially near the potting boundary of the fibres.

3.2.2 Natural organic matter (NOM) fouling

Among the many potential fouling that are ubiquitous in natural waters, natural organic matter (NOM) is one of the most recalcitrant. Membrane distillation fouling can be affected by the characteristics of the NOM and its interaction with the membranes and their associated properties.

Therefore, understanding the causes of membrane fouling by NOM and developing strategies for fouling control are very important. The main components of NOM are humic substances, which are the macromolecular mixtures of humic acids, fulvic

acids, and humin. Humic acids affected flux by forming complexes with the divalent cation (i.e. Ca^{2+}, Mg^{2+}) and resulted in coagulation on the membrane surface.

The important role of NOM in MD fouling is attributed to the specific binding (complexation) with the divalent calcium ions to acidic functional groups of NOM. Such interactions result in a compact and highly resistant fouling layer at the membrane surface, which leads to severe flux decline. In particular, bridging between deposited NOM molecules in the presence of Ca^{2+} ions enhances the compactness of the fouling layer. It is the structure of the fouling layer combined with the deposit mass that governs the flux decline during NOM fouling [26].

Whenever the deposit of humic acid coagulate on the membrane surface is loosely packed, it is rather easily removed. Rinsing of the fouled membrane with clean water and a 0.1M NaOH solution gave 100 % of flux recovery.

3.2.3 Biological fouling in MD

A preliminary assessment of the biofouling due to microorganism growth on the surface of microporous hydrophobic membranes was made by Gryta (2002) [27]. The SEM observations of the membranes taken from modules used MD process indicated that the growth of microorganisms in the MD installation took place, but usually in a limited range. The restriction of microbial growth was significantly affected by the running conditions of the MD process, occurred at a relatively high temperature and salinity of the feed water. The growth of fungi (Aspergillus) and anaerobic bacteria (S. faecalis) was observed on the membrane surface in the examined module used for the treatment of saline wastewater. Aerobic bacteria (Pseudomonas) did not find appropriate conditions for their growth; hence they were not detected in the MD module. As a consequence of a restricted microbial growth in the MD installation, one should not expect acute problems resulting from biofouling in the degree encountered in other membrane processes such as UF, NF or RO.

3.2.4 Wetting and cleaning

Membrane distillation is only possible if the restrictive condition is fulfilled, that the pores of the membrane should not be filled with liquid. Wetting of microporous membranes is mainly influenced by three factors: membrane material, the nature of the penetrating liquid and the membrane structure.

Water and aqueous solutions of inorganic substances have such high values of the surface tension (γ_L>72·10^{-3} N/m) that for a number of hydrophobic microporous membranes with pores in the range of 1 um or less (such as polypropylene, poly-vinylidene fluoride, poly-tetrafluoro ethylene) this non wetting condition is guaranted.

However, as soon as organic solutes are present in aqueous solution, the surface tension γ_L will decrease rapidly. If the concentration of organic liquids exceeds a critical value, the microporous membrane will be wetted and membrane distillation is no longer possible. Penetrating drop method experiments showed that, for instance, for a flat polypropylene membrane (Accurel PP 0.1 um) the following values of γ_L were found: alcohols: ≈ 29 ·10^{-3} N/m; carboxylic acids ≈ 32 ·10^{-3} N/m; DMF/DMAc ≈ 36 ·10^{-3} N/m [28].

The partial reduction of hydrophobicity can be also observed during long-term MD operation working on high concentrated salt solutions. Restoring procedures are based on extensive washing with water/ethanol mixtures, at decreasing ratios, followed by drying of the membrane fibers. Cleaning procedures for hydrophobic membranes are imposed by specific problems, particularly in processes involving fats and proteins that can adhere and foul the membrane, or alcohols and surfactants that can cause leakage. Open literature suggests few approaches to this difficult task. Efficient cleaning methods were assessed by Durham and Nguyen (1994) [29]. The most effective cleaner for membranes with a surface tension greater than 23 mN/m was 1 % NaOH; the hydrophobic integrity of these membranes was destroyed during repeated fouling/ cleaning trials. The most effective cleaner for membranes with a surface tension less than 23 mN/m was P3 Ultrasil 56; water vapour flux was maintained and there was not

salt leakage during repeated fouling/cleaning runs.

References:

[1] J.S. Vrouwenvelder, J.A.M. van Paassen, L.P. Wessels, A.F. van Dam, S.M. Bakker. The Membrane Fouling Simulator: A practical tool for fouling prediction and control. J. Membrane Sci., 2006, 281: 316.

[2] A. Seidel, M. Elimelech. Coupling between chemical and physical interactions in natural organic matter (NOM) fouling of nanofiltration membranes: implications for fouling control. J. Membrane Sci. 2002, 203: 245.

[3] D. Hasson, V. Lumelsky, G. Greenberg, Y. Pinhas, R. Semiat. Development of the electrochemical scale removal technique for desalination applications. Desalination, 2008, 230: 329.

[4] A. Seidel, M. Elimelech. Coupling between chemical and physical interactions in natural organic matter (NOM) fouling of nanofiltration membranes: implications for fouling control. J. Membrane Sci., 2002, 203: 245.

[5] J.W. Cho, G. Amy, J. Pellegrino. Membrane filtration of natural organic matter: initial comparison of rejection and flux decline characteristics with ultrafiltration and nanofiltration membranes. Water Res., 1999, 33: 2517.

[6] A. Braghetta, F.A. DiGiano, W.P. Ball. NOM accumulation at NF membrane surface: impact of chemistry and shear. J. Environ. Eng. ASCE, 1998, 124: 1087.

[7] M. Kabsch-Korbutowicz, K. Majewska-Nowak, T. Winnicki. Analysis of membrane fouling in the treatment of water solutions containing humic acids and mineral salts. Desalination, 1999, 126: 179.

[8] J.W. Cho, G. Amy, J. Pellegrino. Membrane filtration of natural organic matter: factors and mechanisms affecting rejection and flux decline with charged ultrafiltration (UF) membrane. J. Membrane Sci., 2000, 164: 89.

[9] R.K. ller. The Chemistry of silica (Solubility, Polymerization, Colloid and Surface Properties and Biochemistry). Wiley-interscience, New York, 1979.

[10] R.K. Iler. The Chemistry of Silica and Silicates. Cornell University Press, 1955.

[11] I. Bremere, M. Kennedy, J. Schippers. Desalination, 2000, 132: 89-100.

[12] L.F. Comb, Ultrapure Water, 1996, 13: 41-43.

[13] P. Sahachaiyunta, T. Koo, R. Sheikholeslami. Desalination, 2002, 144 (2002: 373.

[14] D. McBride and D. Mukhopadhyay. 450 ppm silica sustained in innovative reverse osmosis technology. Proc. 51th International Water Conference Meeting, 1996: 145-152.

[15] R. Sheikholeslami, J. Bright. Desalination, 2002, 143: 255-267.

[16] J.S.Gill, Colloids and Sur., 1993, 74: 101.

[17] Gary Amy. Fundamental understanding of organic matter fouling of membranes. Desalination, 2008, 231: 44–51.

[18] www.avistatech.com/Solutions/organics_fouling.htm.

[19] Characklis, W.G. Microbial fouling and microbial fouling control. In Biofilms, W.G. Characklis and K.C. Marshall, Eds, pp. 523-633, Wiley, New York, 1990.

[20] M. Gryta. Water purification by membrane distillation process. Sci. Technol., 2006, 41: 1789–1798.

[21] M. Gryta. The fermentation process integrated with membrane distillation. Sep. Purif. Technol., 2001, 24: 283–296.

[22] K. Karakulski, M. Gryta, A. Morawski. Membrane processes used for potable water quality improvement. Desalination, 2002, 145: 315.

[23] K. Karakulski, M. Gryta. Water demineralisation by NF/MD integrated processes. Desalination, 2005, 177: 109.

[24] M. Gryta. Effect of iron oxides scaling on the MD process performance. Desalination, 2007, 216: 88.

[25] F. He, J. Gilron, H. Lee, L. Song, K. K. Sirkar. Potential for scaling by sparingly soluble salts in crossflow DCMD. J. Membrane Sci., 2008, 311: 68.

[26] Ahmed Al-Amoudi, Robert W. Lovitt. Fouling strategies and the cleaning system of NF membranes and factors affecting cleaning efficiency. J. Membrane Sci., 2007, 303: 4.

[27] M. Gryta. The assessment of microorganism growth in the membrane distillation system. Desalination, 2002, 142: 79.

[28] D. Bargeman. Contact angle on non polar solids. J. Colloids and Interface Sci., 1972, 40: 344.

[29] R. J. Durham, M. H. Nguyen. Hydrophobic membrane evaluation and cleaning for osmotic distillation of tomato puree. J. Membrane Sci., 1994, 87: 181.

CHAPTER FOUR

Experimental Activity on $CaCO_3$ Scaling in Presence of Humic Acid

4.1 Introduction

When treating seawater, scaling potential due to sparingly soluble salts dissolved is recognized as a critical problem, and particularly when MD is operated at high recovery factors. Since MD is a thermally driven membrane operation, the scaling event is intensified by the inverse solubility of gypsum and calcium carbonate with temperature [1]. In addition, the presence of dissolved organic matter (DOM), in most part composed by humic substances derived from chemical and biological degradation of micro-organisms, increases the complexity of fouling phenomena.

The precipitation of $CaCO_3$ on the membrane surface, and the consequent flux decline, was observed when tap water was used directly as a feed to nanofiltration/membrane distillation system (NF/MD) for the production of demineralised water; scaling was significantly limited by the acidification of the feed water to pH 4 [2].

Calculations made by Gryta [9] prove that the formation of a deposit layer on the surface of the membrane limits heat transfer in MD and decreases the interfacial feed temperature [3]. DCMD tests carried out by Khayet et al. [4] using polytetrafluoroethylene (PTFE) and polyvinylidene fluoride (PVDF) membranes, demonstrated a preferential absorption of humic acid (HA) at the surface of membranes exhibiting higher hydrophobic character with a consequent more pronounced deterioration of the transmembrane flux.

The attention paid on the investigation of fouling specifically related to membrane distillation slightly increased only in recent years, the level of understanding of this intricate phenomenon still remains poor, and investigation approaches are anchored to traditional ones. So far, studies in literature aiming to understand - from a quantitative point of view - the extent of organic fouling and inorganic scaling in membrane distillation, deeply focus on the chemistry of the solution but almost completely

neglect the effect of physico-chemical properties of the membrane.

The innovative aspects of this work mostly concern the investigation of the role of microporous hydrophobic membranes on:

(1) The heterogeneous nucleation kinetics of CaCO3 (scaling) from seawater solutions at different concentration factors;

(2) The inhibition effect of humic acid on the heterogeneous nucleation and growth rate of CaCO3.

Both theoretical and experimental approaches are used with the aim to investigate the existing interrelations between the energetic aspects of scaling formation, and the alterations

4.2 Theory of $CaCO_3$ scaling

The scaling tendency of $CaCO_3$ is a function of the supersaturation (S), defined as follows [5]:

$$\ln S = \ln \frac{a_{Ca^{2+}}\, a_{CO_3^{2-}}}{(a_{Ca^{2+}}\, a_{CO_3^{2-}})_e} = \ln \frac{a_{Ca^{2+}}\, a_{CO_3^{2-}}}{K_{sp}} \tag{4.1}$$

Where a is the ion activity, subscript "e" identifies the equilibrium condition of the solution (saturation), and K_{sp} the solubility product. Calcium carbonate has three crystal polymorphs, with decreasing order of stability: calcite, aragonite and vaterite. The value in molar units of K_{sp} for each polymorphic form is provided in Appendix A. Gibbs free energy ΔG of the forming phase, assumed as a spherical nucleus of radius r and molecular volume υ, was calculated by an energy balance that considers the sum of surface excess Gibbs energy (positive) and volume excess Gibbs free energy (negative) [6]:

$$\Delta G = 4\pi r^2 \gamma - \frac{4\pi r^3}{3\upsilon} \Delta\mu \tag{4.2}$$

being γ the interfacial energy, $\Delta\mu = kT \ln S$ the chemical potential gradient, k the Boltzmann's constant and T the absolute temperature. The maximum of Gibbs free energy ΔG^* corresponds to a nucleus having a critical radius; below this size the

particle is thermodynamically unstable. For homogeneous nucleation [7]:

$$\Delta G^* = \frac{\beta \gamma^3 \upsilon^2}{(kT)^2} \frac{1}{\ln^2 S} \tag{4.3}$$

being β a geometrical factor (=16π/3 for spheres). According to Classical Nucleation Theory (CNT), the (homogeneous) nucleation rate J is given by [8]:

$$J = A \exp\left[-\frac{\Delta G^*}{kT} \right] \tag{4.4}$$

where A is a pre-exponential factor. For heterogeneous nucleation on microporous hydrophobic membranes, ΔG* is decreased according to the following equation derived by Curcio et al. (2006) [9]:

$$\frac{\Delta G^*_{heterogeneous}}{\Delta G^*_{homogeneous}} = \frac{1}{4}(2+\cos\theta)(1-\cos\theta)^2 \left[1 - \varepsilon \frac{(1+\cos\theta)^2}{(1-\cos\theta)^2} \right]^3 \tag{4.5}$$

where θ is the contact angle between solution and membrane, and ε the membrane porosity. CNT correlates the induction time τ, defined as the time period elapsed from the achievement of supersaturation and the moment at which precipitated particles can be detected, to nucleation rate. Under the assumptions of mononuclear mechanism, constant amount of particles per unit volume (N) necessary for a solid phase to be detected, prevalence of the time to form stable nuclei over relaxation time (necessary for the cluster distribution to respond to imposed supersaturation) and growth time (necessary for the nuclei to grow to a detectable size) [8]:

$$\tau = \frac{N}{J} = \frac{N}{A} \exp\left[\frac{\beta \gamma^3 \upsilon^2}{(kT)^3} \frac{1}{\ln^2 S} \right] \tag{4.6}$$

The interfacial energy was thus estimated from the slope of the straight-line resulting in a plot of ln τ vs ($1/\ln^2 S$).

4.3 Materials and methods

Synthetic seawater solutions were prepared by dissolving reagent grade NaCl (23.27 mg/mL, Carlo Erba 368256), Na_2SO_4 (3.99 mg/mL, Carlo Erba 483007), $MgCl_2$ (11.28 mg/mL, Carlo Erba 349354), KBr (0.095 mg/mL, Carlo Erba 470737),

KCl (0.663 mg/mL, Carlo Erba 471177), $CaCl_2 \cdot 2H_2O$ (1.47 mg/mL, Riedel-deHaen 31307), $NaHCO_3$ (0.193 mg/mL, Fluka 88208), Na_2CO_3 (0.0072 mg/mL, Fluka 71350), Humic Acid (2 mg/L, Fluka 536810), in ultrapure water (Purelab, ELGA). The activity of calcium and carbonate ions are calculated by means of chemical speciation is to evaluate the supersaturation level. Appendix A lists species, reactions, equilibrium constants, and details on the software (Visual MINTEQ v2.61 released by KTH / Department of Land and Water Resources Engineering [10]) used in this research. According to the above-mentioned reference composition, solutions were prepared at different concentration factors and supersaturation in Table 4.1. Adding 1M HCl or 1M NaOH solutions were used to adjust the pH to 8.5.

Table 1. IAP and $CaCO_3$ supersaturation (with respect to vaterite) at the different investigated concentration factors.

Concentration factor (CF)	**IAP ($\times 10^7$)**		**lnS (vaterite)**	
	no HA	**with HA**	**no HA**	**with HA**
4	3.799	3.797	3.755	3.754
4.5	4.573	4.570	3.940	3.939
4.75	4.975	4.973	4.025	4.024
5	5.388	5.385	4.104	4.102
5.5	6.242	6.239	4.251	4.249
6	7.132	7.129	4.385	4.382

pH=8.5; K_{sp} (vaterite at 40 ℃) = -8.051.

Dynamic Light Scattering analysis using a 90 Plus/Bi-Mas Particle Sizing Option (Brookhaven Instruments Corporation) with 15 nW diode laser, operating at a wavelength of 678 nm and thermostated at 40 ℃ was used to determine average particle size and intensity correlation functions versus time. $CaCO_3$ precipitation tests were determined by contacting the supersaturated solutions contained in 4 mL DLS

cuvettes with Accurel PP polypropylene hollow fibers with 0.20 μm pore size and external diameter of 1.8 mm.

SEM micrographs (FEI Quanta 200 instrument) and powder X-Ray diffraction (Phillips PW 1830/1840 using CuKα filter) were used to measure the precipitates. Contact angles were characterized by CAM 200 Contact Angle Meter (KSV Instruments LTD, Helsinki); sessile drops of solutions were deposited on the top surfaces of the membranes by automatic microsyringe.

Long-term Membrane Distillation tests were determined in a semi-pilot plant following in Figure 4.1.

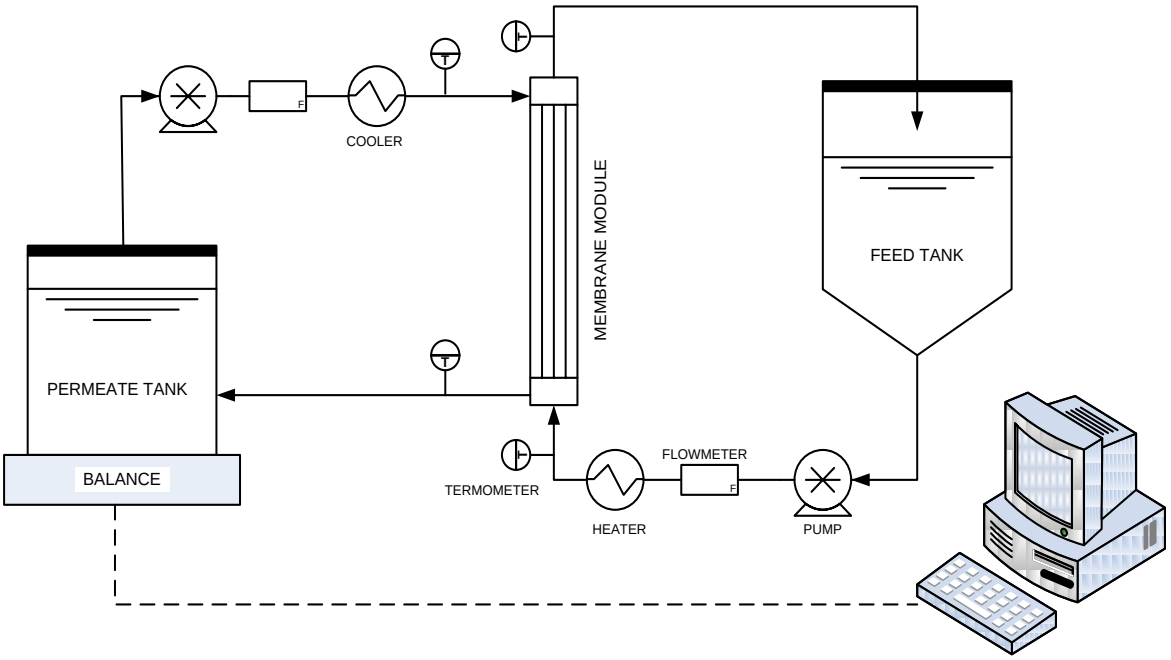

Figure 4.1 Direct Contact Membrane Distillation (DCMD) plant

Feed and distillate currents were recirculated in counter-current by Gear Metering Pump Serie N (Pompe Cucchi) equipped by AC Tech Controler, and Centrifugal Electropump CEA (Lowara), respectively; F14 flowmeters (Blue-White Industries, Ltd) was used to measure the flowrates. The temperatures of distillate and feed at module inlet: 20 ℃ and 40 ℃ were provided by a thermostatic bath Digital Plus RTE201 (Neslab) and a GTR 2000 Heater (Isco), respectively. The transmembrane flux was determined by using industrial balance with HDWE RS485 indicator, connecting to the distillate tank. SPER SCIENTIFIC 800012 Pt multi-channel thermocouples (T) with sensitivity ±0.1 ℃ was used to measure the temperatures.

4.4 Results and discussion

The morphology of precipitates showed in SEM micrographs of Figure 4.2 revealed the characteristic spherical shape of the vaterite crystals (average size ~ 4 μm) adhered at the microporous surface of polypropylene membrane, as also confirmed by X-Ray Diffraction exhibiting reflections for vaterite hkl: 110, 111, 112, 300, 302, 114, 222 [11].

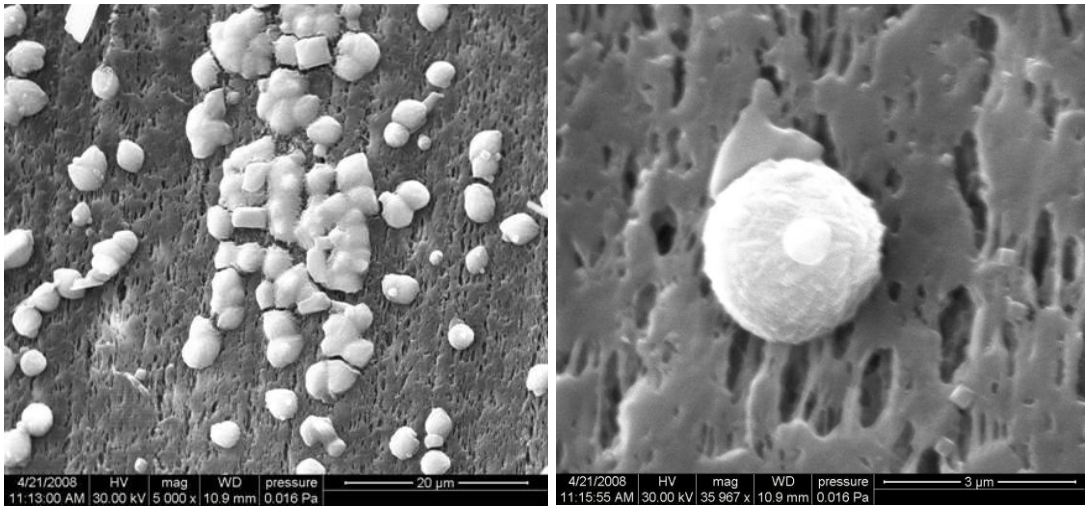

(a) **(b)**

Figure 4.2 SEM micrographs of vaterite spherules grown on the surface of a microporous polypropylene membrane at solution concentration factors of: (a) 4.5 at magnification 5000X; (b) 5.5 at magnification 36000X.

For crystals formed at seawater concentration factors varying from 4 to 6, the precipitation of calcium carbonate was detected in the form of vaterite, nucleation and growth kinetics were investigated in this range with respect to vaterite. Spanos and Koutsoukos (1998) observed in supersaturation at pH around 9 [12].

Our experimental observations well agree with the Ostwald's rule, at high supersaturation the less stable polymorph tends to precipitate, and the metastable vaterite prefers to form [13].

The induction time of calcium carbonate precipitation can be evaluate by DLS measurements, taken in correspondence of the detachment of particle size curves from time axis (when it is possible to observe particles after supersaturation has been imposed to the system).

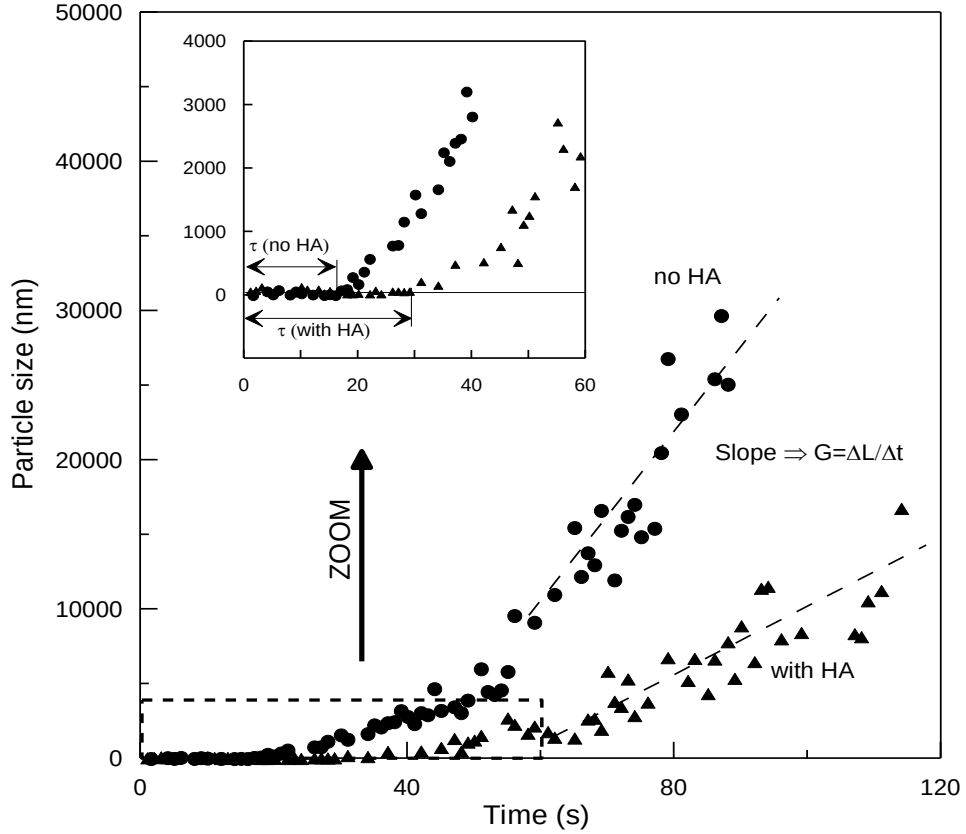

Figure 4.3 The average $CaCO_3$ particle diameter VS time (CF=4.5 and in presence of the membrane, by Dynamic Light Scattering)

In Figure 4.3 (CF=4.5), precipitation tests in presence of membrane resulted in an induction time of 16 seconds, indicating a fast $CaCO_3$ nucleation rate. Humic acid dissolved in solution kinetically inhibited heterogeneous nucleation: induction time increased up to 30 seconds, and the slope of the particle size curve (initial growth rate) was reduced by 67 % from 600 nm/s to 195 nm/s. The presence of micro-porous polypropylene hollow fibres significantly affected the precipitation kinetics of $CaCO_3$: spontaneous experiments carried out in absence of membrane showed that precipitation did not occur within the first 80 seconds of analysis, in substantial agreement with literature [14, 15].

In following Figure 4.4, the linear dependence between the inverse of $\ln^{-2}S$ (as from equation 6) and the logarithm of induction time is reported.

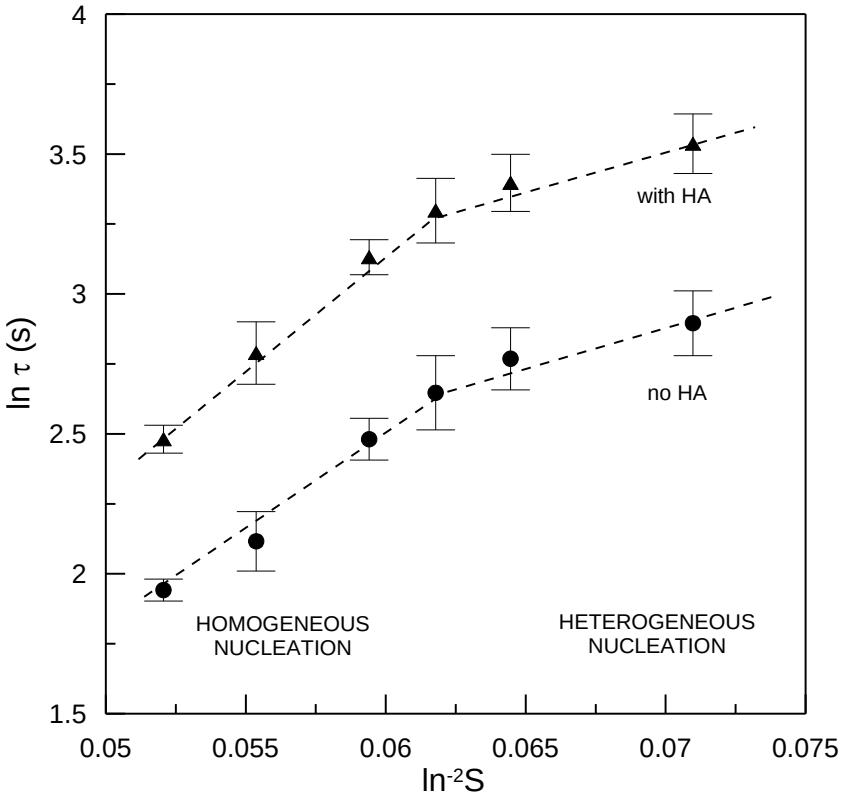

Figure 4.4 Induction time VS Supersaturation in vaterite precipitation

Solution supersaturation was evaluated with respect to vaterite. Changes of the slope reflected the shifting between homogeneous and heterogeneous nucleation mechanisms. Curves exhibited different slopes as a consequence of the inhibiting effect of humic acid on the $CaCO_3$ nucleation kinetics, at high supersaturation level (left side of the diagram); in particular, HA slightly increases the interfacial energy of vaterite by 7% c.a, specifically from 45 mJ/m^2 to 48 mJ/m^2.

It is prevailed the nucleation effect of the micro-porous membrane, at low supersaturation (right side of the diagram). The reduced influence of the chemistry of solution on the nucleation kinetics was experimentally confirmed by the evidence that slopes are substantially identical (independently from the presence or absence of humic acid), and resulting in an interfacial energy of 32 mJ/m^2.

Compared with the interfacial tension of 80 mJ/m^2 calculated for homogeneous vaterite nucleation by Sohnel and Mullin (1978) [16] and theoretically predicted as 90 mJ/m^2 by Kralj (1990) [17], all these values are substantially lower, both related to

homogeneous nucleation conditions as contrasted to our experiments, where the crystal phase is grown on a foreign substrate (the polymeric membrane). However, the values obtained in our study are comparable with those obtained by Gomez-Morales et al. (1996) [18], Verdoes et al. (1992) [19], and Kralj et al. (1990) [17], who reported experimental values of γ for vaterite equal to 40.7, 37.3 and 34 mJ/m^2, respectively. Assuming for calcite a molecular volume ν of $6.13 \cdot 10^{-29}$ m^3 (= molecular weight/(Avogadro's number*density*number of ions in a formula unit)), the experimentally evaluated surface energy values were used to investigate the Gibbs free energy (ΔG) as a function of the nucleus radius (Figure 4.5).

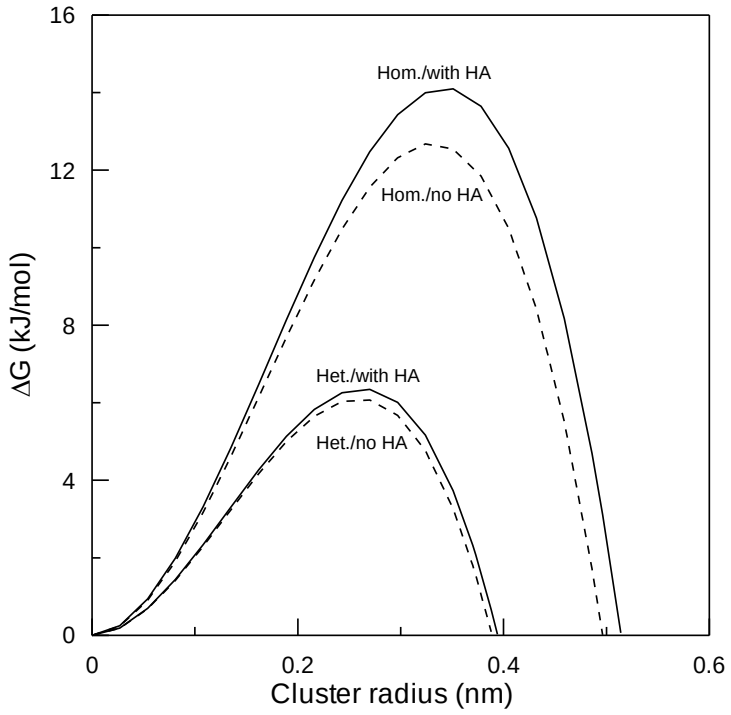

Figure 4.5 Gibbs free energy difference (ΔG) in homogeneous and heterogeneous crystallization of vaterite (CF=4.5)

From solution containing or not humic acid (HA), the coincidence of ΔG curves for heterogeneous nucleation of calcium carbonate crystals is a consequence of the substantially equal values of the corresponding surface energies γ.

The maximum of a ΔG curve corresponds to the energy barrier to overcome when a critical nucleus (having a 50 % of probability to grow or dissolve) is formed. For

calcium carbonate precipitation on Accurel by equation 3 using experimental values of γ for homogeneous (45 mJ/m^2) and heterogeneous (32 mJ/m^2) nucleation kinetics. Gibbs free energies' ratio was slightly reduced to 0.56 when vaterite was precipitated from supersaturated solutions (CF=4.5) containing humic acid as impurity.

Our experimental results also agreed with the expectation that polymeric substrate improves the inhibition effect due to the interaction of HA with calcite crystals nucleating on the membrane surface; moreover, this phenomenon might be also accentuated by concentration polarization phenomena occurring in proximity of the membrane interface.

PP membranes in absence of humic acid, the predicted $\Delta G_{heterogeneous}$ / $\Delta G_{homogeneous}$ ratio (porosity: 0.70, contact angle: 115±2 °) is 0.55, in good agreement with the value of 0.58 calculated.

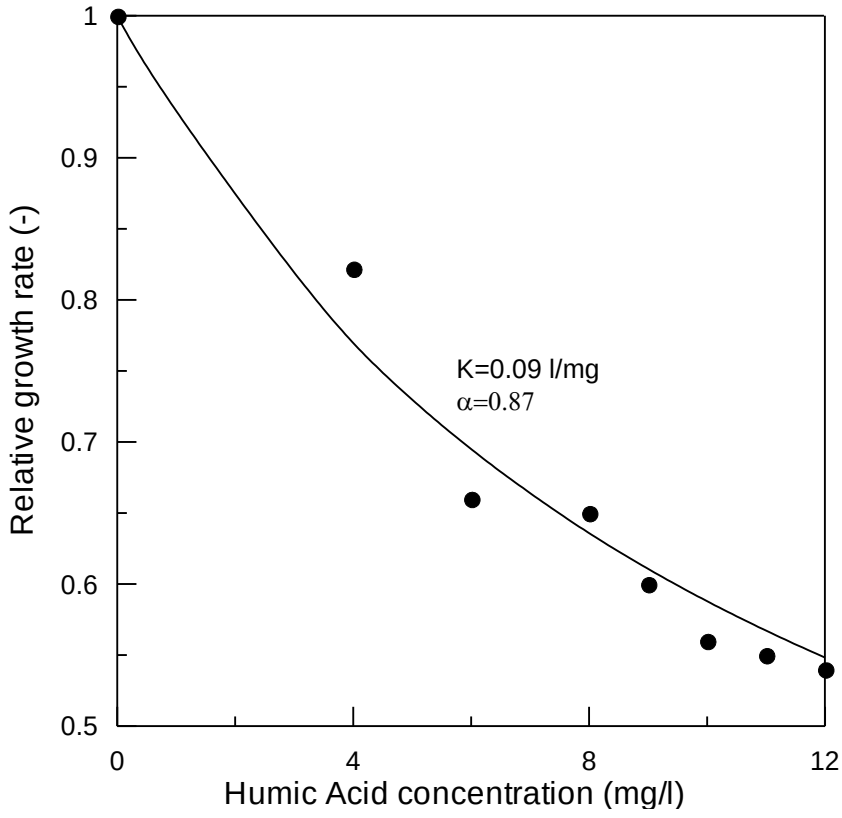

Figure 4.6 Relative growth rate of vaterite (CF=4.5) as a function of humic acid concentration in presence of the membrane

As reported in Figure 4.6, the initial growth rate decreased by 60 % (from $5.3 \cdot 10^{-7}$ to $2.1 \cdot 10^{-8}$ m/s) when humic acid was added to supersaturated solution (CF=4.5). The retarding effect on the growth rare of calcite, due to the presence of citric acid, diethylenetriaminepentaacetic acid (DTPA) and ethylenediaminetetraacetic acid (EDTA), was studied by Westin et al. (2005) [20]; according to their results, the observed retardation at moderate additive concentration (0.04 mmol/L) was around 30 %. From the literature, it is proved that different humic substances (including fulvic acid, humic acid, humin) have dissimilar inhibition effects on calcite crystal growth rate; dissolved organic matter (DOM) insulated from Florida Everglades and Lake Fryxell (Anatrctica) resulted in a $CaCO_3$ rate reduction scattering in the range of 20-80 % at DOM concentration within 1-2 mg/L [21].

Under the assumption that impurities adsorbed at the crystal surface prevent the step advancement during layer growth, the Cabrera-Vermilyea model [22] modified by Kubota and Mullin [19] was used to correlate the relative growth rate (G/G0) to the concentration of HA (c):

$$\frac{G}{G_0} = 1 - \alpha \frac{Kc}{1 + Kc} \tag{4.7}$$

where α is an effectiveness factor ($\alpha \rightarrow 1$ if the relative growth rate approaches zero for increasing coverage) and K is the Langmuir constant. The calculated K was 0.09 L/mg (α=0.87) for vaterite crystals grown in presence of a polymeric membrane. This value, if compared to data reported by Westin et al. (2005), is higher than those found for CIT, DTPA and EDTA (0.07, 0.019 and 0.027 L/mg, respectively) [20], so suggesting that $CaCO_3$ growth is affected by surface adsorption of HA and, in major extent, when crystals nucleation and growth is mediated by a membrane surface.

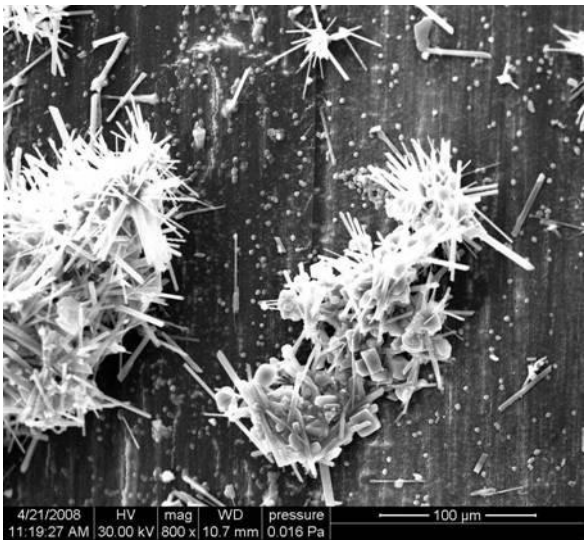

Figure 4.7 SEM micrograph of mixed calcite and gypsum crystals grown on the surface of a microporous polypropylene membrane at solution concentration factors of 8 (magnification 30000X)

A qualitative investigation carried out at concentration factors > 7 (a SEM micrograph at CF=8 is showed in Figure 4.7) reported the presence of crystals exhibiting long needle shape structures (average length ~ 70 μm) typical of calcium sulphate dehydrate in concomitance with $CaCO_3$ deposited on the polypropylene membrane in the form of calcite. These precipitates, characterized by a bimodal crystal size distribution, were excluded from a quantitative kinetic analysis.

At present, systematic studies on the complex phenomena related to combined inorganic fouling in membrane operations are still lacking. Sheikholeslami and Ong (2003) [24] found, although limited to the chemistry of saline solutions, seem to prove that $CaCO_3$ crystals grow without suffering important interferences due to $CaSO_4 \cdot 2H_2O$ crystals because of the higher induction period of gypsum with respect to calcite. Moreover, results showed that the induction period of $CaSO_4 \cdot 2H_2O$ was delayed significantly as the concentration of NaCl increases (and, in general, at increasing solution ionic strength).

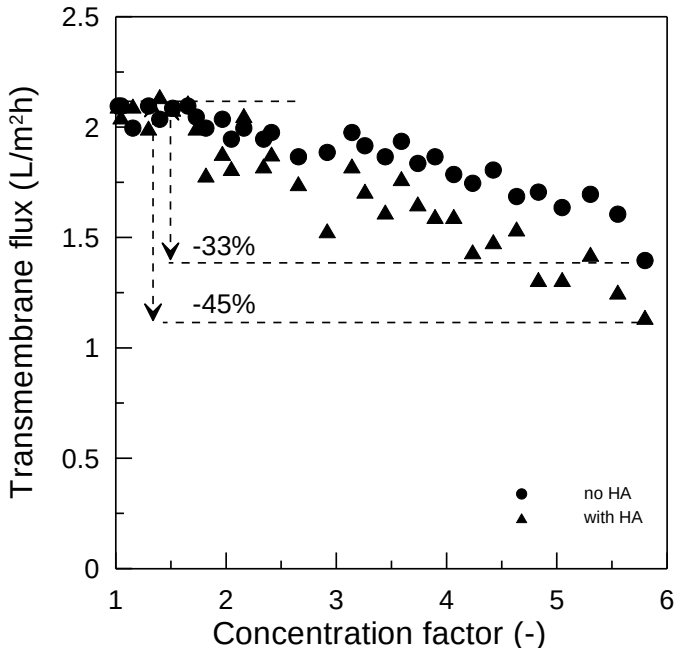

Figure 4.8 Transmembrane flux VS concentration factor in MD test ($T_{feed,in}$=40 ℃ and $T_{permeate,in}$=20 ℃)

In Figure 4.8, flux data from DCMD tests, carried out under a temperature gradient of ~20 ℃ and flowrates of 7 L/min (set equal for both feed and permeate streams), operated over 35 hours. The initial value of permeate flux, substantially not sensitive to the presence of humic acid (2 mg/L) in the feed water, was 2.05±0.05 L/m^{2}h. The progressive deterioration of the MD performance at increasing retentate concentrations is - in most part - due to both progressive reduction of the solution activity coefficients (and, consequently, of the driving force) [25] and to $CaCO_3$ scaling. The permeate flux was reduced by 33 % down to value of 1.40 L/m2h when at concentration factor of 5.8.

At higher concentration factors (>2), the detrimental effect of humic acid (HA) on the trans-membrane flux becomes significant. The permeate rate decreased down to 1.14 L/m^2 h corresponding to a reduction of 45%, at the end of the test. Yuan and Zydney (1999) [26] observed an analogous exacerbation of HA fouling at higher concentration (and, therefore, higher ionic strength), as a consequence of the increased electrostatic shielding among the charged HA molecules that caused a low-permeable deposit on the membrane surface.

The critical influence of dissolved salts appears clearly the same as Khayet et al. (2004) [4] observed a flux decline of only 4.8 % during DCMD tests with water-humic acid solutions (30 mg/mL) using TF200 polytetrafluoroethylene membranes. In particular, divalent ions such as Ca^{2+} considerably affect HA fouling, since they act as binding agents of carboxyl functional groups; Srisurichan and colleagues (2005) [27] found the trans-membrane flux reduction of about 40 % in DCMD tests when operating with solution of humic acid (100 mg/L) and $CaCl_2$ (3.775 mM).

UV-VIS absorbance measurements (at 290 nm) and electrical conductivity of the permeate solutions provided the stability of hydrophobic polypropylene membranes: both analyses excluded the contamination of the distillate due to dissolve HA and salts, respectively.

Two-step cleaning with citric acid aqueous solution at pH 4 (20 min) / 0.1M NaOH aqueous solution (20 min), being each step preceded and followed by extensive washing with deionized water (2 hours), allowed to completely restore the transmembrane flux and the hydrophobicity of the membrane. Srisurichan S (2005) [27] also confirmed the high efficiency of basic cleaning procedure against the deposit of HA, as a consequence of HA dissolution at pH higher than 6. On the other hand, Gryta (2008) [3] recognized the possibility to remove almost completely $CaCO_3$ deposit from polypropylene membranes by using acid solutions.

4.5 Conclusions

The results of this experimental research emphasise the significant role played by microporous membranes in the heterogeneous nucleation mechanisms that control scaling in Membrane Distillation. Not only supersaturation, that depends on the chemistry of the solutions and is partially affected by concentration polarization phenomena, but also morphological and physico-chemical properties of the membrane are important issues in the understanding of the complex phenomena of inorganic fouling.

Induction times, determined by DLS measurements, are significantly reduced if

precipitation occurs in presence of membranes, thus causing an increase of the $CaCO_3$ nucleation rate. In this respect, experimental data are, in part, supported by theoretical predictions of the Gibbs free energy barrier to the formation of critical nuclei, as a function of porosity and contact angle of the solutions.

DCMD tests, carried out on a semi-pilot plant and operated up to 35 hours, demonstrated that scaling significantly reduces the transmembrane permeate flux by 33 %. Humic acid, even at low concentration, retarded the nucleation and growth of vaterite crystals at low supersaturation; on the other side, $CaCO_3$ deposition on the membrane surface (exacerbated at high ionic strength) also contributed – with minor extent with respect to scaling - to decrease the system performance.

References:

[1] F. He, J. Gilron, H. Lee, L. Song, K.K. Sirkar. Potential for scaling by sparingly soluble salts in crossflow DCMD. J. Membrane Sci., 2008, 311: 68-80.

[2] K. Karakulski, M. Gryta. Water demineralisation by NF/MD integrated processes. Desalination, 2005, 177: 109-119.

[3] M. Gryta. Fouling in direct contact membrane distillation process. J. Membrane Sci., 2008, 325: 383-394.

[4] H. Khayet, A. Velazquez, J.I. Mengual. Direct contact membrane distillation of humic acid solutions. J. Membrane Sci., 2004, 240: 123-128.

[5] J.W. Mullin, Crystallization. Butterworth-Heinemann, Oxford, 1993.

[6] G. Madras, B. J. McCoy. Transition from nucleation and growth to Ostwald ripening. Chem. Eng. Sci., 2002, 57: 3809-3818.

[7] J. Gomez-Morales, J. Torrent-Burgues, R. Rodriguez-Clemente. Nucleation of calcium carbonate at different initial pH conditions. J. Crystal Growth, 1996, 169: 331-338.

[8] K.-J. Westin, A.C. Rasmuson. Nucleation of calcium carbonate in presence of citric acid, DTPA, EDTA and pyromellitic acid. J. Colloid and Interface Sci., 2005, 282: 370-379.

[9] E. Curcio, E. Fontananova, G. Di Profio, E. Drioli. Influence of the structural properties of poly(vinylidene fluoride) membranes on the heterogeneous nucleation rate of protein crystals. J. Phys. Chem. B, 2006, 110: 12438-12445.

[10] http://www.lwr.kth.se/English/OurSoftware/vminteq/

[11] M. Sato, S. Matsuda. Structure of vaterite and infrared spectra. Zeitschrift fur Kristallographie, 1969, 129: 405-410.

[12] N. Spanos, P. G. Koutsoukos, Kinetics of Precipitation of Calcium Carbonate in Alkaline pH at Constant Supersaturation. Spontaneous and Seeded Growth, J. Phys. Chem. B 1998, 102: 6679-6684

[13] Y. S. Han, G. Hadiko, M. Fuji, M. Takahashi. Crystallization and transformation of vaterite at controlled pH. J. Crystal Growth, 2006, 289: 269–274.

[14] L. F. Olsson. Induction time of precipitation of calcium carbonate. J. Molecular Liquids, 1995,

65/66: 349-352.

[15] M.G. Lioliou, C. A. Paraskeva, P. G. Koutsoukos, A. C. Payatakes. Heterogeneous nucleation and growth of calcium carbonate on calcite and quartz. J. Colloid and Interface Sci., 2007, 308: 421-428.

[16] Sohnel, O., Mullin, J.W. A method for the determination of precipitation induction periods. J. Crystal Growth,1978, 44: 377–382.

[17] Kralj, D.; Brecevic, L.; Nielsen, A. E. Vaterite Growth and Dissolution in Aqueous Solutions. I. Kinetics of Crystal Growth. J. Crystal Growth, 1990, 104: 793-800.

[18] J. Gomez-Morales, J. Torrent-Burgues, R. Rodriguez-Clemente. Nucleation of calcium carbonate at different initial pH conditions. J. Crystal Growth,1996, 169: 331-338.

[19] D. Verdoes, D. Kaschiev, G.M. Van Rosmalen. Determination of nucleation and growth rates from induction times in seeded and unseeded precipitation of calcium carbonate. J. Crystal Growth, 1992, 118: 401-413.

[20] K.-J. Westin, A. C. Rasmuson. Crystal growth of aragonite and calcite in presence of citric acid (CIT), DTPA, EDTA and pyromellitic acid. J. Colloid. Interf. Sci., 2005, 282: 359-369.

[21] A. R. Hoch, M. M. Reddy, G. R. Aiken. Calcite crystal growth inhibition by humic substances with emphasis on hydrophobic acids from the Florida Everglades. Geochimica et Cosmochimica Acta, 2000, 64: 61-72.

[22] L. Wang, J. J. De Yoreo, X. Guan, S. R. Qiu, J. R. Hoyer, G. H. Nancollas, Constant Composition studies verify the utility of the Cabrera−Vermilyea (C-V) Model in explaining mechanisms of calcium oxalate monohydrate crystallization. Crystal Growth & Design, 2006, 6/8: 1769-1775.

[23] N. Kubota, J.W. Mullin. A kinetic model for crystal growth from aqueous solution in the presence of impurity. J. Crystal Growth, 1995, 152: 203-208.

[24] R. Sheikholeslami, H. W. K. Ong. Kinetics and thermodynamics of calcium carbonate and calcium sulphate at salinities up to 1.5 M. Desalination, 2003, 157: 217-234.

[25] L. Mariah L., C. A. Buckley, C. J. Brouckaert, E. Curcio, E. Drioli, D. Jaganyi, D. Ramjugernath. Membrane distillation of concentrated brines. Role of water activities in the evaluation of driving force. J. Membrane Sci., 2006, 280: 937-947.

[26] W. Yuan, A. L. Zydney. Effect of solution environment on humic acid fouling during

microfiltration. Desalination, 1999, 122: 63-76.

[27] S. Srisurichan, R. Jiraratananon, A. G. Fane. Humic acid fouling in the membrane distillation process. Desalination, 2005, 174: 63-72.

[28] HydroGeoLogic Inc., Allison Geoscience Consultants Inc. MINTEQA2/PRODEFA2, a geochemical assessment model for Environmental systems: User Manual Supplement for Version 4.0; U.S. Environmental Protection Agency: Athens, GA, 1999.

Appendix A

Below are listed equilibrium constants at 40 ℃ for the different components of the system, as from MINTEQA2 database [28] included with the speciation software Visual MINTEQ (latest version 2.61, released on April 2009) [10].

$H_2O = OH^- + H^+$	log K = -13.53
$H^+ + CO_3^{2-} = HCO_3^-$	log K = -10.21
$2H^+ + CO_3^{2-} = H_2CO_3(aq)$	log K = 16.41
$Ca^{2+} + Cl^- = CaCl^+$	log K = 0.43
$Ca^{2+} + CO_3^{2-} = CaCO_3(aq)$	log K = 3.35
$Ca^{2+} + HCO_3^- = CaHCO_3^+$	log K = 11.434
$Ca^{2+} + OH^- = CaOH^+$	log K = -12.158
$Ca^{2+} + SO_4^{2-} = CaSO_4(aq)$	log K = 2.42
$H^+ + SO_4^{2-} = HSO_4^-$	log K = 2.175
$K^+ + Cl^- = KCl(aq)$	log K = -0.334
$K^+ + OH^- = KOH(aq)$	log K = -13.288
$K^+ + SO_4^{2-} = KSO_4^-$	log K = 0.884
$2Mg^{2+} + CO_3^{2-} = Mg_2CO_3^{2+}$	log K = 3.59
$Mg^{2+} + Cl^- = MgCl^+$	log K = 0.633
$Mg^{2+} + CO_3^{2-} = MgCO_3(aq)$	log K = 3.00
$Mg^{2+} + HCO_3^- = MgHCO_3^+$	log K = 11.26
$Mg^{2+} + OH^- = MgOH^+$	log K = -10.85
$Mg^{2+} + SO_4^{2-} = MgSO_4(aq)$	log K = 2.309
$Na^+ + Cl^- = NaCl(aq)$	log K = -0.367
$Na^+ + CO_3^{2-} = NaCO_3^-$	log K = 1.099
$Na^+ + HCO_3^- = NaHCO_3(aq)$	log K = 9.791
$Na^+ + OH^- = NaOH(aq)$	log K = -13.394
$Na^+ + SO_4^{2-} = NaSO_4^-$	log K = 0.748
$Ca^{2+} + SO_4^{2-} = Anhydrite$	log K = -4.387

$Ca^{2+} + CO_3^{2-}$ = Aragonite	log K = -8.318
$Mg^{2+} + CO_3^{2-} + 2OH^- + 3H_2O$ = Artinite	log K = 8.591
$Mg^{2+} + 2OH^-$ = Brucite	log K = 16.14
$Ca^{2+} + CO_3^{2-} + H_2O = CaCO_3 \cdot H_2O$	log K = -7.300
$Ca^{2+} + CO_3^{2-}$ = Calcite	log K = -8.411
$Ca^{2+} + Mg^{2+} + CO_3^{2-}$ = Dolomite (disordered)	log K = -16.93
$Ca^{2+} + Mg^{2+} + CO_3^{2-}$ = Dolomite (ordered)	log K = -17.42
$Mg^{2+} + SO_4^{2-} + 7H_2O$ = Epsomite	log K = -2.029
$Ca^{2+} + SO_4^{2-} + 2H_2O$ = Gypsum	log K = -4.513
$Na^+ + Cl^-$ = Halite	log K = 1.518
$3Mg^{2+} + Ca^{2+} + 4CO_3^{2-}$ = Huntite	log K = -30.67
$5Mg^{2+} + 4CO_3^{2-} + 2OH^- + 4H_2O$ = Hydromagnesite	log K = -10.60
$K^+ + Cl^-$ = KCl	log K = -12.46
$Ca^{2+} + 2OH^-$ = Lime + H_2O	log K = 31.07
$Mg^{2+} + CO_3^{2-}$ = Magnesite	log K = -7.293
$Mg^{2+} + 2OH^-$ = $Mg(OH)_2$ (active)	log K = 18.79
$2\ Mg^{2+} + Cl^- + 3OH^- + 4H_2O = Mg_2(OH)_3Cl \cdot 4H_2O$	log K = 26.00
$Mg^{2+} + CO_3^{2-} + 5H_2O = MgCO_3 \cdot 5H_2O$	log K = -4.540
$2Na^+ + SO_4^{2-} + 10H_2O$ = Mirabilite	log K = -0.447
$2Na^+ + CO_3^{2-} + 10H_2O$ = Natron	log K = -0.758
$Mg^{2+} + CO_3^{2-} + 3H_2O$ = Nesquehonite	log K = -4.874
$Mg^{2+} + 2OH^-$ = Periclase + H_2O	log K = 20.32
$Ca^{2+} + 2OH^-$ = Portlandite	log K = 21.62
$2Na^+ + SO_4^{2-}$ = Thenardite	log K = 0.245
$2Na^+ + CO_3^{2-} + H_2O$ = Thermonatrite	log K = 0.549
$Ca^{2+} + CO_3^{2-}$ = Vaterite	log K = -8.051

Acid-base dissociation

$(HumH)^{Z} = (Hum)^{Z-1} + H^{+}$

for 8 acid sites:

i=1-4; $\log K_i = \log K_A + \frac{(2i-6)}{6}\Delta pK_A$

i=5-8; $\log K_i = \log K_B + \frac{(2i-13)}{6}\Delta pK_B$

$\log K_A$=-4.13, $\log K_B$=-8.99, ΔpK_A=3.03, ΔpK_B=3.03.

Monodentate cation complexation in Stockholm Humic Model (SHM)

$Ca^{2+} + RH = RCa^{+} + H^{+}$ $\log K_m$=-1.9, ΔLK_2=0.3

$Mg^{2+} + RH = RCa^{+} + H^{+}$ $\log K_m$=-2.3, ΔLK_2=0.3

$\log K_{m,x} = \log K_m + x \cdot \Delta LK_2$

CHAPTER FIVE

The effect of sulfate in Nanofiltration-Membrane Crystallization system

5.1 Introduction

Although sodium sulfate is environmentally safe [1] and does not create serious problems, continuous disposal of the wastewater stream may have long term effects. It is necessary to explore feasible methods of treatment and separation of sodium sulfate and investigate the possibility of recycling and marketing.

Membrane technology, because of its intrinsic characteristics of high separation efficiency, low energy consumption, possibility to combine membrane operations in integrated systems, environmental compatibility, and easy scale-up, might offer interesting options to solve this problem [2, 3]. Recently, Bargeman et al. (2009) proposed the use of Nanofiltration (NF) for the production of brines supersaturated in Na_2SO_4; crystallization is then induced in a separate crystallizer outside of the membrane unit by addition of crystal seeds [4].

The concept of membrane crystallization as evaporative process based on the use of microporous hydrophobic membranes has been rationalized by Curcio et al. (2001) [5]. In this innovative unit, chemical-physical properties of the membrane and operating conditions play a key role in two important aspects:

(1) To control supersaturation through evaporation rate of volatile solvent molecules across the membrane according to the principles of membrane distillation [6];

(2) To control nucleation and growth kinetics of crystals [7];

A membrane crystallizer is usually operated at moderate temperatures and low thermal energy is required to warm up the feed solution. Membrane crystallization (MC) process has been tested by Tun et al. (2005) on sodium sulphate; it was confirmed the possibility to operate at high concentrations at feed temperatures of 50 ℃ and 60 ℃ with fluxes up to 20 $L\,m^{-2}\,h^{-1}$ [8].

The synergic effects of a hybrid NF-MC system operated on seawater brines have

been investigated by Drioli et al. (2004): crystallization tests carried out on nanofiltration retentates resulted in the production of sodium chloride and epsomite [9].

In this work, the experimental investigation aims at recovering sodium sulfate by evaporative crystallization through microporous hydrophobic membranes; in order to reduce the load to the membrane crystallizer unit, nanofiltration is used as pre-concentration stage.

5.2 Materials and Methods

Test solutions were prepared by dissolving reagent-grade anhydrous Na_2SO_4 (code n. 375714, Carlo Erba, Italy) in demineralized water (ELGA Labwater Option-S 7BP) with initial concentration of 60 g/L. Nanofiltration tests were carried out in a lab-scale NF unit MATRIX (Matrix desalination Inc.) equipped with three FilmTec^{TM} Nanofiltration Membrane Elements NF90-2540 (2.5"x 40", nominal active surface area: 2.6 m^2) with stabilized rejection (solution test 2,000 ppm NaCl) of 85-95 % (as reported by the manufacturer) at test pressure pf 70 psig. The membrane modules were arranged in parallel configuration. NF pre-concentration tests were carried out at 30 ℃ in complete recycle of retentate until reaching a permeate recovery factor of 50%.

Block flow diagram of the process is shown in Figure 5.1. The concentrated solution is sent to membrane crystallization which is a semi-pilot plant as depicted in Figure 5.2 [10]. Feed and distillate streams were recirculated by Gear Metering Pump Serie N (Pompe Cucchi) with AC Tech Controller, and by Centrifugal Electropump CEA (Lowara), respectively. A thermostatic bath Digital Plus RTE201 (Neslab) and a Julabo Model ED Heating Bath Circulator provided the maintenance of distillate and feed temperatures at the inlet of the membrane module (Accurel PP polypropylene hollow fiber, total membrane area of 0.4 m^2). Temperature at the crystallization tank was set to 35 ℃. Industrial balance with HDWE RS485 indicator connected to the distillate tank was used to estimate the permeate flux. Temperatures were monitored

by SPER SCIENTIFIC 800012 Pt multi-channel thermocouples with sensitivity ±0.1℃, and flowrates measured by F14 flowmeters (Blue-White Industries, Ltd). LabVIEW Control Design Toolkit (National Instruments) was used to implement the automatic plant control.

NF and MDC permeate conductivity was measured by YSI 3200 Conductivity Instruments based on Resistance Ratio Technology. The X-Ray diffraction pattern of the crystalline product was collected using CuKα radiation (Philips Model PW 1730/10 generator equipped with a PW 1050/70 vertical goniometer).

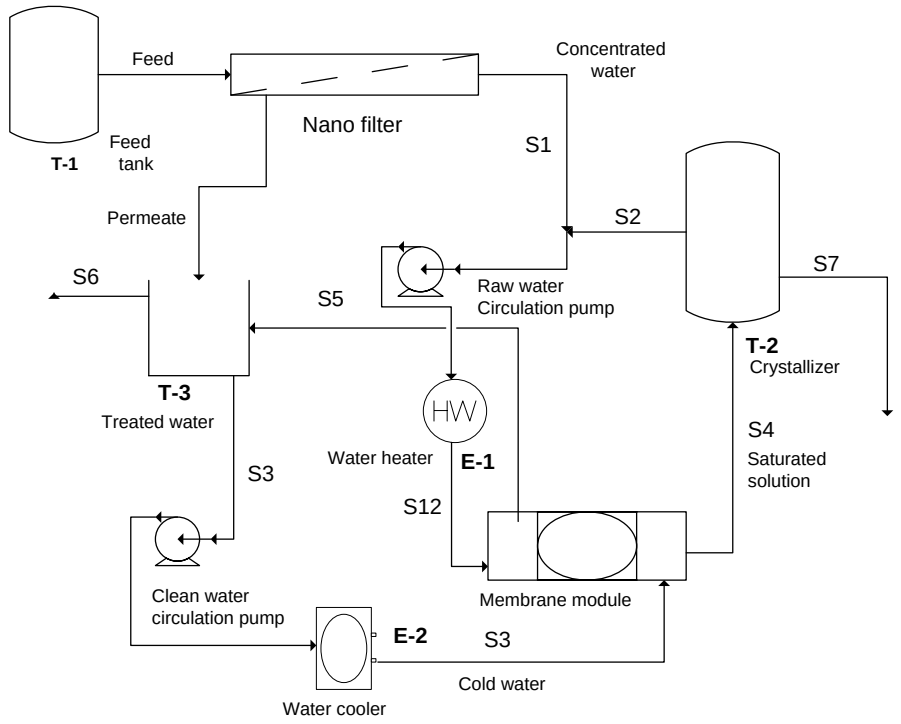

Figure 5.1 Block flow diagram of the experimental setup (S1: concentrated water; S2: recycle stream from crystallizer; S3: cold water; S4: saturated solution; S5: permeate stream; S6: clean water; S7: sodium sulfate crystals; T1: wastewater tank; T2: crystallizer; T3: treated water tank; E1: heater; E2: cooler).

Figure 5.2 Membrane crystallization plant

5.3 Results and discussion

During batch-scale nanofiltration tests, NF90 modules showed excellent performance in terms of Na_2SO_4 rejection (higher than 99 % at operative pressures above 350 psi), that progressively increased at higher feed pressure. The results summarized in Table 5.3 are comparable with the rejection value of 99.7 in the range of 689-1013 kPa reported by Kosutic et al. (2004) for FilmTec^{TM} NF270 [11].

Transmembrane fluxes exhibited the usual linear trend versus pressure (regression of data in Table 5.3 results in R^2=0.986); due to osmotic effect, permeate flux was null for pressures lower than 260 psi. Pre-concentration batch tests were carried out at 500 psi, pH=6.5 and 35 ℃, and protracted until achieving a recovery factor of 50 % (final Na_2SO_4 concentration: 120 g/L). The permeate flux decreased progressively from the initial value of 17.3 L/m^{2}h to almost zero; the retentate solution was fed to the membrane crystallization lab-scale plant for further treatment.

Table 5.3 Nanofiltration rejection test (Na_2SO_4 concentration of feed solution: 60 g/L)

Pressure (psi)	Permeate flux (l/m^{2}h)	Rejection (%)
300	2.61	97.3
350	6.38	99.1
400	11.5	99.4
450	14.6	99.5
500	17.3	99.6

Table 5.3 well exemplifies the dependence of the transmembrane flux of solvent on the feed-distillate temperature difference which is the driving force of the evaporation process. At temperature gradient ΔT of 5 ℃ (T_{feed}=30 ℃ and $T_{distillate}$=25 ℃), the water flux scattered around 0.57±0.07 kg/m^{2}h, a value not practical for large-scale applications. When feed temperature was increased to 40 ℃ (ΔT=12 ℃) the transmembrane flux enhanced by 156 %, reaching an average value of 1.46 ±0.19 kg/m^{2}h. According to conductivity measurements on the permeate solution (<0.6 μS/cm), no loss of membrane hydrophobicity was observed over 2 days of uninterrupted operation. Moreover, the evaporation flux remained stable to a value of 1.6 kg/m^{2}h over the crystallization period.

Detectable sodium sulfate crystals were observed after 46 hours; in all experimental tests, the crystallization operation was protracted for two hours since the appearance of first crystals, up to a Na_2SO_4 supersaturation of 3.93 mol kg^{-1} (corresponding to a supersaturation ratio of 0.05).

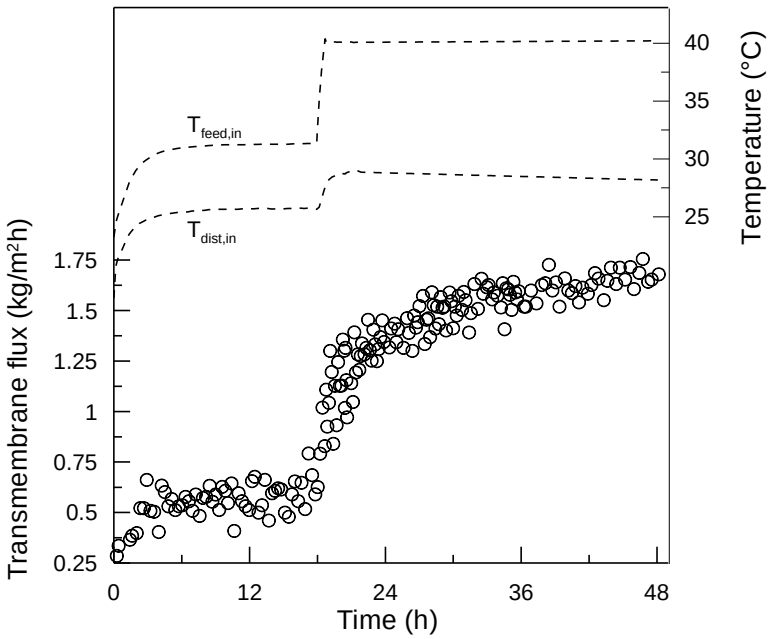

Figure 5.4 Transmembrane flux and inlet feed and distillate temperature profiles versus time.

The population density distribution of Na_2SO_4 crystals (that is the number of crystals per particle size per volume of solution) produced in membrane crystallization batch tests is reported in Figure 5.4 at four time intervals comprised between 30 minutes and 2 hours of operation. Tun et. al (2005), who firstly carried out membrane distillation-crystallization tests on sodium sulfate, reported a value of about 10 #/mm cm^3 (corresponding to ~ 16.9 #/mm dm^3) at 45 minutes and crystal length of 100 μ, that is in good agreement with the value of 16.5 #/mm dm^3 found in our study at 30 minutes and same crystal length [8]. The almost linear shape of population density curves suggests that the behavior of our membrane crystallization system resembles that of evaporative crystallizers described by Mixed Suspension Mixed Product Removal (MSMPR) [12]. A possible explanation is that, under the selected operating conditions, the progressive desupersaturation consequent to crystal formation is counter-balanced by the transmembrane flux, thus resulting in a process with supersaturation able to reach a profile almost constant in time.

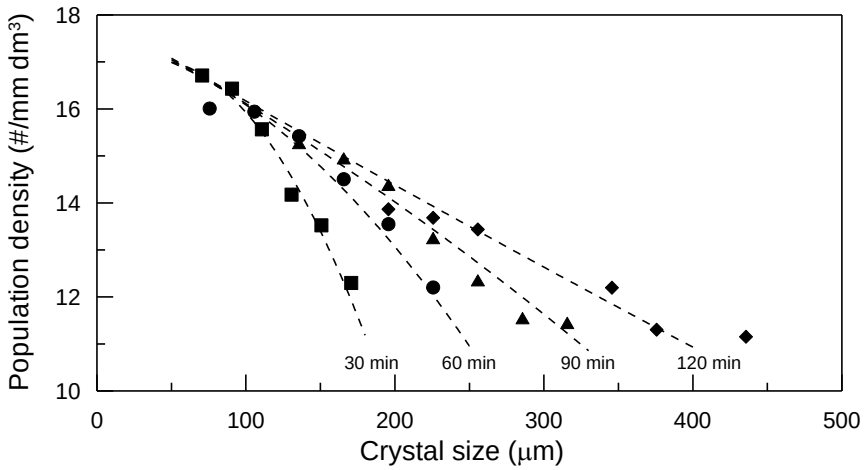

Figure 5.5 Population density vs crystal size as measured within 2 hours. Dashed lines are guide to eyes.

The crystals length distribution at 30 minutes (Figure 5.6), comprised between 45 μm and 165 μm, is comparable with data reported by Klug et al. (1989) in a flow-cell batch crystallization operated at higher supersaturation ratio (0.088) and temperature (61 ℃) [13]. This result proves the accelerated crystallization kinetics observed in the membrane crystallizer, as an effect of the heterogeneous nucleation occurring at the polymeric surface of the membrane. In general, the mean crystal size increased form 84.5 μm at 30 min to 170 μm at 120 min. Na_2SO_4 crystals exhibited the conventional elongated habit with orthorhombic symmetry and shape factor of about 0.65. A linear growth rate of 1.56 10^{-8} m/s has been calculated by optical-microscopy observations carried out every 30 minutes on crystalline samples.

The coefficient of variation (CV), defined as the ratio of standard deviation to mean value, is an industrially relevant parameter since it measures the scatter of crystal product size around its mean: a low CV corresponds to a narrow CSD curve. Crystal samples collected at 30 minutes showed the lowest CV (23 %); this good result is comparable with a CV interval of 20-30 % for $Na_2SO_4 \cdot 10H_2O$ reported in [14]. The dispersion of CSD increases with time and reaches a constant value of 40±1 % after 90 minutes (typical residence times in industrial crystallizers). As a comparison, the coefficient of variation for ideal MSMPR is 50 % for size-independent growth, but becomes significantly higher for size-dependent growth [12].

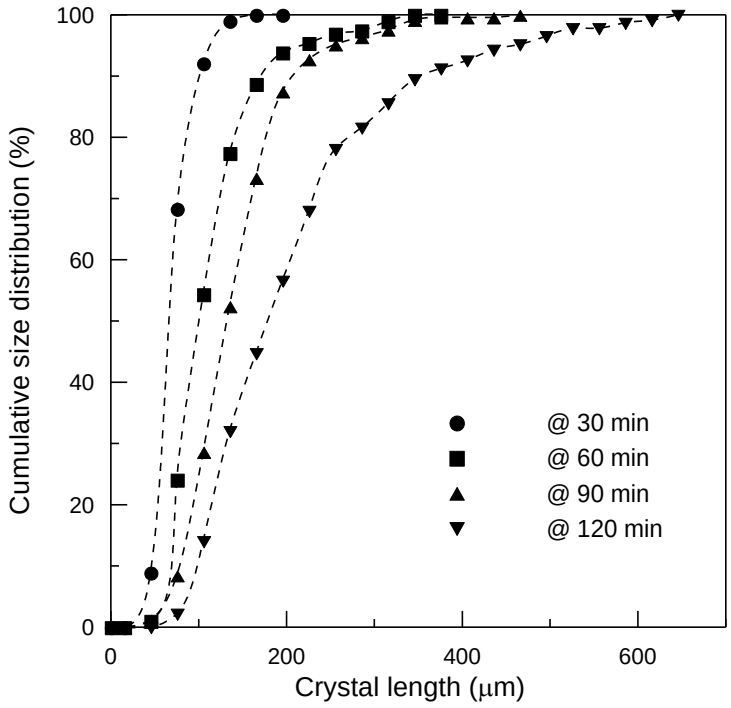

Figure 5.6 Cumulative size distribution of the crystalline product

The increase with time of slurry density is depicted in Figure 5.7; experimental data exhibit an almost linear trend within the first hour of operation, with rate of 0.31 kg/m^{3}h of crystals produced, followed by a smooth increase up to a final detected value of 21 kg/m^3. As a term of comparison, typical slurry density of Glauber salt (the decahydrate form of sodium sulfate, where water amounts to somewhat more than 55 per cent) in conventional evaporative crystallizer spans within 4-25 % wt for a residence time over the range of 0.56-1.25 hours [14].

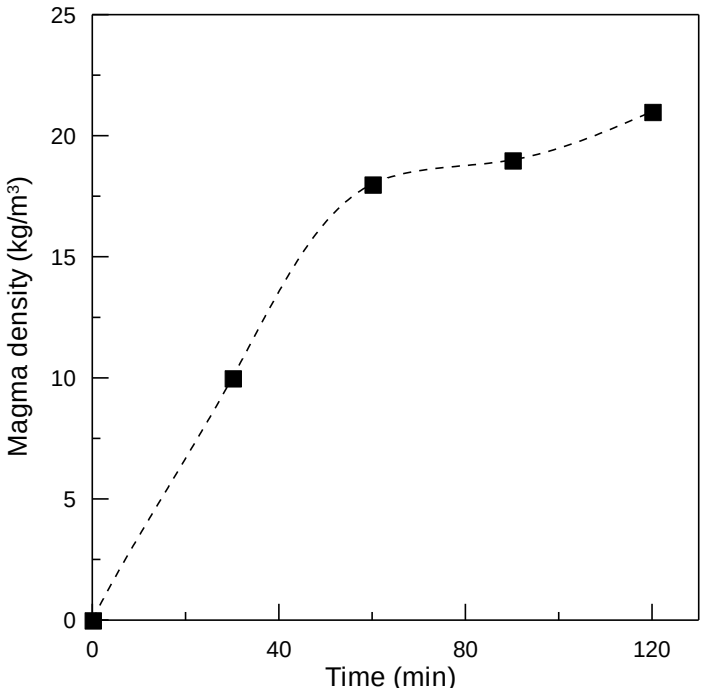

Figure 5.7 Increase in time of the magma density.

The XRD pattern of the solid product shown in Figure 5.8 reveals that crystals are of the anhydrous form of sodium sulfate (through peaks observed at 2θ degree: 18.5 °, 23.2 °, 28.1 °, 29.0 °, 33.9 °, 38.7 ° and maximum intensity at 32.2 °), as from matching it with JCPDS standard 36-0397 of thenardite [15]. No hydration of thenardite Na_2SO_4(V) to mirabilite $Na_2SO_4 \cdot 10H_2O$ (the only stable phases at temperatures close to ambient), or formation of the metastable anhydrous form Na_2SO_4(III), was observed under the crystallization conditions investigated. In the latter case, however, investigations of Xu and Schweiger [16] suggested that the presence of small amounts of water can cause the complete conversion of form III to form V. These observations are not trivial: recent studies demonstrated that Na_2SO_4 phase transition reactions are closely related to the generation of deleterious high stresses and damage in porous materials: In particular, Steiger predicted a crystallization pressure of 9 MPa for Na_2SO_4 crystals confined in a porous structure growing from a supersaturated solution with molality of 3.9 mol kg^{-1}, limiting condition at which thenardite and mirabilite exhibit the same solubility [17].

The precipitation of thenardite from solution at temperatures above 32.4 ℃ is also

reported in Rodriguez-Navarro et al. (2000) [18]. In our work, batch crystallization experiments were extended up to a Na_2SO_4 supersaturation of 3.93 mol kg-1, slightly exceeding the previously mentioned limiting value. In this situation, confined mirabilite crystal is not stable any more with respect to dehydration, confirming the experimental findings that solid phase is only thenardite.

The cleaning procedure at the end of each crystallization test, mainly consisting in extensive washing with de-mineralized water, has been carried out at temperature above 35 ℃ in order to avoid membrane damage due to mechanical stress induced by volume expansion of hydrated forms that might crystallize inside the porous structure (conversion from thenardite to mirabilite causes a volume expansion of 314 % [19]). After cleaning, both hydrophobic character and permeability have been completely restored.

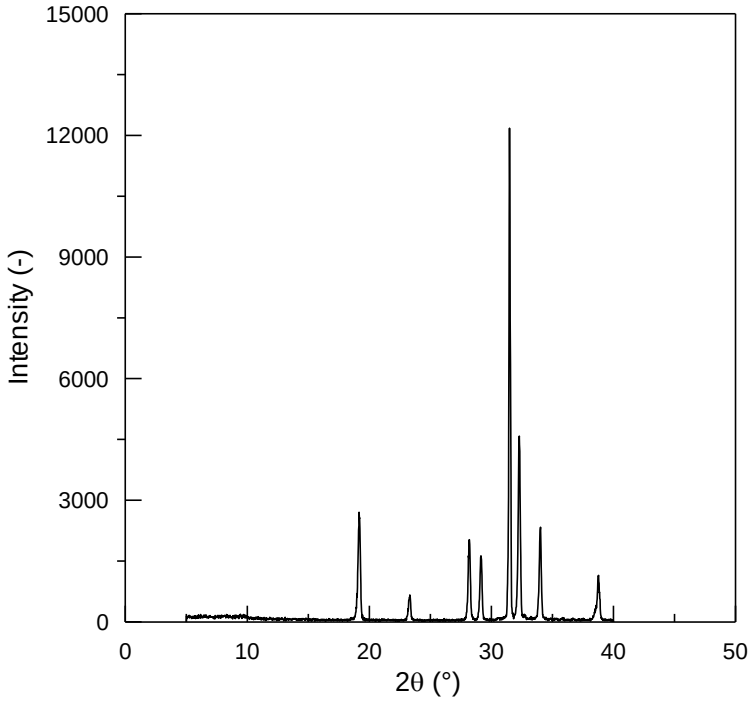

Figure 5.8 X-Ray diffraction pattern of crystalline product: characteristic peeks reveal thenardite, the anhydrous form of sodium sulfate.

5.4 Economical aspects

The preliminary cost analysis of the process revealed that the separation of Na_2SO_4 by Membrane Crystallization integrated with Nano-filtrarion can substantially reduce the number of membrane modules or the required membrane surface area (about 30 %). The cost associated with membranes and their susceptibility to fouling are of major concern in such operations. Although the revenue generated from crystalline sodium sulphate is not significant due to the low price of this chemical, such an approach may result in considerable saving in capital and operating costs. The clean water from the permeate tank can be recycled into the main process, reducing the water consumption in the plant, which has a positive impact on cost and environment. It is expected to cover about 25 % of annual operating cost of the wastewater treatment plant by marketing sodium sulphate.

5.5 Conclusions

In this work, Na_2SO_4 was efficiently removed from aqueous sulphate wastes by evaporative crystallization through microporous hydrophobic membranes, preceded by a nanofiltration pre-concentration step. The experimental investigation performed on lab-scale plants confirmed the feasibility of this approach. NF90-2540 membrane modules exhibited rejection values higher than 99 % when operated above 350 psi, and ability to achieve a permeate recovery factor of 50 %. Membrane crystallization tests carried out at moderate temperature (~ 40 ℃) resulted in the formation of thenardite in a reasonably amount (slurry density up to 21 kg/m^3) and good product quality (coefficient of variation below 30 % within the first hour); the hydrophobic character of polypropylene hollow-fibres membranes was stable over two days of continuous operation. The commercial implementation of the treatment plant will: protect the environment, generate a marketable product and result in clean water consumption due to the recycling of treated water.

References:

[1] J. A.Young. Sodium Sulfate. J. Chem. Educ., 2007, 84/8: 1272.

[2] E. Drioli, E. Curcio. Membrane engineering for process intensification: a perspective. J. Chem. Technol. Biotechnol., 2007, 82: 223–227.

[3] K. Karakulski, M. Gryta, M. Sasim. Production of process water using integrated membrane processes. Chemical Papers, 2006, 60/6: 416-421.

[4] G. Bargeman, M. Steensma, A. ten Kate, J.B. Westerink, R.L.M. Demmer, H. Bakkenes, C.F.H. Manuhutu. Nanofiltration as energy-efficient solution for sulfate waste in vacuum salt production. Desalination, 2009, 245: 460–468.

[5] E. Curcio, A. Criscuoli, E. Drioli. Membrane Crystallizers. Ind. Eng. Chem. Res., 2001, 40: 2679-2684.

[6] M. Qtaishat, T. Matsuura, B. Kruczek, M. Khayet. Heat and mass transfer analysis in direct contact membrane distillation. Desalination, 2008, 219: 272-292.

[7] E. Curcio, E. Fontananova, G. Di Profio, E. Drioli. Influence of the structural properties of poly(vinylidene fluoride) membranes on the heterogeneous nucleation rate of protein crystals. J. Physical Chem. B., 2006, 110 /25: 12438-12445.

[8] C. M. Tun, A. G. Fane, J. T. Matheickal, R. Sheikholeslami. Membrane distillation crystallization of concentrated salts—flux and crystal formation. J. Membrane Sci., 2005, 144-155.

[9] E. Drioli, E. Curcio, A. Criscuoli, G. Di Profio. Integrated system for recovery of $CaCO_3$, NaCl and $MgSO_4 \cdot 7H_2O$ from nanofiltration retentate. J. Membrane Sci., 2004, 239: 27-38.

[10] S. Al Obaidani, E. Curcio, F. Macedonio, G. Di Profio, H. Al-Hinai, E. Drioli. Potential of membrane distillation in seawater desalination: Thermal efficiency, sensitivity study and cost estimation. J. Membrane Sci., 2008, 323: 85-98.

[11] K. Kosutic, I. Novak, L. Sipos, B. Kunst. Removal of sulfates and other inorganics from potable water by nanofiltration membranes of characterized porosity. Separation and Purification Technology, 2004, 37: 177-185.

[12] S. J. Jancic, P. A. M. Grootscholten, Industrial crystallization, Delft University Press, Delft (Holland) 1984

[13] D. L. Klug, R. L. Pigford. The probability distribution of growth rates of anhydrous sodium sulfate crystals. Ind. Eng. Chem. Res., 1989, 28/11: 1718-1725.

[14] D.E. Garrett. Sodium Sulfate: handbook of deposits, processing, properties, and use. Academic Press, San Diego (USA), 2001.

[15] K. Linnow, A. Zeunert, M. Steiger. Investigation of sodium sulfate phase transitions in a porous material using humidity- and temperature- controlled X-ray diffraction. Anal. Chem., 2006, 78: 4683-4689.

[16] B. Xu, G. Schweiger. In-situ Raman observation of phase transformation of Na_2SO_4 during the hydration/dehydration cycles on single levitated microparticle. J. Aerosol Sci., 1999, 30: 379-380.

[17] M. Steiger. Crystal growth in porous materials - I: The crystallization pressure of large crystals. J. Cryst. Growth, 2005, 282: 455-469.

[18] C. Rodriguez-Navarro, E. Doehne, E. Sebastian. How does sodium sulfate crystallize? Implications for the decay and testing of building materials. Cement and Concrete Res., 2000, 30: 1527- 1534.

[19] N. Tsui, R. J. Flatt, G. W. Scherer. Crystallization damage by sodium sulphate. J. Cultural Heritage, 2003, 4: 109–115.

CHAPTER SIX

Membrane Bioreactor For Water Treatment

6.1 Introduction

In Membrane Distillation / Crystallization system, the membrane material was always transformed from hydrophobic into hydrophilic by organic matter, and the salt crystal process was further destroyed. For the purpose of removing the organic matter, we utilized pre-treatment to improve the Membrane Distillation / Crystallization performance.

The MBR is a compact-built purification system combining the biological degradation step with the membrane separation step. The influent is feed to the bio-reactor where the organic components are oxidized by the activated sludge. The aqueous activated sludge solution passes through a membrane filtration unit separating the water from the sludge. The latter returns to the bio-reactor, while the permeate is discharged or re-used as particle-free effluent [1-3].

The first MBR concept for wastewater treatment was developed by Dorr-Oliver Inc. in the late 1960s [4]. In the Membrane Sewage Treatment system, wastewater entered a suspended growth bioreactor where mixed liquor was continuously withdrawn via a rotating screen to an ultrafiltration membrane module. The membrane configuration was plate and frame.

6.2 Compare MBR with CAS

In conventional activated sludge (CAS) system in generally as showed in Figure 6.1 volves four stages：Mechanic treatment, Primary clarifier, Activated sludge, Secondary clarifier.

(1) Screening, The influent water is strained to remove all large objects carried in the sewage stream, such as rags, sticks, tampons, cans, fruit, etc.

(2) Primary clarifiers, to produce both a generally homogeneous liquid capable of being treated biologically and a sludge that can be separately treated or processed.

(3) Primary treated sewage combined with organisms to develop a biological floc which reduces the organic content of the sewage. The combination of raw sewage and biological mass is commonly known as Mixed Liquor.

(4) Substantially degrade the biological content of the sewage.

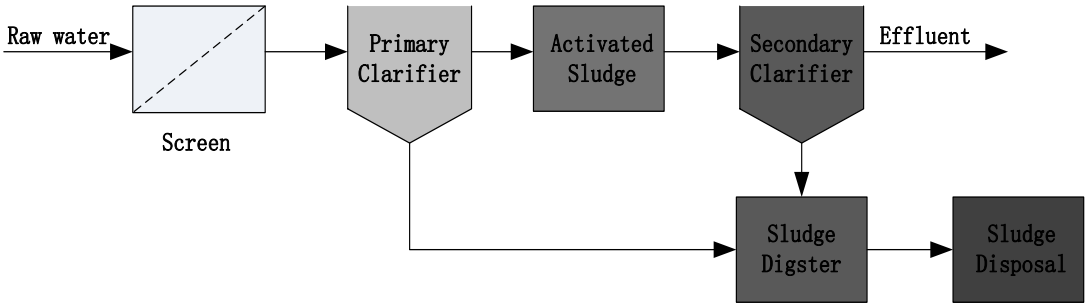

Figure 6.1 Conventional activated sludge process

Membrane bioreactors (MBR) combines activated sludge treatment with a membrane liquid-solid separation process. The membrane component uses low pressure microfiltration or ultra filtration membranes and eliminates the need for clarification and tertiary filtration. The membranes are typically immersed in the aeration tank (however, some applications utilize a separate membrane tank).

The combination of biological treatment with membrane filtration offers several significant advantages over a conventional activated sludge system as presently being used for municipal wastewater treatment, such as a higher biomass concentration and less sludge carry-over. The technology permits bioreactor operation with considerably higher mixed liquor suspended solids (MLSS) concentration than CAS systems, which are limited by sludge settling. The process is typically operated at MLSS in the range of 8,000–12,000 mg/L, while CAS is operated in the range of 2,000–3,000 mg/L. The elevated biomass concentration in the membrane bioreactor process allows for very effective removal of both soluble and particulate biodegradable materials at higher loading rates. Thus increased Sludge Retention Times (SRT)—usually exceeding 15 days — to ensure complete nitrification even in extremely cold weather [5].

The higher biomass concentration results in a more compact system being an advantage for both highly populated (space requirement) as remote areas (flexibility). The decrease in sludge carry-over in the effluent reduces the need of post-treatment of the effluent protecting ecologically sensitive areas.

The cost of building and operating a MBR is usually higher than conventional wastewater treatment, however, as the technology has become increasingly popular and has gained wider acceptance throughout the industry, the life-cycle costs have been steadily decreasing. The small footprint of MBR systems, and the high quality effluent produced, makes them particularly useful for water reuse applications.

MBR technology and the use of membrane separation bioreactor combination, highly efficient solid-liquid separation membrane role in strengthening the role of the biological treatment, it has many other biological processes can not match the obvious advantages:

(1) efficiently carry out solid-liquid separation, separation is far better than the conventional sedimentation tank, good water quality, suspended solids and turbidity of the water close to zero, can be directly used to achieve the water resource.

(2) the role of membrane retention of high-performance, so completely cut-off micro-organisms in the reactor, the reactor to achieve a hydraulic retention time (HRT) and sludge age (SRT) of the complete separation, the stability of a more flexible operation.

(3) Reactor at high concentrations of microbial resistance, the impact load.

(4) Free to control the sludge age. Membrane separation of macromolecules sewage refractory composition, in a limited volume within the bioreactor have sufficient residence time has greatly increased the degradation of refractory organic matter effects. Reactor load in high-volume, low sludge load, long sludge age run under the conditions can be achieved without excess sludge basic emissions.

(5) Compact structure, small footprint, process equipment, easy integration of automatic control.

MBR are considered as a good integration of conventional activated sludge (CAS) system and advanced membrane separation, thus enabling the independent control of

sludge retention time (SRT) and hydraulic retention time (HRT) and retaining a high concentration of sludge biomass in the reactors. Compared with CAS processes, MBR process has great advantages including a smaller footprint, less sludge production and better effluent quality.

6.3 MBR configuration

MBR systems are generally comprised of two configurations as showed in Figure 6.2: submerged (immersed or integrated) MBR and side-stream (recirculated or external) MBR.

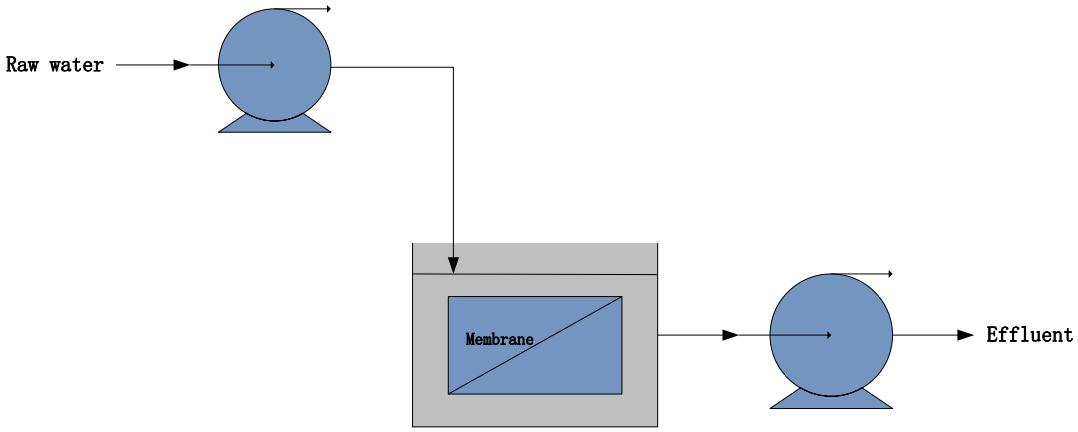

Figure 6.2 Schematic of membrane bioreactor: immersed membranes

Yamamoto et al. [6] were the first to put forward the concept of submerged MBR by introducing submerged membranes in an aeration tank for solid/liquid separation in 1989. Submerged MBR consume much less power than side-stream MBR due to the absence of a high-flow recirculation pump as showed in Figure 6.3. Compared with side-stream MBR, submerged MBR is more popular in water and wastewater treatment because of its lower operational cost [7].

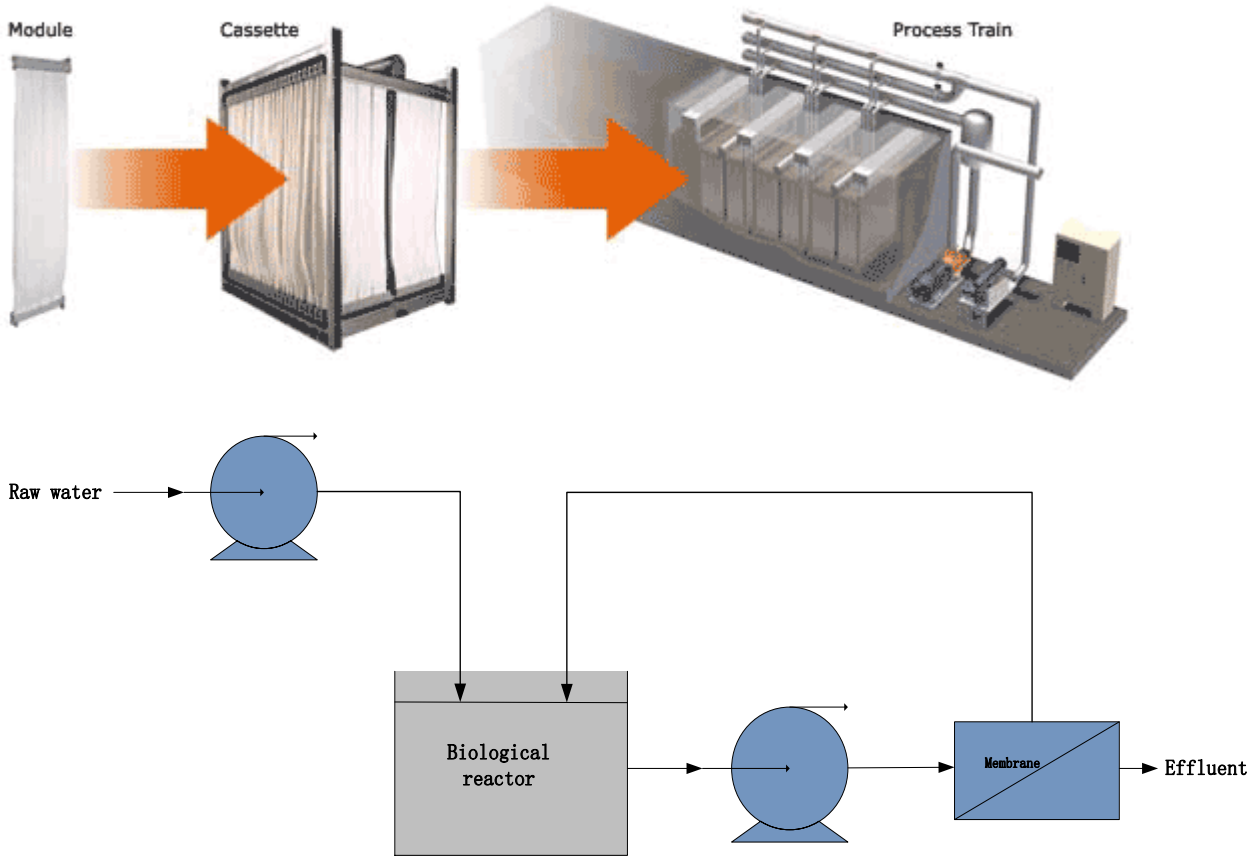

Figure 6.3 Schematic of membrane bioreactor：external membranes

External MBR were considered to be more suitable for wastewater streams characterized by high temperature, high organic strength, extreme pH, high toxicity and low filterability. Accordingly, the membranes are easily accessible and cleaned without having to touch or smell the sludge. Moreover, because the membrane filtration is completely separated from the bioreactor, the entire process is running more efficiently as showed in Figure 6.4 [8].

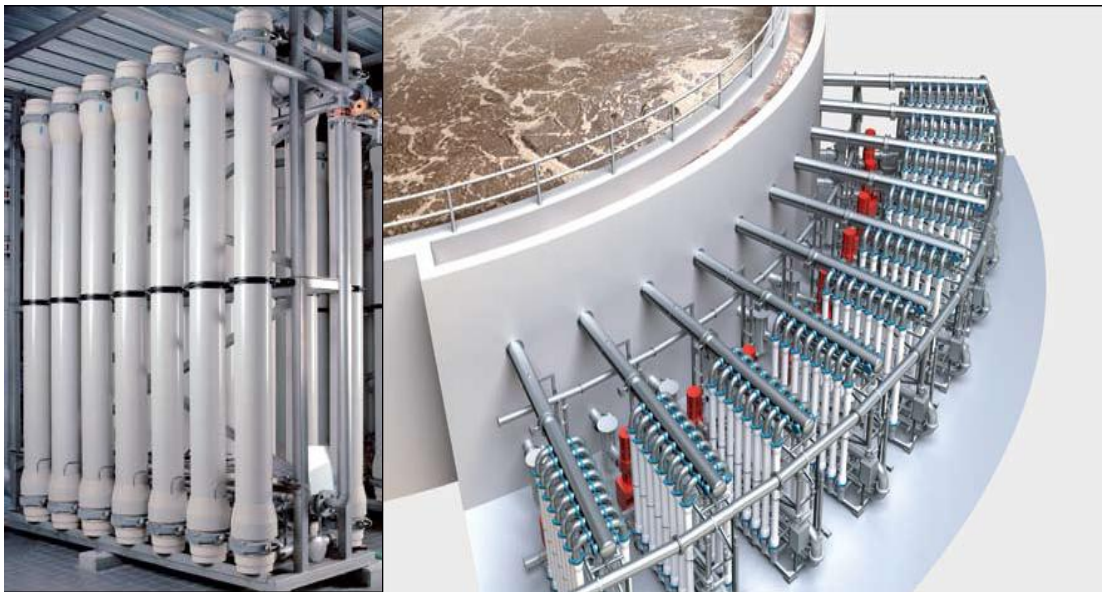

Figure 6.4 MBR plant in industry

6.4 Membrane materials and modules

The two more popular kinds of flat-sheet and hollow fiber membranes are made of PVDF and PES compared with the rest PP and polyacrylonitrile (PAN) materials as showed in Table 6.5 [9].

Table 6.5 Five main MBR manufacturers

	GE（Zenon）	**Siemens（US Filter）**	**Kubota**	**Koch（Puron）**	**Norit**
Membrane type	Hollow fiber	Hollow fiber	Flat sheet	Hollow fiber	Hollow fiber
Material	Proprietary	PVDF	Polyethylene	PVDF	PVDF
Cleaning method	Backwash	Backwash	Relax	Relax	Backwash
Recovery method	Chemical soak	Chemical soak	Chemical soak	Chlorine Backwash	Chemical soak

6.5 MBR Market Overview

Over the past decade, a strong growth momentum had arisen in the MBR market

and it will continue into the next decade. In 1995, the revenue on global MBR market was only 0.1 million U.S. dollars, however, by 2000 to 2005, the revenue reached 217 million U.S. dollars, and with the annual growth rate of 10.9 %, it is expected to reach 360 million U.S. dollars. During this period, an average of 1,000 sets of MBR installations will be put into operation. While in Europe, the revenue of 253 million euro in 1999 has arising to 328 million euro in 2002 in MBR market, and since from 2004, the annual growth rate has become 6.7 %. And in 2006, the revenue reached 500 million euro, which is expected to double within the next five years.

At present, the market, basically share in the United Kingdom, Ireland, Germany , France, Italy, the Benelux Economic Union and the several major areas, is expected to be double the size of above after seven years. From 2004 to 2006, MBR market in the United States experiences an extraordinarily rapid growth period, not only the hydraulic development of industry which develops better than other aspects in the United States, but also has brought about a number of ancillary industries (for example, the filter market, membrane filtration technology or ultraviolet radiation technology), the growth rate of which is more than 15 %. The next decade, the United States and Canada MBR market will continue to grow. Asia, which develops rapid, is also a typical MBR market, only in 2005 in South Korea about 1400 sets of MBR installations has been put into operation on the completion. [10].

6.6 Challenges for developing MBR technology

Although the commercialization of MBR has expanded substantially in past 20 years, target markets have not been tapped to a large extent and new potential areas of applications are continually developing. MBR technology is currently facing some research and development challenges which, when tackled, will lead to a more competitive and mature market for MBR applications. Some of these challenges include [11, 12]:

(1) Membrane fouling: further understanding the mechanisms of membrane fouling and developing more effective and easier methods to control and minimize membrane

fouling;

(2) Pretreatment: effective methods to limiting membrane clogging and operational failures;

(3) Membrane lifespan: increasing membrane mechanical and chemical stability;

(4) Cost: reducing costs for maintenance and replacement of membranes, energy requirement and labor requirements;

(5) Plant capacity: scaling up for large plants;

6.7 Objective

It is well known that the nature and the amount of organic molecules existing in the highly concentrated brines of NF and RO. Moreover, these substances might act directly as foulant for the membranes or as nutrient for bio-fouling.

Advanced water pre-treatment operations are necessary to reduce/remove natural (organic) marine substances and organic polluting molecules deriving from human activities, with the consequent advantage of:

(1) Reducing organic fouling and bio-fouling of membranes.

(2) Avoiding hindrance/influence on the crystallization kinetics and crystals characteristics.

In the study, we want to investigate submerged ultrafiltration membrane separation as seawater pre-treatment in the logic of an integrated membrane desalination system.

References:

[1] T. Melin, B. Jefferson, D. Bixio, C. Thoeye, W. De Wilde, J. De Koning, J. van der Graaf, T. Wintgens. Membrane bioreactor technology for wastewater treatment and reuse. Desalination, 2006, 187: 271–282.

[2] W. Yang, N. Cicek, J. Ilg. State-of-the-art of membrane bioreactors: worldwide research and commercial applications in North America. J. Membrane Sci. 2006, 270: 201-211.

[3] E.J. McAdam, S.J. Judd. A review of membrane bioreactor potential for nitrate removal from drinking water. Desalination, 2006, 196: 135-148.

[4] P.M. Sutton, P.N. Mishra, J.R. Bratby, D. Enegess. Membrane bioreactor industrial and municipal wastewater application: long term operating experience, in: Proceedings of WEF 75th Annual Conference and Exposition, Chicago, IL, October 2002.

[5] http://en.wikipedia.org/wiki/Sewage_treatment

[6] Yamamoto K et al. Direct solid - liquid separation using hollow fiber membrane in an activated sludge aeration tank. Wat . Sci. Tech, 1989, 21 (4～5): 43.

[7] www.ge.com

[8] www.norit.com

[9] Wenbo Yang a, Nazim Cicek a, John Ilg. State-of-the-art of membrane bioreactors: Worldwide research and commercial applications in North America. J. Membrane Sci., 2006, 270: 201–211.

[10] www.jsbwater.com

[11] H.F. van der Roest, A.G.N. van Bentem, D.P. Lawrence. MBR technology in municipal wastewater treatment: challenging the traditional treatment technologies. Water Sci. Technol., 2002, 46: 273–280.

[12] J.A. Howell, T.C. Arnot, W. Liu. Membrane bioreactors for treating waste streams. Adv. Membr. Technol., 2003, 984: 411–419.

CHAPTER SEVEN

Removal of the Organic matter by Submerged Ultrafiltration

7.1 Introduction

Bacteria live on food. Membrane Bioreactor, whose energy resource is from organic matter, was often utilized for wastewater treatment. But the concentration of organic matter is very low in fresh seawater. Ultrafiltration has been widely used as membrane pretreatment to obtain consistent seawater with high quality prior to RO [1－20].

Compared with the conventional pretreatments, UF showed many advantages, such as improved water quality, smaller footprint, smaller amount of chemicals required and more stable operation [19], while the overall cost was also very low[6,20].However, serious membrane fouling limited its application. Because this delicate problem led to the increase of the hydraulic resistance, the reduction of recovery factor and flux, thus increased operational costs.

On the other side, in submerged UF, a cross-flow stream over the membrane surface is produced by air bubbling which induces a moderate shear stress generating the back transport of deposited matter [21]; this will have a great significance for reducing particles deposition on the membrane surface and for prolonging the operation period [22]. Furthermore, the technology is worthy of consideration because of the lower energetic consumption and cleaning requirements compared to tangential filtration mode [23,24], while hollow fibers would be preferred over flat sheet membrane configuration due to the higher energy efficiency in terms of creating completely mixed conditions [25] and the increased available membrane surface for module unit volume.

Even though UF systems have been widely used for the treatment of surface water and wastewater, like in membrane bioreactors, not much attention has been devoted so far to the application of this technology as pretreatment desalination, and only few papers can be found in the literature [26, 27]. However, natural seawater composition

in terms of main foulants is quite different from surface water and wastewater. In addition, the higher salt concentration can also affect the interactions existing between membrane-foulant and foulant-foulant, so that a different fouling dynamics is expected to occur. In this situation, the influence on the process of several operating conditions, like the filtration mode, air scouring procedure and back flushing and their effect on membrane fouling needs investigations. Accordingly, this work focuses on the study of submerged hollow fibers UF as pretreatment for controlling natural organic matter content in seawater. Before the suitable microorganism was found, the effects of different operating conditions on process performance and fouling dynamics under subcritical flux conditions for a relatively long operation time was investigated.

7.2 Materials and methods

Polyethersulfone (PES) hollow fiber membranes (UltraPes from Membrana GmbH, Germany; 70 *kDa* MWCO; nominal permeance was reported by the manufacturer: L_p > 0.65 *mL/cm ²s bar* - 3.9 *L/m ²h kPa*) were used to assemble the one-side potted modules (the total membrane area A is 0.068 m^2). The asymmetric structure of membrane fibers as showed in Figure 7.1.

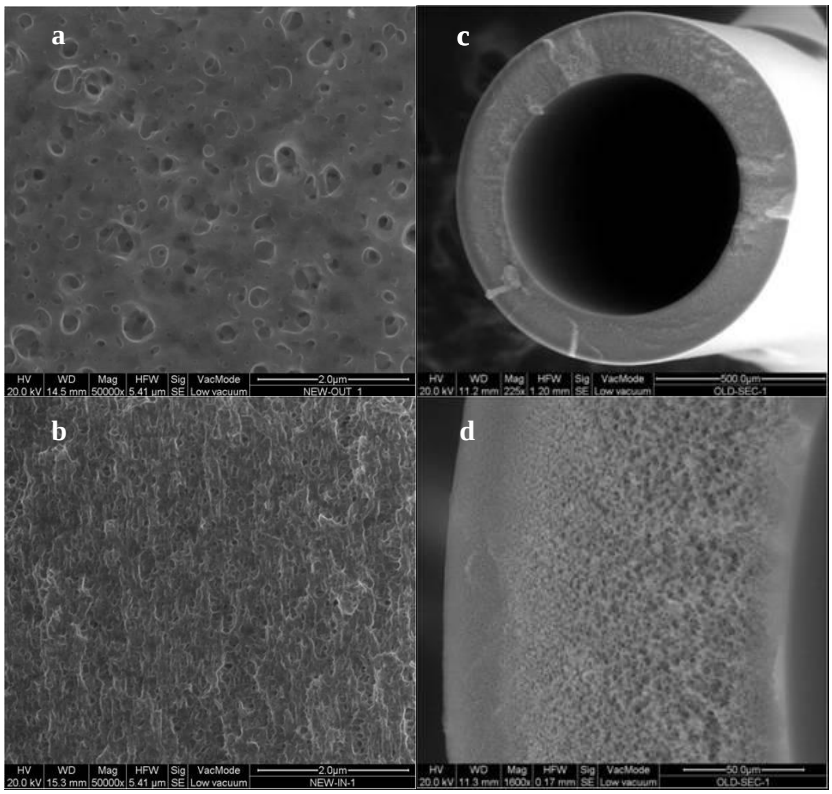

Figure 7.1 SEM images of membrane fibers: (a) shell side; (b) lumen side; (c) cross-section; (d) asymmetric structure of the cross-section.

Figure 7.1 a and b are at the same magnification. Modules were prepared in non-carterised configuration to allow more freedom for fibers motion to reduce fouling under aeration conditions.

Membrane, in vertical arrangement, were used in the bench-scale plant, with a maximum working volume *V* of 20 L, and operated in submerged configuration as showed in Figure 7.2.

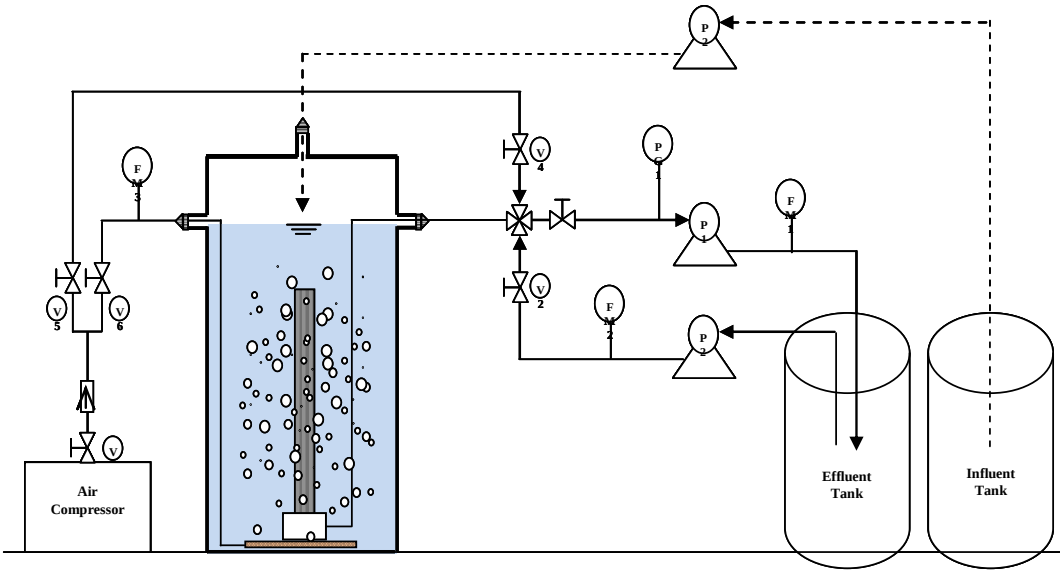

Figure 7.2 Laboratory-scale plant

Filtration was carried out in outside-to-inside filtration mode. Air sparging, through a diffuser, was operated from the bottom of the module, by using an air compressor, at 8 *LPM*. The effluent has been drawn through the module by a peristaltic pump towards an effluent tank. Back-flushing have been operated by using a back-flushing pump with pure water. An air line was inserted in the plant to allow air back-pulse to check, when necessary, module integrity.

Seawater (SW) without any initial pre-treatment (from the Tyrrhenian coast, Belvedere Marittimo, Southern Italy), was used to feed the plant. Water was uptake 2-3 meters far, on the sea side, from the estuarine of a little river in which the effluent from a traditional municipal wastewater depuration plant is discharged after treatment. Sodium Acetate and Humic Acid (from Sigma-Aldrich) were added to seawater in order to increase the initial TOC content to stimulate biological activity.

Ion composition of water characterization was carried out by ion chromatography (Metrohm IC861 compact system) and by a TOC analyzer (Shimadzu VCSN) for TOC measurements according to standard procedure for seawater.

Experiments have been carried out by operating at constant flux J (L/m^2 h) or constant trans-membrane pressure TMP (kPa) and intermitted or continuous aeration operation mode. Membrane compactions have been carried out by a sequence of

increasing and reducing pressure filtration cycles with pure water before the experimental trials. The filtration resistance of the membrane module was determined through measuring the flux to pure water for different trans-membrane pressures after membrane compaction and before the experimental session by using Equation 7.1:

$$J = \frac{TMP}{\mu R_t} \tag{7.1}$$

where μ ($Pa\ s$) is the viscosity of the permeate (water) and R_t (m^{-1}) is the total membrane resistance coinciding with the intrinsic module resistance R_m (m^{-1}) at the beginning of the experiments. Equation 7.1 was also used to evaluate the increase in resistance to permeation during the experiments with seawater due to membrane fouling. The membrane surfaces were examined by a Quanta 200 F FEI Philips scanning electron microscopy (SEM).

7.3 Results and Discussions

The variation of the membrane permeance LP to pure water with the applied trans-membrane pressure TMP for increasing and decreasing pressure cycles as showed in Figure 7.3.

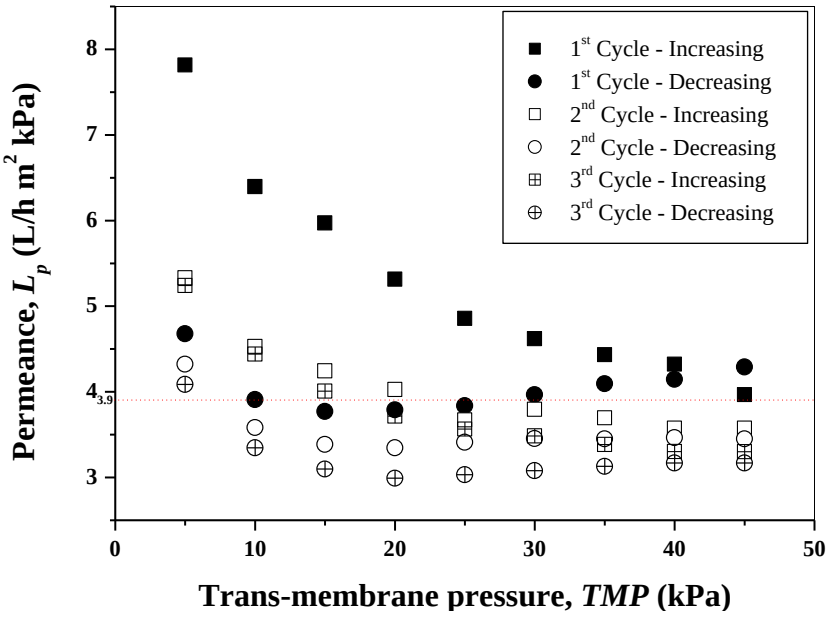

Figure 7.3 Membrane compaction experiments before the seawater filtration.

Dotted line indicates the reference value of 3.9 L/m ² h *kPa* from the membrane manufacturer. The hysteresis due to membrane compaction is clearly visible for three consecutive cycles. This is due to mechanical deformation of the solid polymer, trans-membrane pressure difference causing a decrease in membrane permeability.

Because of the asymmetric structure in the hollow fiber membrane (Figure 7.1), the increase of pressure causes densification of the more porous support layer leading to a thickening of the skin layer (selective barrier). Consequently, thicker membranes result in lower permeability. Indeed, gradual decrease in permeability over the duration of compaction time was observed for each cycle. In the first cycle L_p decreases almost 50% when increasing *TMP* from 5 to 45 *kPa*. At the end of the first relaxation sequence L_p at 5 *kPa* (corresponding to the maximum variation) reduced to the 40 % of its initial value for the same *TMP*. In the successive cycles, for *TMP* at 5 *kPa*, L_p reduced of 22 % and 19 % with respect to the initial value for the 2nd and 3rd cycle respectively. Compaction sequences was completed when the maximum variation of L_p reduced to less than 15 % (for the highest variation) with respect to the initial value, which occurred after the 5th cycle. At the end of compaction process L_p stabilized at a value somewhat lower than that indicated by the manufacturer of 3.9 *L/m ²h kPa*.

In order to identify the appropriate operating conditions for avoiding (or reducing) fouling, the critical flux (J_c) has been estimated. In fact, the critical flux is defined as that value below which, on start-up, a decline of flux with time does not occur [28, 29]; when the permeation flux is below J_c (conditions referred to as sub-critical), no particle accumulation occurs in the region of the membrane and, if the physicochemical solute/membrane interactions are negligible, filtration can take place in stable conditions close to a permeation operation in clean water.

It is possible to observe the transition between constant and non-constant permeability at the onset of fouling by plotting flux against *TMP*. A common practice to estimate J_c is to incrementally increase the flux for a fixed duration for each increment, giving a stable *TMP* at low flux but an ever-increasing rate of *TMP* increase at fluxes beyond J_c [30-32]. This method is preferred over the *TMP*-step

method since it provides better control of the flow of material deposition on the membrane surface, as the convective flow of solute towards the membrane is constant during the run [33, 34].

The trans-membrane pressure as function of the flux for increasing *J* procedure was showed in Figure 7.4.

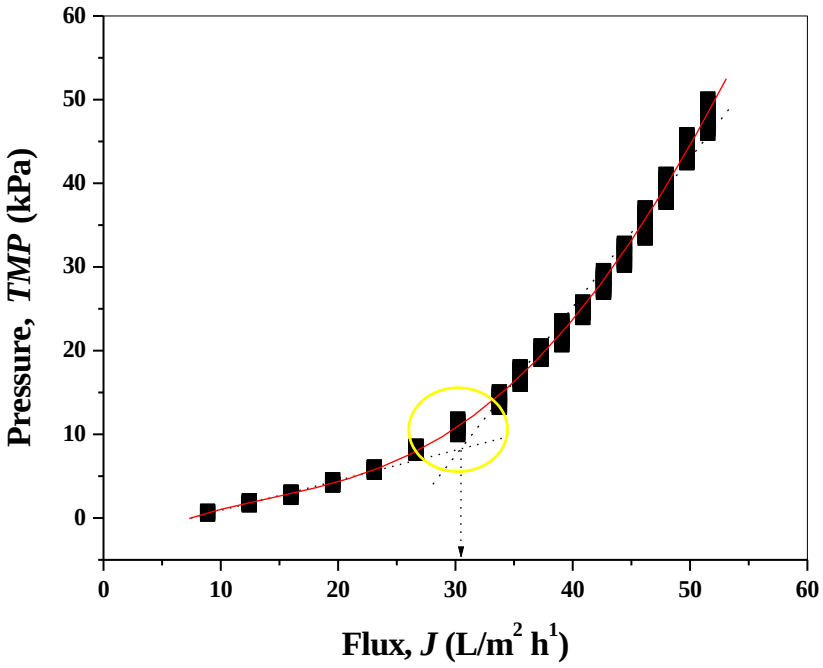

Figure 7.4 Trans-membrane pressure (*TMP*) with function of the flux (*J*) for seawater filtration test at increasing flux steps. Circle evidences the range of values for *J* where the critical flux falls.

In the curve, experimental points can be separated two regions. In the first region, *TMP* increases with *J* when *J* up to 26 L/m^2 *h*, indicating that fouling at somewhat extent occurred even for low flux values. For *J* greater than 34 L/m^2 *h*, the increase of *TMP* was steeper, accounting for a more severe fouling in these permeation conditions. Thence, J_c lies in the range between these two values although reduction of *J* was appreciable below J_c.

Bacchin [35] defined two distinct forms of the concept of critical flux. In the first form, the flux obtained during sub-critical flux is equated to the clean water flux

obtained under the same conditions, but the *TMP vs. J* curve starts to deviate from that of pure water after J_{cs} (strong form) has been reached. In the alternative form, it is assumed that there is very rapid fouling on start-up and so the *J - TMP* relationship is below that of the pure water line (weak form). The critical flux (weak form) J_{cw} is the point at which this line becomes non-linear. Clean water fluxes are rarely attained for most real feed-waters due to irreversible adsorption of organic components which had not been removed other than by chemical cleaning.

The *J - TMP* relation for constant pressure filtration experiments of pure and seawater as reported in Figure 7.5.

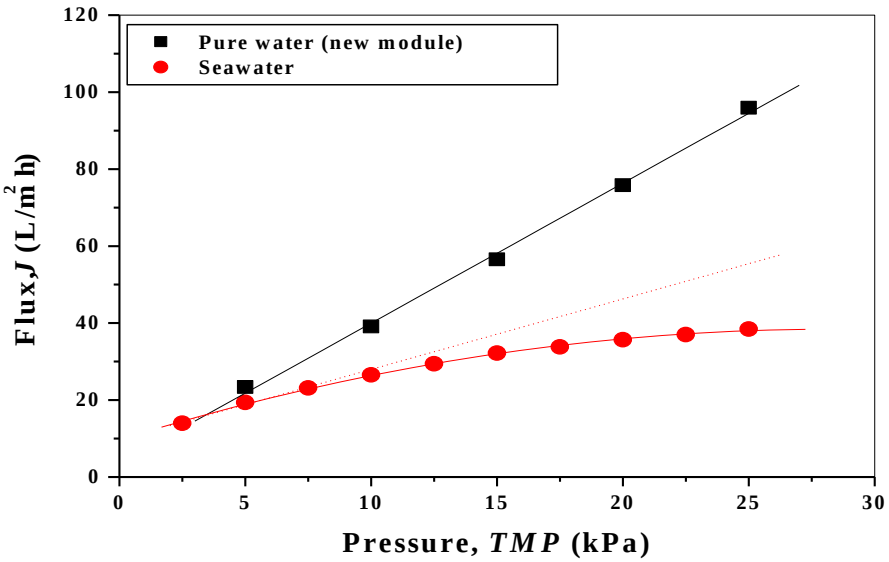

Figure 7.5 Flux (*J*) as function of the trans-membrane pressure (*TMP*) for pure water (squares) and seawater (circles) filtration test at increasing pressure steps.

This is due to the adsorption of foulants at the beginning of the test, the two curves diverge since the lower values of pressure. This is consistent with a weak-form of critical flux which can be individuated already for low values of *J*. From the figure 7.4, in accordance with data reported in Figure 7.5, the *J - TMP* curve starts to be not linear already for $J > 26\ L/m^2\ h$, this value representing J_{cw}. Accordingly, filtration experiments with at the flux of $26\ L/m^2\ h$ were carried out in the subsequent tests at constant *J*.

Pressure cycling experiments have been carried out, so as to better determine membrane fouling dynamics [30, 36].

Figure 7.6 a shows Trans-membrane pressure varied in the time with cycling steps.

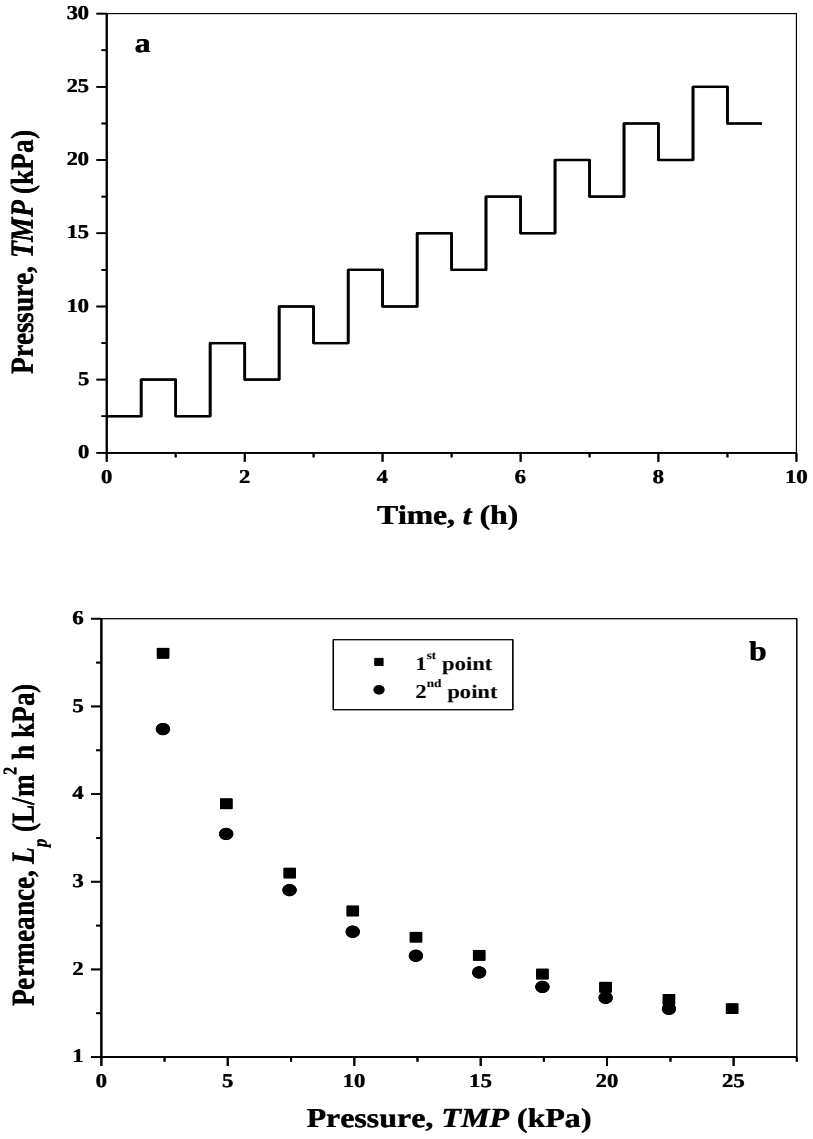

Figure 7.6 Cycling pressure experiment (a) and corresponding membrane permeance measurements (b) for the seawater filtration experiment.

TMP was increased up to 25 *kPa*, when the critical flux was overcome already for low pressure values. From Figure 6.6-b, the corresponding values of permeance were registered as function of *TMP*. According to this procedure, the impact of the reversible/irreversible fouling contribution to flux limitations can be estimated.

From the Figure 7.6, for low *TMP* the main part of fouling was irreversible as L_p decreased of almost 15% when cycling *TMP* in the range 2.5-5-2.5 *kPa*. This effect consistently decreased by increasing pressure and for the higher *TMP* values fouling was almost completely reversible as irreversible adsorption of foulants occurred already during the initial stages of the test. This result is consistent with previous considerations. Since the beginning, for pure water filtration, membrane permeability will decreased, because the irreversible introduction of foulants inside the pores of the membranes at low *TMP*. For higher *TMP* reversible polarization phenomena, combined with the irreversible pore constriction, is responsible for the reduction of L_p. When seawater was filtered instead of pure water, the consistent decreased in membrane permeance well below a value of 2 *L/m ²h kPa*.

Filtration tests in subcritical conditions (J = 26 $L/m^2\ h^1$) were performed to study the effect of aeration and back-flushing on the process performance. The variation of the trans-membrane pressure with the time for a constant flux experiment as reported in Figure 7.7.

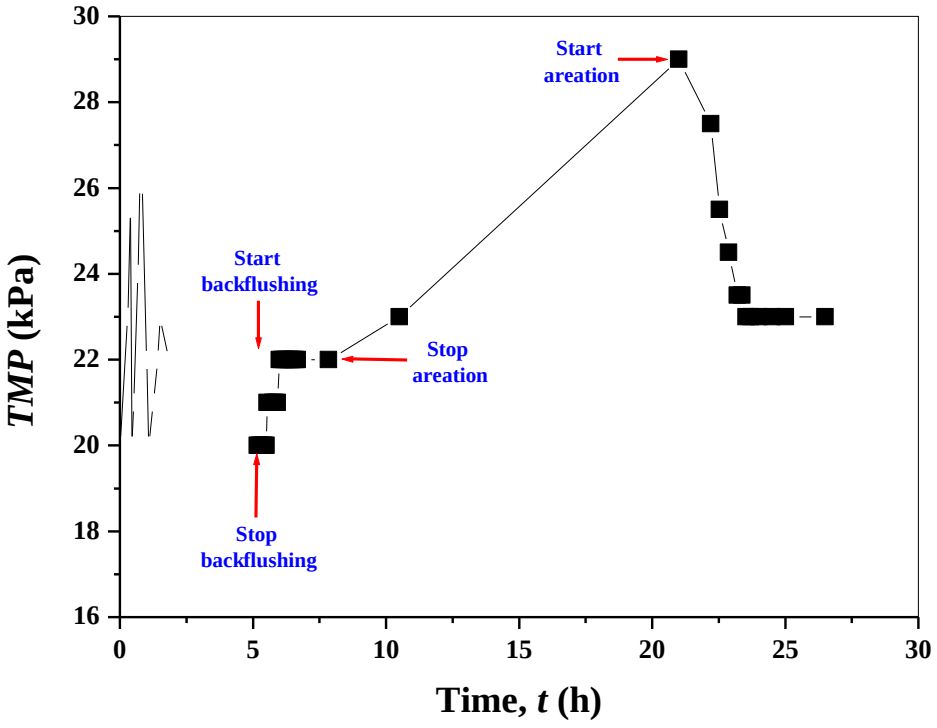

Figure 7.7 Variation of the trans-membrane pressure *TMP* VS the time *t* in different operating conditions.

At the time t = 0 the *TMP* was 20 *kPa* and air was supplied continuously with a flux of 7.1 $m^3/h\ m^2$. The system reached a stationary condition of 22 *kPa TMP* which remained constant for 4 *h* of operation, after a period of almost 1 *h*. This means that over one hour of operation, even in continuous aeration conditions, a certain extent of membrane fouling occurred. At this point filtration was interrupted and a back-flushing section of 10 *min* was operated for the complete recovery of the initial *TMP*. However, *TMP* increased again to 22 *kPa* and remained stable at this value after almost 50 minutes after back-flushing. This phenomenon might be due to the partial plugging of the membrane pores by particles existing in the untreated feed water. After almost 2 *h* of operation, while registering a constant *TMP* of 22 *kPa*, aeration was stopped and the system was left to operate in quiescent conditions for 13 *h*. In this stage, this is due to accumulation of particles nearby the membrane surface, the *TMP* increased dramatically from 22 to 29 *kPa*. Upon restarting aeration, *TMP* decreases and in 2.5 *h* it stabilized at 23 *kPa*. This demonstrated that upon restarting aeration, reversible fouling and/or polarization phenomena were eliminated while irreversible fouling occurred in the initial operation time. However, as the *TMP* were not completely recovered, some increase of irreversible fouling occurred during this aeration idle time. Therefore, results reported in Figure 7.7 demonstrated that whilst increase in liquid transfer resistance might occur in a reversible way while keeping aeration, polarization phenomena and/or reversible fouling, which also promotes some irreversible fouling, occurs in absence of aeration. This would induce severe loss of performance in the case of long operation time. In order to study the effect of aeration/suction operation mode on process performances, different experimental sections were performed: continuous aeration and suction, (2) continuous suction and intermitted aeration (10 *min* ON/10 *min* OFF), (3) intermitted suction (8 *min* ON/2 *min* OFF) and aeration. Figure 7.8 shows fluxes against *TMP* for SW filtration in the different modes.

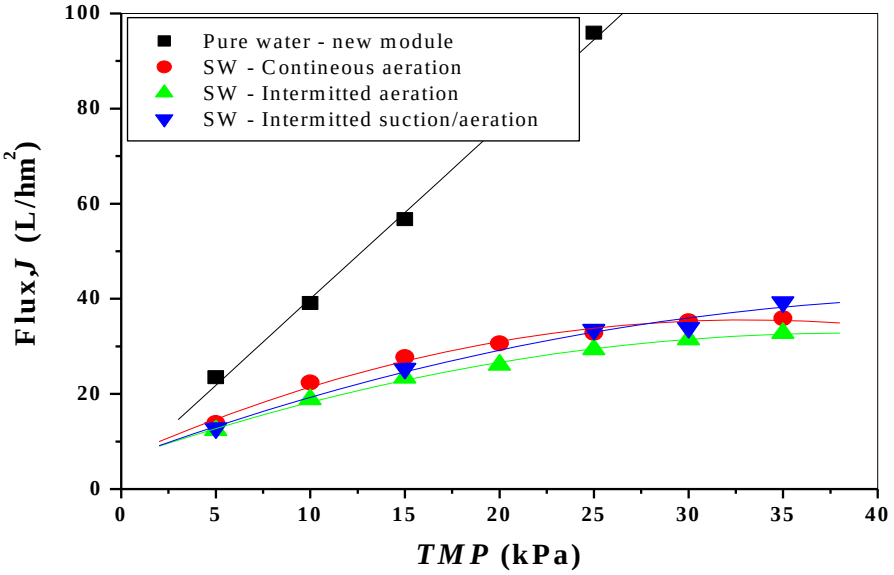

Figure 7.8 Trans-membrane flux *J* as function of *TMP* during filtration of SW in continuous and intermitted aeration/suction regimes.

The curves in the figure, demonstrates that in continuous aeration conditions slightly lower fluxes were observed with respect to intermitted conditions. Accordingly, system performance in intermitted aeration conditions does not substantially decrease with respect to continuous aeration mode, with consequent gain, however, in terms of energy consumption. However, for both intermitted suction and aeration conditions the highest limiting flux J_∞ was obtained, resulting in the more efficient operation mode in terms of energy consumption provided effluent production requirements.

Taking into account results above, in a subsequent filtration test plant were operated for more than 60 hours overall by using intermitted aeration/suction conditions at the constant filtration flux of 26 $L/m^2\ h$ registering *TMP* (Figure 7.9).

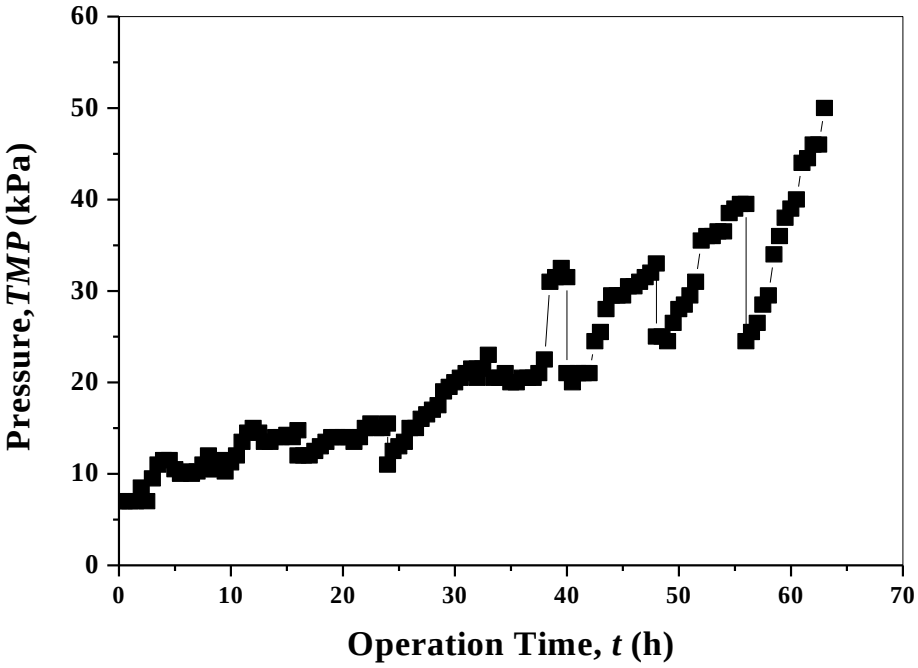

Figure 7.9 The trans-membrane pressure *TMP* VS the time *t*

In the Figure 7.9 the sharp decreases in *TMP* correspond to idle conditions of about 14 hours. Although the reduction of *TMP* after an idle period has been observed, a continuous increase of *TMP* was registered over the overall operation time, caused by the continuous accumulation of foulants inside the membrane.

Membrane resistance was estimated by using Equation 7.1 performing pure water filtration tests and registering *J* at constant *TMP*. The variation of the total module resistance R_t with the total amount of filtered volume during the experimental work as showed in Figure 7.10.

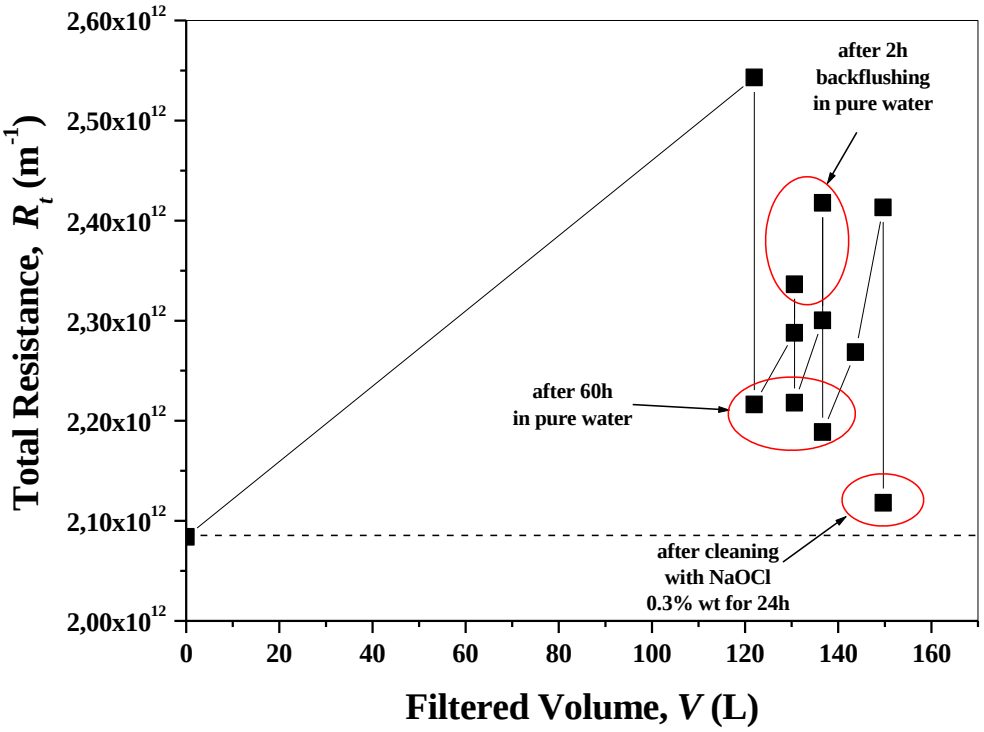

Figure 7.10 Total module resistance R_t as function of the SW volume filtered over the experimental runs.

R_m was found to be 2.08 m^{-1}, when for $V = 0$ (new module). R_t increased up to 2.54 m^{-1}, after almost 120 L of filtered seawater. At this point, the module was cleaned by soaking in pure water for 60 h, so that R_t deceased to 2.22 m^{-1}, indicating however, that some loss of permeability due to fouling occurred. Afterwards, two short SW filtration runs were operated. The module resistance increased due to fouling and a sequence of back-flushing and pure water soaking were performed to clean the membrane at this stage. From the Figure 7.10, it is evident that back-flushing steps induced an increase in R_t while soaking with pure water was effective in recovering to some extent membrane permeability. This indicated that back-flushing induced compaction of the fouling deposits on/in the membrane with consequent loss in permeability. At the end of the filtration runs R_t increased up to 2.4 m^{-1} so that cleaning by NaOCl solution was performed. By chemical cleaning almost complete membrane permeability was recovered as showed in the figure.

SEM images of the membrane surface after the SW filtration experiments and after chemical cleaning with NaOCl as showed in Figure 7.11.

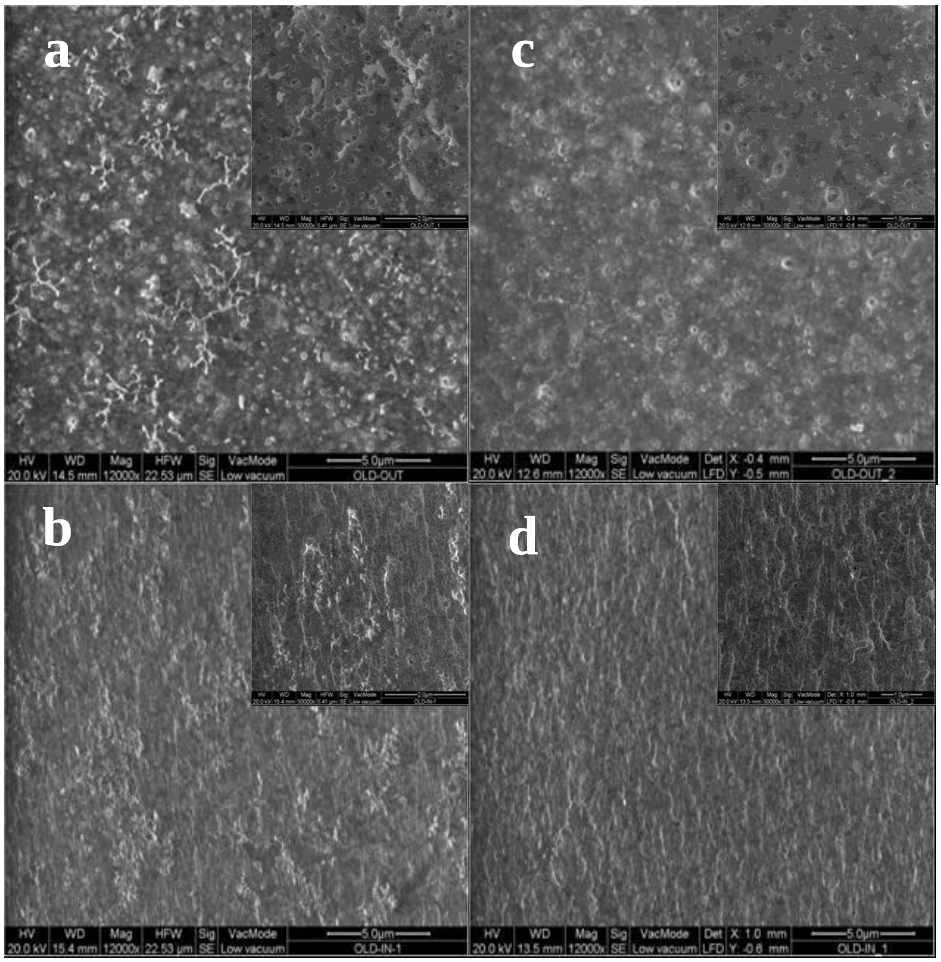

Figure 7.11 SEM images of membrane fibers: (a) shell side at the end of SW filtration tests; (b) lumen side at the end of SW filtration tests; (c) shell side after cleaning with NaOCL 0.3% *wt*; (d) lumen side after cleaning with NaOCL 0.3 % *wt* (insets in the figures are at higher magnification).

Organic particles deposited on both shell and lumen sides of the membrane after SW filtration were showed in Figure 7.11 a and b. As organic fouling is present even on the lumen side of the membranes, compaction of these deposits by back-flushing explains the increase of R_t. After chemical cleaning, these deposits were efficacy removed on both sides of the membrane as demonstrated in Figure c and d. Figure 7.12 shows the rejection of TOC after membrane filtration with respect to *J*.

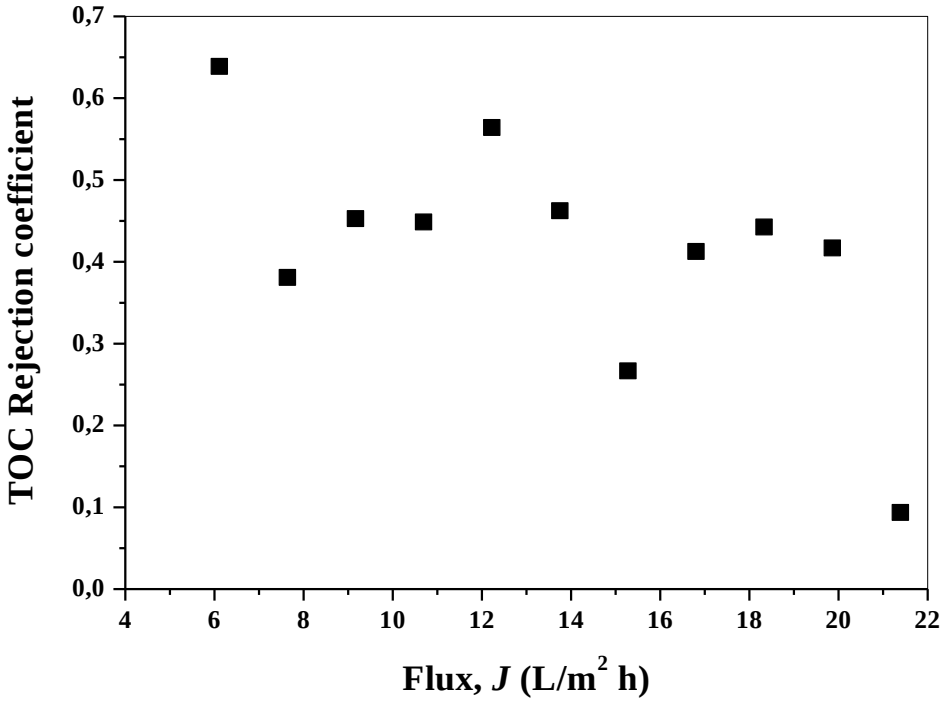

Figure 7.12 Trans-membrane flux *J* and TOC removal in seawater filtration test as function of *TMP*.

From the Figure 7.12, for the lowest flux the maximum value of 63 % in TOC rejection was achieved. TOC rejection decreased *J* Increased. Because of the fact that as *J* increases polarization phenomena, which encourage small organic particles to permeate the membrane, raise as well with consequent reduction in TOC removal.

7.4 Conclusions

This previous study tries to explore the use of submerged membrane operations as pre-treatment step in the logic of integrated membrane desalination systems to reduce natural/polluting organic matter existing in feed seawater. In this respect, by achieving this purpose would allow to reduce significantly RO membranes bio-fouling and to eliminate exogenous molecules that will affect/hinder crystallization kinetics in membrane crystallizers.

Results demonstrated that irreversible particles adsorption on/in the membrane surface occurs during the early stages of filtration while reversible polarization

phenomena/fouling become dominant for higher fluxes. Before the significant loss of performance, the plant can be operated for more than 60 hours without any chemical cleaning. At this stage, simple cleaning with NaOCl allows the almost complete recovery of module permeability.

Excessive back flushing with the permeate, containing not-retained low molecular weight NOM, might not only lead to increased energy consumption and reduced water productivity, but also induces pore blocking and fouling cake compaction on the lumen side of the asymmetric membrane, thus enhancing the overall resistance to mass transport.

Intermitted aeration/suction operation represent the best compromise between process efficiency and energy consumption, provided the requirements of effluent production.

For the sole filtration stage, TOC can be removed up to 63 % for low values of flux by using 70 kDa MWCO membranes, although polarization phenomena supported the decrease in TOC rejection for higher trans-membrane fluxes. For this reason, TOC removed will increase the overall efficiency of the proposed system by stimulating biodegradation before membrane filtration.

According to the results, submerged UF hollow fiber has been demonstrated as a feasible pretreatment to seawater in reducing NOM, thus supporting its utilization as seawater pretreatment in the logic of integrated membrane desalination systems, provided the identification of the operating conditions and their opportune optimization. These preliminary results encourage further researches addressed to increase the biological degradation of organic matter in seawater and to increase TOC rejection in the filtration step by using membranes with lower MWCO.

References:

[1] S.C.J.M. van Hoof, A. Hashim, A.J. Kordes. The effect of ultrafiltration as pretreatment to reverse osmosis in wastewater reuse and seawater desalination applications. Desalination, 1999, 124: 231-242.

[2] A. Teuler, K. Glucina, J.M. Lain. Assessment of UF pretreatment prior RO membranes for seawater desalination. Desalination, 1999, 125: 89-96.

[3] A. Brehant, V. Bonnelye, M. Perez. Comparison of MF/UF pretreatment with conventional filtration prior to RO membranes for surface seawater desalination. Desalination, 2002, 144 (1-3): 353-360.

[4] P.Glueckstern, M. Priel, M. Wilf. Field evaluation of capillary UF technology as a pretreatment for large seawater RO systems. Desalination, 2002, 147: 55-62.

[5] C.K.Teng, M.N.A. Hawlader, A. Malek. An experiment with different pretreatment methods. Desalination, 2003, 156: 51-58.

[6] G.K. Pearce, S. Talo, K. Chida, A. Basha, A. Gulamhusein. Pretreatment options for large scale SWRO plants: Case studies of UF trials at Kindasa, Saudi Arabia, and conventional pretreatment in Spain. Desalination, 2004, 167: 175-189.

[7] P.H. Wolf, S. Siverns, S. Monti. UF membranes for RO desalination pre-treatment. Desalination, 2005, 182: 293-300.

[8] D. Gille, W. Czolkoss. Ultrafiltration with multi-bore membranes as seawater pretreatment. Desalination, 2005, 182: 301-307.

[9] M. Kumar, S.S. Adham, W.R. Pearce. Investigation of seawater reverse osmosis fouling and its relationship to pretreatment type. Environmental Sci. and Technol., 2006, 40 (6): 2037.

[10] W. Ma, Y. Zhao, L. Wang. The pretreatment with enhanced coagulation and a UF membrane for seawater desalination with reverse osmosis. Desalination, 2007, 203 (1-3): 256-259.

[11] O. Lorain, B. Hersant, F. Persin, A. Grasmick, N. Brunard, J.M. Espenan. Ultrafiltration membrane pre-treatment benefits for reverse osmosis process in seawater desalting. Quantification in terms of capital investment cost and operating cost reduction. Desalination, 2007, 203 (1-3): 277-285.

[12] G.K. Pearce. The case for UF/MF pretreatment to RO in seawater applications. Desalination, 2007, 203: 286-295.

[13] J. Xu, G.L. Ruan, X.Z. Chu, Y. Yao, B.W. Su, C.J. Gao. A pilot study of UF pretreatment without any chemicals for SWRO desalination in China. Desalination, 2007, 207: 216-226.

[14] J. Xu, G.L. Ruan, X.L. Gao, X.H. Pan, B.W. Su, C.J. Gao. Pilot study of inside‐out and outside‐in hollow fiber UF modules as direct pretreatment of seawater at low temperature for reverse osmosis. Desalination, 2008, 219 (1-3): 179-189.

[15] N.Prihasto, Q.-F. Liu, S.-H. Kim. Pre-treatment strategies for seawater desalination by reverse osmosis system. Desalination, 2009, 249: 308-316.

[16] F. Knops, R. te Lintelo. Long-term operating experience of Seaguard UF as pretreatment to SWRO in the Mediterranean region. Desalination and Water Treatment, 2009, 5: 74-79.

[17] V. García-Molina, R. Chang, M. Busch. First year performance review of Magong UF/RO seawater desalination plant. Desalination and Water Treatment, 2010, 13: 203-212.

[18] N. Voutchkov. Considerations for selection of seawater filtration pretreatment system. Desalination, 2010, 261: 354-364.

[19] D.F. Halpern, J. McArdle, B. Antrim. UF pretreatment for SWRO: Pilot studies. Desalination, 2005, 182: 323-332.

[20] M. Wilf, M.K. Schierach. Improved performance and cost reduction of RO sweater systems using UF pretreatment. Desalination, 2001, 135: 61-68.

[21] Z.F. Cui, S. Chang, A.G. Fane. The use of gas bubbling to enhance membrane processes. J. Membrane Sci., 2003, 221: 1-35.

[22] J. Tian, Y.-P. Xu, Z.-L. Chen, J. Nan, G.-B. Li. Air bubbling for alleviating membrane fouling of immersed hollow-fiber membrane for ultrafiltration of river water. Desalination,2010, 260 (1-3): 225-230.

[23] M. Gander, B. Jefferson, S. Judd. Aerobic MBRs for domestic wastewater treatment: A review with cost considerations. Separation and Purification Technol., 2000, 18: 119-130.

[24] A.G. Fane, A. Yeo, A. Law, K. Parameshwaran, F. Wicaksana, V. Chen. Low pressure membrane processesdoingmorewith less energy. Desalination, 2005, 185: 159-165.

[25] Y. Wang, M. Brannock, G. Leslie. Membrane bioreactors: Overview of the effects of module geometry on mixing energy. Asia-Pacific J. Chem. Eng., 2009, 4: 322-333.

[26] P. Cote, J. Cadera, J. Coburn, A. Munro. A new immersed membrane for pretreatment to reverse osmosis. Desalination, 2001, 139 (1-3): 229-236.

[27] J.-B. Castaing, A. Massé, M. Pontié, V. Séchet, J. Haure, P. Jaouen. Investigating submerged ultrafiltration (UF) and microfiltration (MF) membranes for seawater pre-treatment dedicated to total removal of undesirable micro-algae. Desalination, 2010, 253 (1-3): 71-77.

[28] Field, R.W., Wu, D., Howell, J.A., Gupta, B.B. Critical flux concept for microfiltration fouling. J. Membrane Sci., 1995, 100: 259-272.

[29] Wu, D., Howell, J.A., Field, R.W. Critical flux measurement for model colloids. J. Membrane Sci., 1999, 152: 89-98.

[30] Chen, V., Fane, A.G., Madaeni, S.S., Wenten, I.G. Particle deposition during membrane filtration of colloids: transition between concentration polarization and cake formation. J. Membrane Sci., 1997, 125: 109-122.

[31] Bouhabila, E.H., Ben Aim, R., Buisson, H. Microfiltration of activated sludge using submerged membrane with air bubbling (application to wastewater treatment). Desalination, 1998, 118: 315-322.

[32] Defrance, L., Jaffrin, M.Y. Reversibility of fouling formed in activated sludge filtration. J. Membrane Sci., 1999, 157: 73-84.

[33] Defrance, L., Jaffrin, M.Y. Comparison between filtrations at fixed transmembrane pressure and fixed permeate flux: application to a membrane bioreactor used for wastewater treatment. J. Membrane Sci., 1999, 152: 203-210.

[34] Le Clech P. et al. J. Membrane Sci., 2003, 227: 81-93.

[35] Bacchin, P., Aimar, P., Field, R.W. J. Membrane Sci., 2006, 281: 42-69.

[36] Espinasse B. et al. Desalination, 2002, 146: 91-96.

CHAPTER EIGHT

Membrane Distillation /Crystallization of Reverse Osmosis brines

8.1 Introduction

One of the main problems related to seawater desalination plants is that of brine disposal. At present the majority of desalination facilities discharge their concentrate waste streams into surface waters or oceans. However this disposal method may damage the environment if safe and scrupulous measures to mitigate and to control the impact of the discharged brine are not adopted. According to Fritzmann et al. (2007) [1], the capacity of RO desalination industry is today around 20 million m^3/day; the water recovery in seawater RO operations generally varies from 30 to 50 %, being the remaining part rejected. Recent studies in literature confirmed the impact of discharged RO concentrates on soil, on groundwater (contamination by residual chlorine, heavy metals [2]), and on marine fauna and flora (increase of mortality of Posidonia Oceanica [3]), damage of benthic organisms due to coagulants [4]. In this context, innovative techniques and approaches aiming to reduce the volume of wastes and to extract dissolved salts from RO reject brines can represent an interesting opportunity towards sustainability, also in terms of cost-saving [5].

In recent years, the innovative process of membrane distillation-crystallization (MDC) has been investigated for the recovery of valuable salts from nanofiltration brines produced by desalination operations [6]. MDC exploits the excellent ability of Membrane Distillation (MD), a thermally driven operation, to concentrate aqueous solutions up to supersaturation. MD can operate with reasonable fluxes under moderate temperature gradients at high solution concentrations, whilst Reverse Osmosis fails as a consequence of the suppression of driving force caused by the increase of osmotic pressure [7].

The application of MDC to the crystallization of sodium chloride has been firstly addressed by Curcio et al. (2001) [8] by operating at moderate temperature gradient (feed and distillate inlet temperatures of 29 ℃ and 9 ℃, respectively) in order to keep

low the transmembrane flux (~$1.1 \cdot 10^{-4}$ kg/m^2s), so reducing the influence of the concentration polarization on the supersaturation profile, and preventing eventual incrustation at the membrane surface [8].

Integrated MD-crystallization system has been operated by Gryta (2002) [9] to produce 100 kg m^{-2} d^{-1} of NaCl crystals. Anhydrous sodium sulphate crystals with a relatively narrow crystal size distribution have been obtained at high feed temperatures (50-60 ℃) with fluxes up to 20 l m^{-2} h^{-1} by Tun et al. (2005) [10]; it was also found that, due to a high evaporation rate and relevant polarization phenomena, the transmembrane flux gradually declined. NaCl crystals from aqueous solutions showing a coefficient of variation within 25-35 % and an average size of 43 μm have been obtained by Konig and Weckesser (2005) [11].

Our work quantitatively investigates the crystallization kinetics of sodium chloride (NaCl) from RO brines by MDC, as essential requisite to optimize the membrane-assisted crystallization process in terms of productivity, controlled size and shape distribution. The empirical approach is based on a transient crystal size distribution (CSD) data acquired by immage analysis, and an experimental measurement of solution concentration and suspension density curves during batch crystallization tests.

The proposed comparison between artificial and natural RO concentrates aims at quantifying the effect of organic matter dissolved in raw seawater on the distillate flux, suspension density, and NaCl nucleation and growth rates.

8.2 Theory

Mass balance on NaCl during batch crystallization is given as follows:

$$[c(t) + M(t)]V(t) = \text{constant} \tag{8.1}$$

where c is the solution concentration, M the suspension density (weight of crystals per volume unit of suspension), and V the solid-free volume of the solution (subscript 0 refers to initial condition), that progressively decreases with time (t) depending on the flux of water J removed through the microporous hydrophobic membrane having total

area A:

$$V(t) = V_0 - \int_0^t J(t) A\, dt \approx V_0 - A \sum_j J_j(t)\left(t_{j+1} - t_j\right) \qquad (8.2)$$

Suspension density M(t), experimentally measured, was correlated through NaCl density (ρs=2.163 kg/m^3 (Perry and Green, 1984) [12] to the number of crystals $N_i(t)$ in the i-th class of the CSD (counted from the micrographs) having a characteristic size Li at time t:

$$M(t) = \int_{L_1}^{L_n} \rho_s \phi_v L^3 n(L,t) dL \approx \sum_{i=1}^{n} \rho_s \phi_v L_i^3 N_i(t) \qquad (8.3)$$

where ϕ_v is the shape factor (1 for cubic NaCl crystals) and n(L,t) is the population density. By definition:

$$N_i(t) = \int_{L_i}^{L_{i+1}} n(L,t) dL \qquad (8.4.a)$$

and

$$\sum_{i=1}^{n} N_i(t) = N_{t\,o}(t) \qquad (8.4.b)$$

where $N_{tot}(t)$ is the total number of crystals in suspension at time t. If indicating αi(t) the fraction $N_i(t)/N_{tot}(t)$, experimentally determined by CSD measurements (figure 8.5 clarifies this point), equation 8.3 can be rewritten as:

$$N_{tot}(t) \approx \frac{M(t)}{\sum_{i=1}^{n} \rho_s \phi_v L_i^3 \alpha_i(t)} \qquad (8.5)$$

being all the terms in the right side known. The NaCl linear growth rate G was calculated as:

$$G = \frac{d\bar{L}(t)}{dt} \approx \frac{\bar{L}(t_{j+1}) - \bar{L}(t_j)}{\left(t_{j+1} - t_j\right)} \qquad (8.6.a)$$

where $\bar{L}$ (t), the average length of crystals at time t, is:

$$\bar{L}(t) \approx \sum_{i=1}^{n} \alpha_i(t) L_i \qquad (8.6.b)$$

As in Garside et al. (2002) [13], the relationship between G and the overall mass

growth rate R_G is:

$$R_G = \frac{3\phi_v}{\phi_a}\rho_s G \tag{8.6.c}$$

The surface shape factor ϕa, for the cubic NaCl crystals, takes the value of 6. Nucleation rate B was obtained as:

$$B = \frac{1}{V(t)}\frac{dN_{tot}(t)}{dt} \tag{8.7.a}$$

and

$$\frac{dN_i(t)}{dt} \approx \frac{N_{tot}(t_{j+1}) - N_{tot}(t_j)}{(t_{j+1} - t_j)} \tag{8.7.b}$$

8.3 Materials and methods

Raw seawater was collected from Tyrrenian Sea facing the coastal city of Amantea (Calabria), and then pre-filtered through 0.5 μm cartridge filters. Reverse Osmosis concentrates were obtained by processing seawater in a RO lab-scale unit MATRIX (Matrix desalination Inc.) equipped with 3 modules OSMONICS AD 2540 FF 2.5", and operated at 800 psi and 25 ℃ in complete recycle of retentate until reaching a global recovery factor of 30 %.

The solution composition of both raw and RO concentrated natural seawater was determined by ion chromatographer 861 Advanced Compact IC (Metrohm AG, Switzerland) equipped with METROSEP C2-150 columns for cations and anions analysis. The TOC content was evaluated by TOC-VCSN Total Organic Carbon Analyzer (Shimadzu, Japan).

Synthetic RO concentrates were prepared according to the ionic composition reported in Table 8.1 by dissolving reagent grade NaCl (Carlo Erba 368256), $CaCl_2 \cdot 2H_2O$ (Riedel-deHaen 31307), $MgCl_2$ (Carlo Erba 349354), $NaHCO_3$ (Fluka 88208), Na_2CO_3 (Fluka 71350), Na_2SO_4 (Carlo Erba 483007), and KCl (Carlo Erba 471177) in ultrapure water (Purelab, ELGA) without any organic content.

Table 8.1 Natural feed seawater analysis

Parameter	Feed Concentration (mg/L)†	Retentate Concentration (mg/L)‡
TOC	1.5	2.1
Cl^-	20,250	28,800
Na^+	10,900	15,500
SO_4^{2-}	2,150	3060
Mg^{2+}	1,420	2,020
Ca^{2+}	440	625
HCO_3^-	140	199
TDS	35,300	50,200

† Temperature: 25 ℃, pH=8.2

‡ Recovery factor.

Conventional lime/soda ash softening process was used to reduce calcium and magnesium hardness of the RO concentrates and to limit scaling problems [14].

The initial volume V_0 of brine charged to the membrane distillation-crystallization plant was 50 l; batch operations were protracted for 80-90 hours. The MDC bench-scale experimental setup used in this work is shown in Figure 8.1.

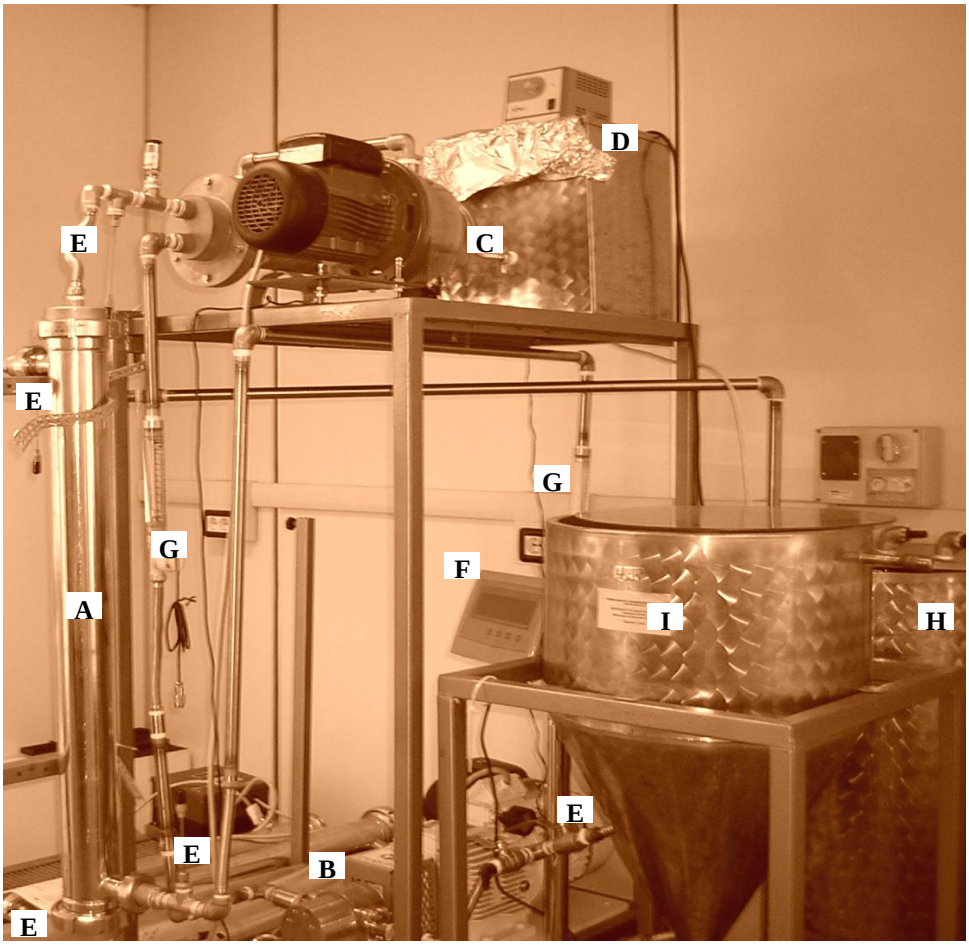

Figure 8.1 Membrane Distillation-Crystallization bench-scale plant

It consists of: A) a home-made membrane module assembling Accurel PP polypropylene hollow-fibers with a total membrane area of 0.4 m^2; B) a gear pump SERIE N (Pompe Cucchi, ITALY) automated by AC TECH Intelligent Drive, recirculating the concentrate solution; C) a centrifugal pump BGM5/A (Lowara, Italy) recirculating the solvent (water) that permeates through the membrane; D) a heater Mod. 112A (VWR, USA) that increases the solution temperature up to 40 ℃ at the entrance of the membrane module; E) five SPER SCIENTIFIC 800012 Pt multi-channel thermocouples; T) with sensitivity ±0.1 C monitoring temperatures at the inlet and outlet of the membrane module (on both permeate and concentrate sides); F) an industrial balance with HDWE RS485 indicator connected to the distillate tank to estimate the transmembrane flux of water; G) two F14 flowmeters (Blue-White Industries, Ltd) operating on both permeate and concentrate lines. The temperatures in

the distillate reservoir; H) and jacketed retentate/crystallization tank; I) were maintained at 20 ℃ and 30 ℃, respectively, by thermostatic baths Digital Plus RTE201 (Neslab, USA).

Suspension density was experimentally measured by collecting samples of mother liquor at various intervals of time, corresponding to different supersaturation levels of the solution; the time interval chosen between two successive sampling was 30 min, enough to yield detectable changes in crystal size distribution. Crystals were filtered, weighted, deposited on a glass side and visually analysed by transmitted optical microscopy LEICA DFC 420 with monochrome camera connected to PC in order to determine the crystal size distribution (CSD). The images captured, at least 50 per sample, corresponded to more than 1000 classified crystals for each experimental run.

8.4 Results and discussion

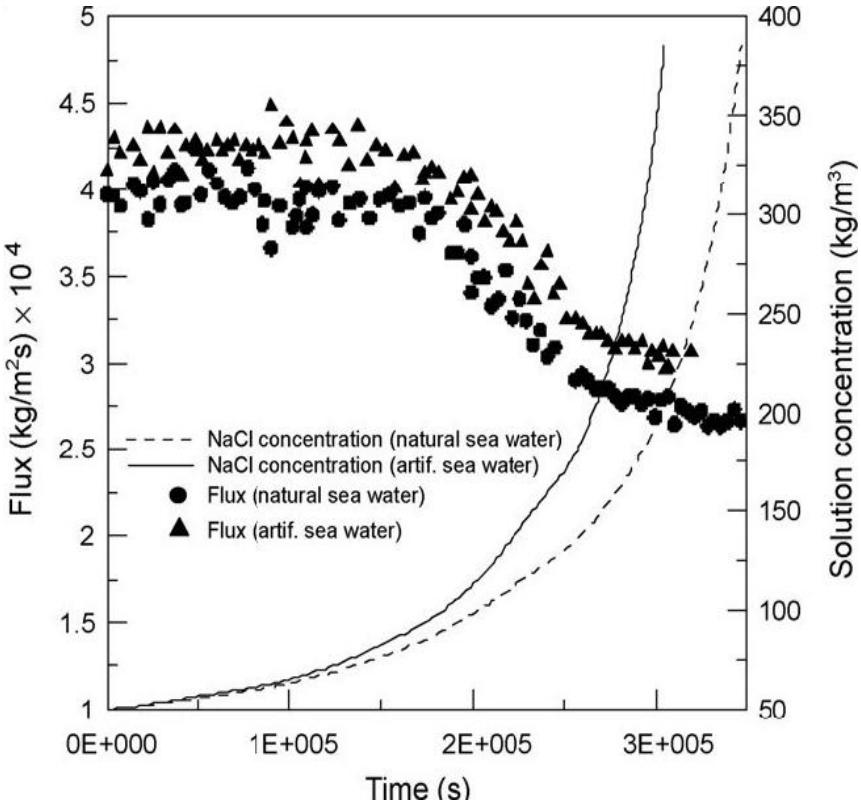

Figure 8.2 Transmembrane flux and seawater concentration vs operation time

Figure 8.2 illustrates the time-dependent water flux and NaCl concentration profiles

registered during MDC tests carried out at moderate temperature gradient ($\Delta T \approx 20$ ℃), that resulted in a initial transmembrane flux of 4-4.2 $kgm^{-2}s^{-1}$. The subsequent progressive flux decline (~30 % at the end of each test) was caused by the vapour pressure decrease due to the increase in solute concentration. The achievement of NaCl supersaturation (reached after 81 and 92 hours when treating natural and synthetic RO retentates, respectively) did not result in a significant flux decrease. Therefore, crystallization tests were carried out under almost constant transmembrane fluxes of $3.1 \cdot 10^{-4}$ and $2.7 \cdot 10^{-4}$ kg $m^{-2}s^{-1}$ for natural and synthetic brines, respectively. These findings confirmed the good countermeasures (appropriate control of evaporation rate and hydrodynamics) taken against encrustation and deposit of particles on the membrane surface that caused drastic reduction of permeability noticed in Tun et al. (2005) [10].

The persistence of a significant distillate flux was able to sustain the supersaturation ratio S (that progressively increased from 1 to 1.15 during batch experiments) against the reduction caused by the crystallization of NaCl.

When treating RO brines from natural seawater, the observed average reduction of the distillate flux with respect to artificial retentates was 8%, that became more prominent (-13 %) at NaCl concentration approaching the solubility limit. These observations agree with the expectation of a deterioration of MDC performance as a consequence of the membrane fouling due to the presence of natural organic matter (NOM) in the feed seawater. The decline of membrane permeability in MD caused by the deposition of organic matter on the membrane surface has been investigated by Gryta et al. (2001) [15]; SEM-EDS and FTIR-DSR analyses indicated that forming fouling layer comprises a hydrated gel layer, from which the evaporation of water was still possible, but at reduced rates (up to a 30 % decline of the maximum transmembrane flux has been noticed during tests carried out at 358K). However, two-step cleaning with citric acid aqueous solution (20 min)/NaOH aqueous solution (20 min) allowed us to completely restore the permeation performance of the membrane.

At the end of a MDC test, the total water recovery factor achieved was higher than

90 %, thus confirming the potentiality of this innovative approach towards the goal of zero liquid discharge.

Polarization phenomena occurring at the membrane surface might affect the supersaturation profile along the membrane module. In particular, concentration polarization refers to the increase of solute concentration (c_s) at the membrane interface (wall) with respect to its bulk value as a consequence of the solvent evaporation. According to the film model:

$$CPC\,(Concentration\,Polarization\,Coefficien\,t) = \frac{c_{s,wall}}{c_{s,bulk}} = \exp\left(\frac{J}{\rho\, k}\right) \qquad (8.8.a)$$

where J is the transmembrane flux, ρ the solution density and k is the mass transfer coefficient, estimated in laminar regime using the Leveque equation [16]:

$$k = 1.62\left(\frac{d\,u}{l}\right)^{1/3} D^{2/3} \qquad (8.8.b)$$

In equation 8.8.b, d is the fibre inner diameter, v the solution velocity, *l* the fibre length and D the diffusion coefficient. Our strategy, devoted to minimize this effect by keeping the flux low, resulted in CPC values varying between 1.014-1.008. As a term of comparison, Tun et al. (2005) [10] who observed the complete suppression of permeability due to severe clogging of the membrane surface due to crystals formed - have reported an initial CPC value of 1.2-1.3 (resulting from initial permeation rates of 10^{-20} kg m^2h^{-1}) that decreased gradually during the batch run as the transmembrane flux dropped.

The concomitant effect of temperature polarization on NaCl supersaturation was considered negligible due to the insensitive behaviour of sodium chloride solubility with temperature: +0.2 % every 10 ℃ [17]. The increase of suspension density during batch MDC tests is reported in Figure 8.3.

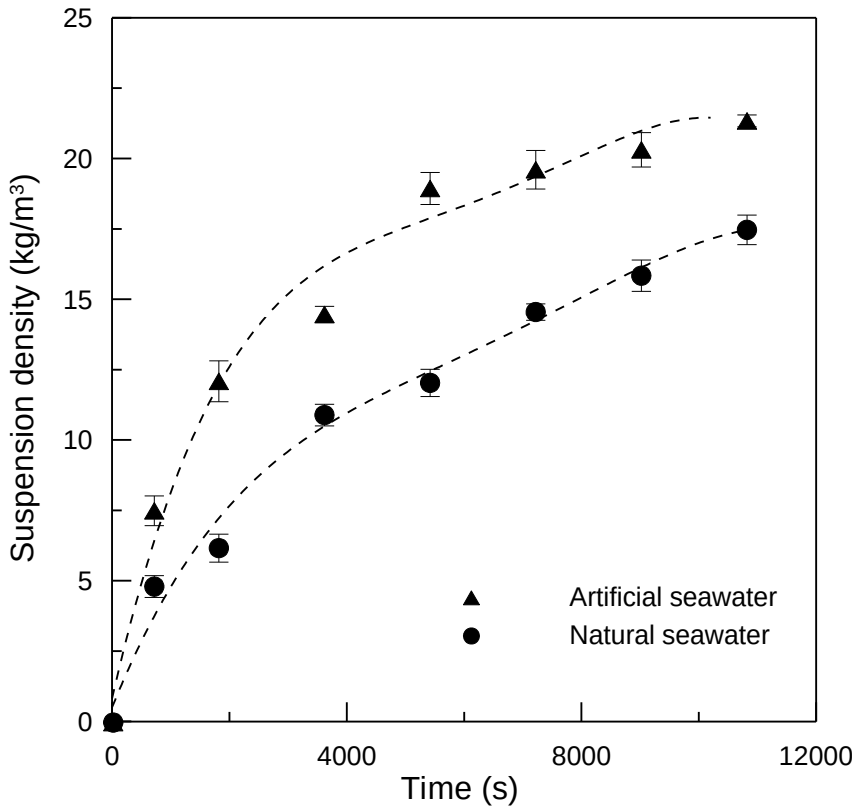

Figure 8.3 Suspension density VS crystallization time

The yield of NaCl crystals approaches 21 kg per cubic meter of RO artificial brine after three hours since the achievement of supersaturation. A lower amount of solids (-20 %) was produced from natural RO brines, thus evidencing the negative impact on the crystallization kinetics of organic matter dissolved in natural seawater.

The presence of NaCl crystals on the membrane surface confirmed that the polymeric surface acts as promoter of heterogeneous nucleation.

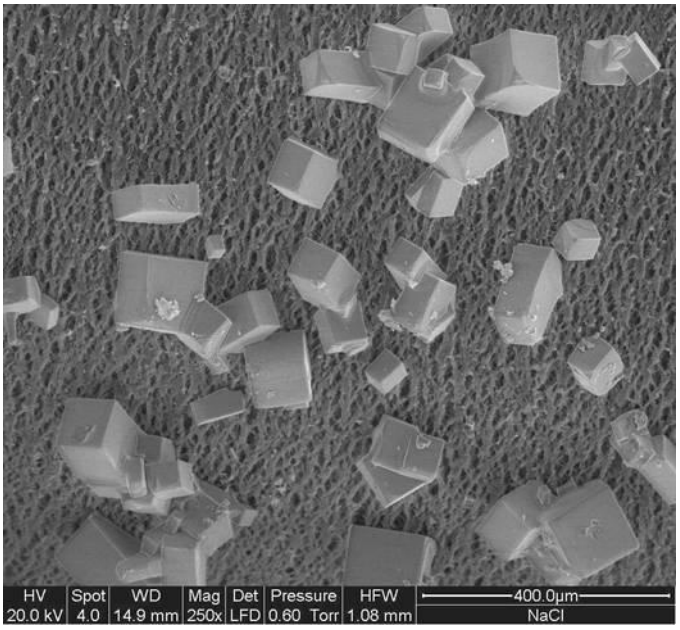

Figure 8.4 Sodium chloride crystals grown on Accurel PP hollow fiber membrane (from natural RO brines at 210 min).

As shown in Figure 8.4, crystals of sodium chloride nucleating at the membrane surface showed the ordinary cubic shape; some exception concerned the moderate morphological changes (slight elongation) most probably due to the presence of different ions in the RO brines acting as impurities. The size of detected crystals typically varied between 20 and 200 μm, showing reduced values (-10 % c.a.) when NaCl crystals grew from natural seawater RO concentrates.

Crystals were continuously removed from the membrane surface as a consequence of the recirculation of the solution along the hollow fiber module (placed in vertical to avoid deposition by gravity, as in Figure 8.1), and transmembrane flux remained almost stable during the crystallization tests.

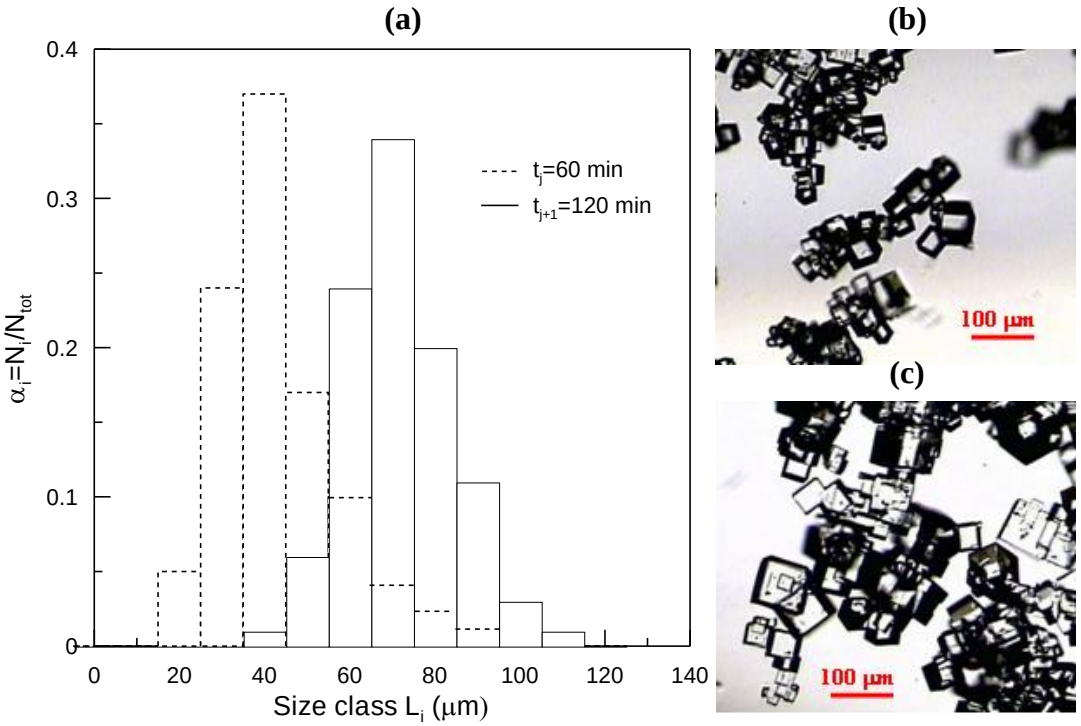

Figure 8.5 a) NaCl crystal size distribution grown from natural RO brines, Images of crystals at b) 60 min, c) 120 min after reaching supersaturation

The characteristic development of CSD is exemplified in Figure 5 at 60 and 120 minutes: detected size distributions were mononodal, and the single peaks move towards a larger size with time. The dispersion of CSD curves was relatively low, with coefficient of variation in the interval of 35-40 %.

The following empirical expression usually correlates the mass growth rate RG to the overall concentration driving force (c-c*):

$$R_G = k_G (c - c^*)^g \tag{8.9}$$

In equation 8.9, the value of the solubility c* of NaCl in the concentrated brines at the working temperature of 35 ℃ was 305 kg/m^3 (experimentally measured), about 15 % lower than the solubility value of NaCl in pure water; analogous solubility decrease as a consequence of impurities (and, in particular, $MgCl_2$) present in the mother solution have been reported in Ferreira et al. (2005) [18].

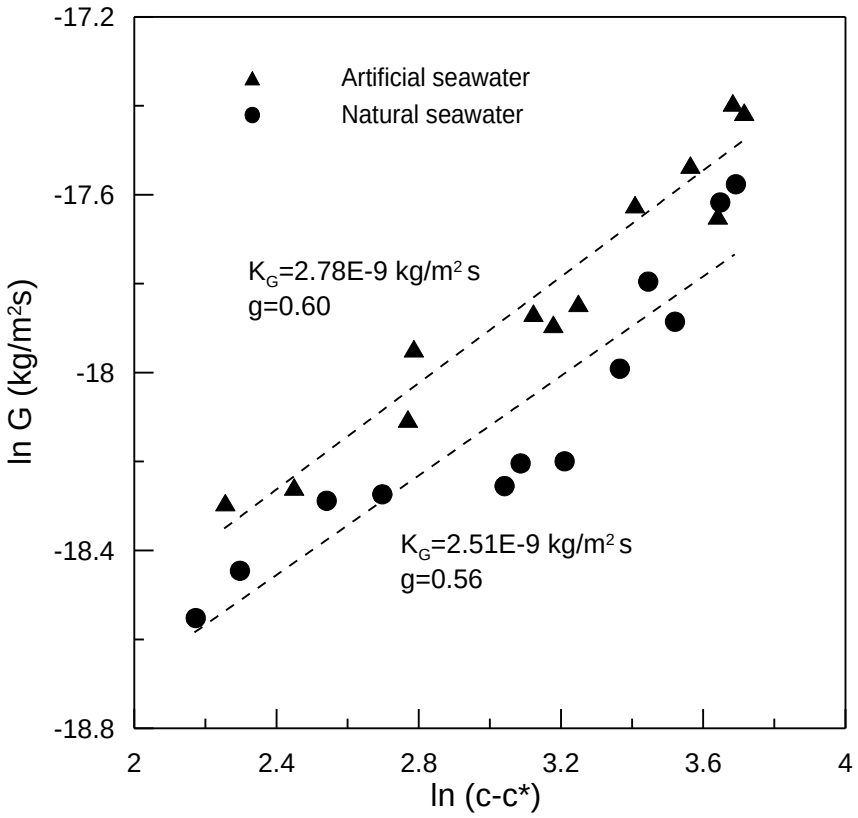

Figure 8.6 Mass growth rate of NaCl crystals vs supersaturation (c* = 305 kg/m^3)

The values of kinetic parameters kG (kg/m^{2}s) and g were determined from the logarithmic plot reported in Figure 8.6. The NaCl growth rate order g showed a substantial independence from the low organic content present in natural seawater (g=0.56, lower by 7 % with respect to value found for artificial RO concentrates). The measured of g were generally lower than those reported in literature and related to the crystallization of inorganic compounds, i.e: 0.77 for $KAl(SO_4)_2 \cdot 12H_2O$ in Tavare and Garside (1986) [19]; 1.3 for KNO_3 in Chung et al. (2000) [20]; 1.6 for $CuSO_4 \cdot 5H_2O$ in Zumstein and Rousseau (1987) [21]. Al-Jibbouri and Ulrich (2002) [22] verified that $MgCl_2$ inhibits the growth rate of NaCl and this effect was more pronounced at higher impurity concentration, confirming the important role of the integration step (incorporation of the growth units into the crystal lattice) in the crystal growth phenomenon; in the $MgCl_2$ concentration range of 0-250 pm, they found a growth rate of 1.21. The inhibition effect was more evident when referring to the growth rate constant kg: the highest value obtained in our work (2.78·10-9 kg/m^{2}s for NaCl

crystallized from artificial RO concentrates) was 4 order of magnitude lower with respect to that measured by Al-Jibbouri and Ulrich (2002) [22].

Growth rate of NaCl from real seawater RO brines varied within 0.8 10^{-8} - 2.5 10^{-8} m/s, exhibiting a reduction of 15-23 % with respect to what measured on artificial concentrates. These data compares favourably with literature: in Asselbergs (1978) [23], a traditional reference for NaCl crystallization, the values of G range within 3.5-13·10^{-8} m/s for suspension density of 25-200 kg/m^3. The work of Garside and Shaha (1980) [24] showed that most of inorganic salts exhibit a growth rate in the order of 10^{-8} m/s.

During crystallization tests, the value of supersaturation (S-1) remained relatively low and always below 0.15. Takiyama et al. (1998) [25] observed, in drowning-out precipitation experiments of NaCl, that heterogeneous nucleation mechanism was predominant for (S-1) <0.7. In our system, hydro-dynamically characterized by a laminar regime of the recirculating mother solution (Re~900), and where unseeded crystallization occurred in presence of a polymeric membrane, primary heterogeneous nucleation was assumed to initiate the crystallization process and to prevail over secondary nucleation. According to Classical Nucleation Theory (CNT), the primary nucleation rate B is related to supersaturation S by the expression:

$$B = a \exp\left(\frac{-b}{\ln S^2}\right) \qquad (8.10.a)$$

where a is a pre-exponential factor, and b is a constant (Mersmann et al., 1992) [26]. According to predictions of CNT, and regardless from brine typology, the number of NaCl crystals increased at higher supersaturation ratios, being in the order of 109-1011 crystals per cubic meter of solution.

The total number of crystals generated from natural brines was at average 27 % lower than that observed when processing artificial retentate.

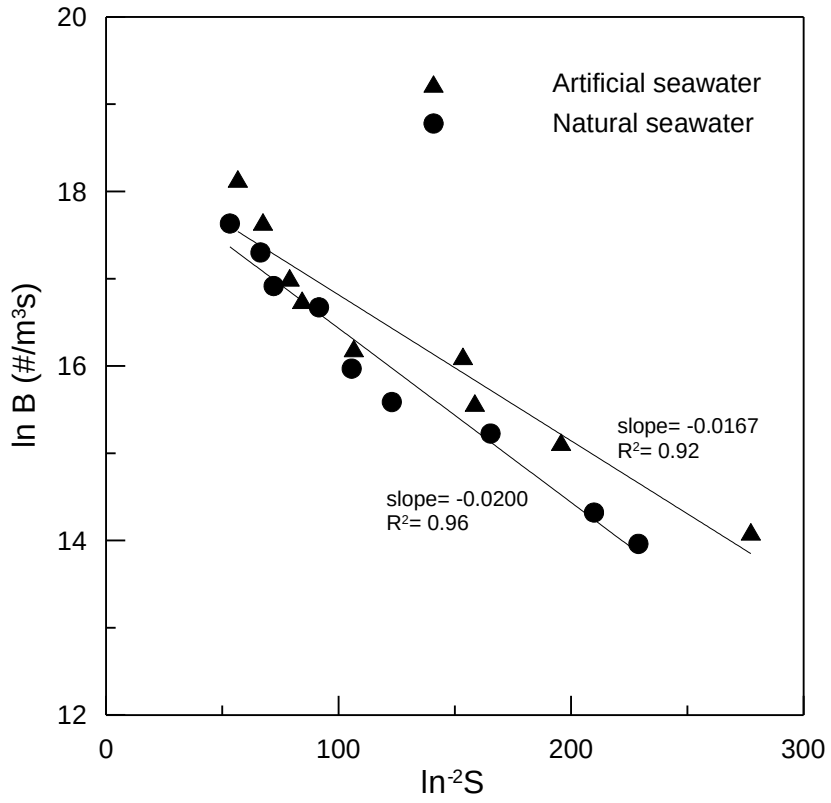

Figure 8.7 Experimental nucleation rate of NaCl crystals vs supersaturation

The logarithm plot of nucleation rate B vs $\ln^{-2}S$, reported in Figure 8. 7, confirmed the good agreement of experimental results with the linear trend expected from equation 8.10.a. Slopes for NaCl nucleation rates measured in artificial and natural seawater RO concentrates, mathematically corresponding to the term b in equation 8.10.a, differed by 16 %. The coefficient b can be expressed as in Gomez-Morales et al. (1996) [27]:

$$b = \frac{\phi 16\pi\sigma^3\upsilon^2}{3(kT)^3} \qquad (8.10.b)$$

where σ is the interfacial energy, ν the NaCl molecular volume ($1.12\cdot10^{-29}$ m^3 = molecular weight/(Avogadro's number*density*number of ions in a formula unit)), k the Boltzmann's constant and T the absolute temperature. The factor ϕ accounts for the reduction of the Gibbs free energy of the system due to heterogeneous nucleation on porous membranes and, according to Curcio et al. (2006) [28], depends on the membrane porosity ε and the contact angle θ:

$$\phi = \frac{1}{4}(2+\cos\theta)(1-\cos\theta)^2\left[1-\varepsilon\frac{(1+\cos\theta)^2}{(1-\cos\theta)^2}\right]^3 \qquad (8.10.c)$$

For ε=0.70 and θ=120 °, ϕ=0.66. Based on the different slopes of Figure 7, the values of σ calculated using equation 10.b were $9.6\cdot10^{-3}$ and $10.2\cdot10^{-3}$ J/m^2 for NaCl crystals nucleated from artificial and natural brines, respectively. These results nicely compare with experimental values of interfacial energy in supersaturated solutions for some inorganic salts as reported in Toyokura (1995) [29]: $10.5\cdot10^{-3}$ J/m^2 for $CuSO_4\cdot5H_2O$, $8.9\cdot10^{-3}$ J/m^2 for K-Alum, $7.3\cdot10^{-3}$ J/m^2 for $MgSO_4\cdot7H_2O$.

8.5 Conclusions

This study confirms the ability of MDC to extremely concentrate RO brines. So achieve a total water recovery factor greater than 90 % and an analogous volumetric reduction of the waste to be discharged. Moreover, batch runs carried out on natural RO concentrates resulted in the production of 17 kg/m^3 of NaCl crystals, representing the 34 % c.a. of the total content of dissolved solids in the brine.

Transmembrane fluxes in the order of 10^{-4} kg m^{-2}s^{-1} allowed limit concentration polarization at the membrane surface where heterogeneous nucleation took place; the possibility to prevent encrustations or irremovable deposits of solids due to uncontrolled supersaturation was recognized as a crucial task in order to achieve long-term stability of MDC.

It was also observed that the relatively low content of organics in natural RO retentate (TOC: 2.1 mg/L), increasing progressively during concentration tests, significantly affects the crystallization kinetics in terms of reduced magma density, nucleation and growth rates, as well as the transmembrane flux. Therefore, adequate pre-treatment before RO stage is needed to reduce the negative effect of dissolved organic matter on the MDC performance.

All these data outline the potential impact of MDC on the economical and environmental aspects of membrane desalination industry, and more research efforts in this field should be encouraged.

References:

[1] Fritzmann, C., Löwenberg, J., Wintgens, T. and Melin, T. State-of-the-art of reverse osmosis desalination. Desalination, 2007, 216: 1-76.

[2] Mohamed, A.M.O., Maraqa, M. and Al Handhaly, J. Impact of land disposal of reject brine from desalination plants on soil and groundwater. Desalination, 2005, 182: 411-433.

[3] Latorre M. Environmental impact of brine disposal on Posidonia seagrasses. Desalination, 2005, 182: 517-524.

[4] Lattermann, S. and Höpner, T. Environmental impact and impact assessment of seawater desalination. Desalination, 2008, 220: 1-15.

[5] Ahrned, M., Arakelb, A., Hoey, D., Thumarukudyd, M. R., Goosen, M. F.A., Al-Haddabi, M. and Al-Belushi, A. Feasibility of salt production from inland RO desalination plant reject brine: a case study. Desalination, 2003, 158: 109-117.

[6] Drioli, E., Curcio, E., Criscuoli, A. and Di Profio, G. (2004) Integrated system for recovery of CaCO3, NaCl and MgSO4·7H2O from nanofiltration retentate. J. Membrane Sci., 2004, 239: 27-38.

[7] Curcio, E. and Drioli, E. Membrane Distillation and related operations - A review. Separation and Purification Reviews, 2005, 34: 35-86.

[8] Curcio, E., Criscuoli, A. and Drioli, E. Membrane Crystallizers. Ind. Eng. Chem. Res., 2001, 40: 2679-2684.

[9] Gryta, M. Concentration of NaCl solution by membrane distillation integrated with crystallization. Sep. Sci. Tech., 2002, 37: 3535-3558.

[10] Tun, C.M., Fane, A.G., Matheickal, J. T. and Sheikholeslami, R. Membrane distillation crystallization of concentrated salts – flux and crystal formation. J. Membrane Sci., 2005, 257: 144-155.

[11] Konig, A. and Weckesser, D. Membrane based evaporation crystallization. VDI Berichte 1901 II, 2005: 1171-1176.

[12] Perry, L.R. and Green, D. Perry's Chemical Engineering Handbook 6th Ed. McGraw-Hill, New York, 1984.

[13] Garside, J., Mersmann, A. and Nyvlt, J. Measurement of crystal growth and nucleation rates.

IChemE, Rugby (UK), 2002.

[14] Baruth, E.E. Water treatment plant design. 4th Ed. McGraw-Hill (New York), 2005.

[15] Gryta, M., Tomaszewska, M., Grzechulska, J. and Morawski, A.W. Membrane distillation of NaCl solution containing natural organic matter. J. Membrane Sci., 2001, 181: 279-287.

[16] Shrivastava, A., Kumar, S. and Cussler, E.L. Predicting the effect of membrane spacers on mass transfer. J. Membrane Sci., 2008, 323: 247-256.

[17] Ferreira, A. and Lopes A. A new potentiometric method to evaluate supersaturation in aqueous systems. Proceedings of 15th International Symposium on Industrial Crystallization, Sorrento (Italy), 2002: 1377-1382.

[18] Ferreira, A., Faria, N., Rocha, F., Feyo De Azevedo S. and Lopes A. Using image analysis to look into the effect of impurity concentration in NaCl crystallization. Chem. Eng. Res. Des., 2005, 83: 331-338.

[19] Tavare, N.S. and Garside, J. Simultaneous estimation of crystal nucleation and growth kinetics from batch experiments. Chem. Eng. Res. Dev., 1986, 64: 109-117.

[20] Chung, S.H., Ma, D.L. and Braatz, R.D. Optimal model-based experimental design in batch crystallization. Chemometrics and Intelligent Laboratory Systems, 2000, 50: 83-90.

[21] Zumstein, R.C. and Rousseau, R.W. (1987) Utilization of industrial data in the development of a model for crystallizer simulation. AIChE Symposium Series No 253 (83), 130–139

[22] Al-Jibbouri, S. and Ulrich, J. The growth and dissolution rate of sodium chloride in a fluidized bed crystallizer. Journal of Crystal Growth, 2002, 234: 237-246.

[23] Asselberg, A.J. (1978) PhD Thesis. Delft Technical University

[24] Garside, J. and Shah, M.B. Crystallization kinetics from MSMPR Crystallizers. Ind. Eng. Chem. Process Dev., 1980, 19: 509-514.

[25] Takiyama, H., Otsuhata, T. and Matsuoka M. Morphology of NaCl Crystals in drowning-out precipitation operation. Trans IChemE, 1998, 76: 809-814.

[26] Mersmann, A., Angerhofer, M., Gutwald, T., Sangl, R. and Wang, S. General prediction of median crystal sizes. Separation Technology, 1992, 2: 85–97.

[27] Gomez-Morales, J., Torrent-Burgues, J. and Rodriguez-Clemente, R. Nucleation of calcium carbonate at different initial pH conditions. Journal of Crystal Growth, 1996, 169: 331-338.

[28] Curcio, E., Fontananova, E., Di Profio, G., Drioli, E. Influence of the Structural Properties of

Poly(vinylidene fluoride) Membranes on the Heterogeneous Nucleation Rate of Protein Crystals. J. Phys. Chem. B, 2006, 110: 12438-12445.

[29] Toyokura, K. New aspects of industrial crystallization. J. Chem. Eng. Japan, 1995, 28: 361-371.

Conclusions

Membrane Distillation/Crystallization (MD/Cr), as a stand-alone unit or in combination with RO, offers the opportunity to increase the overall water recovery factor (WRF).

To reduce the volume of brines:

This study confirmed the ability of membrane distillation/crystallization to concentrate RO brines to achieve a water recovery above 90% with a concomitant reduction in volumetric waste discharged to the environment.

To produce valuable crystals:

Followed after a nanofiltration pre-concentration step, Na_2SO_4 was efficiently removed by evaporative crystallization through microporous hydrophobic membranes. The nanofiltration pre-concentration step operated at 3.45×10^6 Pa exhibited rejection values above 99%, and the unit recovery factor reached up to 50%. Membrane crystallization tests carried out at moderate temperature (40 $^{\circ}$C) resulted in the formation of thenardite in a reasonable amount (slurry density up to 21 kg/m^{-3}h) and good product quality (coefficient of variation below 30% within the first hour);

The possibility to drive MD/Cr at high WRF depends on the ability to control scaling. DLS measurements showed that induction times were significantly reduced when precipitation occured in presence of membranes, which accelerated the rate of $CaCO_3$ nucleation. DCMD tests, carried out on a semi-pilot plant and protracted for 35 h, demonstrated that scaling significantly reduced the transmembrane permeate flux by 33%. Humic acid, even at low concentration, retarded the nucleation and growth of vaterite crystals with low supersaturation. On the other side, $CaCO_3$ deposition on the membrane surface (exacerbated at high ionic strength) also contributed – in minor extent with respect to scaling – to decrease the system performance.

Dissolved Organic Matter in real seawater:

(1) To decrease both growth rate and yield of NaCl crystals;

(2) Submerged UF hollow fiber has been demonstrated as feasible seawater

pretreatment in reducing NOM, thus was of great use in the integrated membrane desalination systems, and provided the identification of the operating conditions and their opportune optimization.

Experiments performed on direct seawater pretreatment by submerged hollow fiber ultrafiltration demonstrated that:

(1) Periodical aeration/filtration represented the best compromise between process efficiency and energy consumption, and provided the requirements of permeate production.

(2) The plant could be operated for more than 60 h without any chemical cleaning, however, the fouling rate increased yet after 24 h, even when back flushing, with significant loss of performance.

(3) Irreversible particles adsorption on/in the membrane surface occured yet during the early stages of seawater filtration, even under subcritical flux conditions.

(4) Amino compounds with small molecular weight permeated the membranes, while biopolymers and, to some extent, humic substances were more effectively retained.

(5) Excessive back flushing with the permeate, containing not-retained NOM with low molecular weight, might not only led to increased energy consumption and reduced water productivity, but also induced pore blocking and fouling cake compaction on the lumen side of the asymmetric membrane, thus enhanced the overall resistance to mass transport.

(6) DOC average removal was around 46%, with a maximum of 67% at lower transmembrane flux, with an average content in the permeate well below 1 mg/L.

(6) Simple cleaning with NaOCl allowed almost complete recovery of original membrane permeability.

Costs analysis showed that large-scale MD was competitive under the following constraints:

(1) Availability of waste thermal energy or renewable energy sources (i.e. solar);

(2) Integrated with conventional pressure-driven membrane systems.

All the results outline the potential of Membrane Distillation integrated with

seawater desalination systems on the economical and environmental aspects of membrane desalination industry, and more research efforts in this field should be encouraged.

Acknowledgements

I would like to express my deepest gratitude to my supervisor, Professor Enrico Drioli from University of Calabria, for his constant encouragement and guidance during my Ph.D. studies. In the preparation of the thesis, he has spent much time reading through each draft and provided me with inspiring advice. Without his illuminating instruction, insightful criticism and expert guidance, the completion of this thesis would not have been possible.

I thank Dr. Efrem Curcio from University of Calabria, for his help in the academic affairs.

I thank Dr. Gianluca Di Profio from University of Calabria, who has instructed and helped me a lot in the past three years.

I thank Dr. Al Obaidani Sulaiman from University of Calabria for his technical support during my Ph.D. studies.

I thank Dr. F. Macedonio for her good suggestions about thesis writing.

Finally, I greatly appreciate the support from my parents and all my friends.

Publications:

1. Gianluca Di Profio, Xiaosheng Ji, Efrem Curcio, Enrico Drioli, Submerged hollow fiber ultrafiltration as seawater pre-treatment in thelogic of integrated membrane desalination systems, Desalination (accepted)

2. Efrem Curcio, Xiaosheng Ji, Abdul Matin Quazi, Shahzad Barghi , Gianluca Di Profio, Enrica Fontananova, Trevor Macleod, Enrico Drioli, *Hybrid Nanofiltration-Membrane Crystallization system for the treatment of sulfate wastes*, Journal of Membrane Science, Volume 360, Issues 1-2, 15 September 2010, Pages 493-498

3. Xiaosheng Ji, Efrem Curcio, Al Obaidani Sulaiman, Gianluca Di Profio, Enrica Fontananova, Enrico Drioli,*Membrane Distillation Crystallization of seawater Reverse Osmosis brines*, Separation and Purification Technology, Volume 71, Issue 1, 29 January 2010, Pages 76-82

4. Efrem Curcio, Xiaosheng Ji, Gianluca Di Profio, Enrico Drioli, *Membrane Distillation operated at high seawater concentration factors: role of the membrane on CaCO3 scaling in presence of humic acid*, Journal of Membrane Science, Volume 346, Issue 2, 15 January 2010, Pages 263-269

5. Xiaosheng Ji, Efrem Curcio, Gianluca Di Profio, Enrica Fontananova, Enrico Drioli, *The effect of carbonate scaling and humic acid fouling in Membrane Distillation*, Asia-Pacific Conference on Desalination & Water Reclamation,2010

6. E. Curcio, G. Di Profio, Xiaosheng Ji, F. Macedonio, E. Drioli, *Pretreatment for membrane distillation operated at high seawater concentration factors*, EU－CHINA workshop, 2009

7. E. Curcio, J. Xiaosheng, G. Di Profio, S. Al-Obaidani, E. Drioli, Seawater desalination by membrane distillation-crystallization: troubles at high recovery factors, EUROMEMBRANE 2009

8. F. Macedonio, Xiaosheng Ji, E. Drioli, E. Curcio, G. Di Profio, CRYSTALS RECOVERY FROM NF RETENTATE STREAMS THROUGH MEMBRANE CRYSTALLIZER DEVICES, ECCM5,2008